1995

A New Photocatalytic Reactor For The Photodegradation Of Organic Contaminants In Water

Julio E. Valladares

A NEW PHOTOCATALYTIC REACTOR FOR THE PHOTODEGRADATION OF ORGANIC CONTAMINANTS IN WATER

by

Julio E. Valladares

Department of Chemistry

Submitted in partial fulfilment
of the requirements for the degree of
Doctor of Philosophy

Faculty of Graduate Studies
The University of Western Ontario
London, Ontario, Canada
March 1995

ISBN 0-315-99285-9

ABSTRACT

The TiO_2 photocatalytic degradation and mineralization of organic pollutants in water has been broadly demonstrated at the laboratory level for a wide number of organic pollutants. However, there are still some problems that need to be addressed in order to make this technology more practical. The design of heterogeneous photocatalytic reactor systems, still in the infancy their development, is facing different problems such as light scattering, oxygen starving, particle separation and mass transfer. Additionally, there have also been a lack of a general method to evaluate the performance of the different reactor systems.

The present work addresses these problems by presenting a new photoreactor system (PHOTO-CREC II) and a general method called the Photochemical Thermodynamic Efficiency Factor, PTEF (based on known thermodynamic and photocatalytic principles) for the evaluation and comparison of the performance of different photoreactor systems.

The new photocatalytic reactor concept (PHOTO-CREC, reactor) was designed, built and successfully tested with model pollutants (Methylene Blue and Phenol). The characteristic parameters of adsorption and reaction kinetics for the photodegradation of methylene blue were determined. The effects on the reaction rate of initial concentration of the model compound, flow rate of the solution through the reactor and light intensity were also determined and a kinetic model proposed. Quantum yields and EE/Os for the photodegradation reaction were determined and compared with other values reported in the literature.

The new efficiency index (PTEF), was utilized to compare the performance of the PHOTO-CREC reactor with other photoreactor systems. It was demonstrated that PTEFs, obtained using data from a number of literature references, are independent or weakly dependent on pollutant chemical structure and characteristic of the specific photocatalytic reactor used.

PTEF values in PHOTO-CREC II were in the range of 1×10^{-9} mol J^{-1}, which is considered in the high range for PTEF values. This was particularly relevant considering that the unit studied was with the largest volume for this range of PTEF.

AKNOWLEDGEMENTS

I want to express my gratitude to my superb team of advisers, Professors Jim Bolton and Hugo de Lasa. Their support, help, advice and encouragement throughout this work have been invaluable. I will forever be grateful.

I want to thank as well my coworkers at the Chemical Reactor Engineering Centre (CREC) and the Environmental Photochemistry Laboratory for their help and support. Finally, I want to thank the Ministry of Environment of Ontario, for the financial support to this research.

DEDICATION

To my beloved wife, Marta Gloria

and my Children Julio Jr., Marta Maria and Eduardo.

TABLE OF CONTENTS

LIST OF FIGURES

LIST OF TABLES

CHAPTER I

GENERAL REVIEW

I.1 INTRODUCTION

During the last decade, chemical and bacteriological contamination of water streams have become an issue of worldwide concern. Nowadays it is frequent to find reports in the press about the contamination of ground and surface waters: sea, lakes, rivers, ponds, creeks and wells. In developed countries, water contamination originates frequently from industrial activity and from the large number of household chemicals used at home and the office, while in developing countries, water contamination is due largely to agricultural activities, transportation, untreated industrial wastewater discharges and social problems. The consequences of drinking contaminated water are numerous. Contaminated waters may be linked with new diseases and epidemics and also contributes to the destruction of the natural environment, such as the eutrophication of lakes and rivers (Edwards, 1995).

In general, sources of organic contaminants can be related to petroleum refining, organic synthesis industries, pulp and paper milling, textile processing, agroindustries and the use of pesticides, insecticides, herbicides and fertilizers in agriculture. Also, chlorine used for waste water disinfection can form a broad range of low molecular weight, halogenated organic compounds. These chlorinated compounds, so-called chlorinated byproducts, are potentially hazardous substances.

Fifteen years ago, the U.S. Environmental Protection Agency (EPA), identified 114 chemical compounds of concern that could be found in water. These compounds were classified into nine groups:

1. Pesticides and metabolites,
2. Polychlorinated biphenyl (PCB) and related compounds,
3. Halogenated Aliphatics,
4. Ethers,
5. Monocyclic Aromatics,
6. Phenols and Cresols,
7. Phthalate Esters,

8. Polycyclic Aromatics,

9. Nitrosamines and other nitrogen containing compounds.

Given the continuous progress in new chemical processes, many more compounds have been synthesized and eventually released to the environment.

Fortunately, nature plays an important role in the decontamination of surface waters. The natural purification of surface waters is caused mainly by sunlight and natural photocatalysts, such as iron salts (Matthews, 1991) which break down organic molecules into simpler molecules and ultimately to carbon dioxide and other mineral products. However, direct solar photolysis encounters significant difficulties given the poor sunlight absorption by many substrates, since in many natural aquatic bodies, sunlight is strongly attenuated at shallow penetrations. As well, contaminants are frequently adsorbed on sediments, both in lakes and rivers, creating physicochemical barriers to the natural process (Serpone, 1994).

Given these facts, it is necessary to consider other processes to decontaminate water, other than by purely natural means. The best strategy appears to be the removal of the pollutant by destruction at the source of contamination. Thus, industrial waste waters should be treated at the effluent site of the chemical plant before they are released into the aquatic system.

Classical technologies for wastewater treatment and purification are mainly based on the transfer of contaminants from one phase to another, leaving the second phase contaminated. An example of such technologies is the use of activated carbon. This process involves adsorption of pollutants on the surface of activated carbon particles with contaminants being transferred from the liquid to the solid phase (carbon particles). Following this operation, it is necessary to dispose of the unit or to regenerate the activated carbon. Deactivated carbon particles can be regenerated by desorption of the pollutants at higher temperatures, transferring again the pollutants from one phase to another (solid to gas/liquid phase). In summary, the activated carbon process leaves the original pollutant essentially intact transferring from one phase to another with still the additional problem of having to dispose of the noxious substance.

Thus, there is an increasing need for new and effective methods for cleaning polluted air and water streams. This has resulted in a renewed interest in developing

environmentally benign methods for the detoxification and complete mineralization of a wide range of organic compounds.

In this respect, there is a group of emerging technologies for the destruction of organic water pollutants known as Advanced Oxidation Processes (AOPs). These processes can bring about a nearly complete mineralization of pollutants to yield CO_2, water and mineral acids. These technologies are based on the generation of free radicals, such as hydroxyl ($\cdot OH$), as initiators of the photochemical degradation. There are two main possible routes to achieve these ends: homogeneous and heterogeneous methods for pollutant photodegradation.

In the homogeneous process, formation of the $\cdot OH$ radicals takes place directly in the water phase (Bolton and Cater, 1994). Frequently the photocatalyst or photochemical enhancer employed is consumed in the photoreaction. A typical example of homogeneous process is the photolysis of hydrogen peroxide. A new process is the Solaqua® process of Solarchem,[1] which is based on the use of a water soluble ferrioxalate complex plus hydrogen peroxide (Bolton, 1995).

In the heterogeneous process, the formation of the $\cdot OH$ radicals takes place as a result of light excitation of a photocatalyst such as TiO_2, CdS, or ZnO (Serpone, 1986). The TiO_2, in the anatase crystalline form, is a powdered solid employed either suspended in water or immobilized onto a matrix with water contacting this matrix. TiO_2 is an innocuous material with no secondary effects and is quite active. Thus, it offers very interesting features for water decontamination: i) it is clean, inexpensive and does not require the addition of extraneous chemical substances, and ii) sunlight, with 3% in the ultraviolet wavelength range for TiO_2 excitation, can be employed. Furthermore, the bactericide activity of the TiO_2 (Zhang, 1994), may lead to solar powered water disinfection systems at remote sites. Simple designs and use of solar energy could become a viable alternative to chlorination for water disinfection.

Photoreactor systems, still in the infancy of their development, are facing different problems such as light scattering, oxygen starving, particle separation and mass transfer. There is also a lack of a general and reliable method to evaluate the performance of the

---

[1] A Canadian wastewater treatment company based in Markham, Ontario

different reactor systems. The present work addresses these problems by introducing a novel photoreactor (PHOTO-CREC) as well as a general method for the evaluation and comparison of the performance of different photoreactor systems. Thus, in the context of the present thesis work the following chapters are considered:

Chapter I presents an introduction and a general literature review and scope of the thesis.

Chapter II introduces some aspects about the design of photoreactors in the context of the conceptualization of the PHOTO-CREC reactor.

Chapter III describes the experimental method of preparation, characterization and optimization of the photocatalyst used, as well as the interpretation of the phenomenon of bonding of TiO_2 particles.

Chapter IV describes the different photochemical efficiency factors reported and introduces the new Photochemical-Thermodynamic Efficiency Factor (PTEF).

Chapter V describes the experimental methodology used.

Chapter VI describes and discusses the experimental results of the physicochemical parameters of the system that were measured using the PHOTO-CREC unit in a comparative evaluation with other reactors. A kinetic model is also proposed.

Chapter VII presents the conclusions of the Thesis and suggestions.

I.2 CONVENTIONAL WASTEWATER TREATMENT PROCESSES

Sundstrom and Klei (1979) indicate that the main goals of conventional wastewater treatment processes are the reduction of biochemical oxygen demand (BOD), suspended solids, and pathogenic organisms. In addition, it is necessary to remove toxic and non-biodegradable compounds and dissolved solids. Since most contaminants are present at low or very low concentrations, the treatment processes must be able to function effectively with very dilute streams.

Conventional wastewater treatment processes are classified into primary, secondary and tertiary treatments and sludge disposal.

Primary treatment usually refers to the removal of suspended solids by settling

or floatation. Coarse solids are screened out, the average solid size is reduced, floating oils are separated and flow or concentration fluctuations are equalized through short term storage. Some chemicals may be added in the primary treatment to neutralize the stream or to improve the removal of small suspended solid particles.

Secondary treatment generally involves a biological process to remove organic matter through biochemical oxidation. The particular biological process selected depends on such factors as the quantity of wastewater, biodegradability of the waste and availability of landfill areas. Activated sludge reactors and trickling filters are the most commonly used biological processes.

Tertiary treatment or advanced wastewater treatment are designed to remove specific contaminants or to prepare water for reuse. It is in this operation where activated carbon and air stripping can be employed for the removal of organic chemicals. Also, water effluents are often treated with chlorine or ozone to destroy pathogenic organisms. It is in this tertiary step of the wastewater treatment, where advanced oxidation processes, with their many advantages and features, appear to be appropriate as a substitute for classical methods.

Sundstrom and Klei (1979) also state that currently used methods for cleaning liquid or gaseous streams involve stoichiometric addition of oxidizing reagents, usually either chlorine or ozone, to oxidatively degrade organic contaminants. These chemical treatments have limited effectiveness and accomplish incomplete purification. As well, these processes involve the comsumption of large quantities of oxidizing reagents to be consumed in the operation. Therefore, there is a significant possibility that by using AOP methods, detoxification can be achieved at lower costs.

In Canada, an increasing number of companies are manufacturing systems using these advanced methods on a demonstration and a full scale. Examples of such companies are: Trojan Technologies and Matrix Photocatalytic in London, Ontario and Solarchem Environmental Systems in Markham, Ontario.

I.3. ADVANCED OXIDATION PROCESSES

The oxidation of organic pollutants in water is an important approach toward water treatment, given that, if carried to completion, it yields the mineralization of

organics to harmless materials such as carbon dioxide, water and dilute inorganic salts. As it is well known that the direct oxidation (without a photocatalyst or photoenhancer) of organic compounds with oxygen takes place, in most cases, at too low rate to be of practical interest.

As stated before, a possible approach to oxidizing organics in wastewater treatment is to use chemical reagents with a high oxidizing potential. Usually, the addition of highly oxidizing chemicals is expensive and requires large quantities of oxidizing reagents. As well, this approach may yield a waste solution that might result in a new waste treatment problem with significant levels of reduced products of oxidizing agents.

Carey (1990) states that the water treatment processes which have the most potential are the following: a) processes involving addition of energy to initiate oxidations, b) processes considering addition of non-polluting oxidizing agents such as hydrogen peroxide and ozone, c) processes that achieve in situ generation of reactive species, primarily the hydroxyl radical.

Table I.1 shows a list of different oxidizing reagents and their thermodynamic standard reduction potentials. As shown, the most highly oxidizing species is the hydroxyl radical. Based on this fact, it can be argued that AOPs which are based on the formation of hydroxyl radicals to initiate oxidations are promising methods for wastewater treatment.

Table I.1

TYPE OF OXIDANT AGENT AND THE REDUCTION POTENTIAL

OXIDIZING AGENT	STANDARD REDUCTION POTENTIAL, E° (V)
Hydroxyl Radical	2.80
Ozone	2.07
Hydrogen Peroxide	1.77
Permanganate Ion	1.67
Chlorine Dioxide	1.50
Chlorine	1.36

In a recent publication, Bolton and Cater (1994) consider that there are four major AOP techniques under development: a) homogeneous photolysis (UV/Ozone, and UV/H_2O_2), b) dark homogeneous oxidation (Fenton reaction, ozone at high pH and ozone/hydrogen peroxide), c) heterogeneous photolysis (UV/TiO_2) and d) radiolysis (high energy radiation).

Concerning the homogeneous photolysis, the combined use of UV/ozone or UV/H_2O_2 stimulates the oxidation of organic pollutants in the water. This oxidative degradation occurs at least partially through the photochemical generation of highly reactive radicals such as the hydroxyl (•OH) radical. Light absorption by a photocatalyst is, of course, needed to initiate the reaction.

There is also the possible use of a dark homogeneous oxidation with no UV light irradiation required. These processes, such as the Fenton reaction, ozone at high pH and ozone/hydrogen peroxide, are alternative methods to generate •OH radicals.

In heterogeneous photocatalysis (UV/TiO_2) •OH radicals are also generated. In this method, a dispersion or immobilized solid particles of TiO_2 absorb light in the near UV to generate chemical oxidants in situ using dissolved oxygen or water. Given that there is no special reagent requirement, other than an adequate supply of water and oxygen, heterogeneous photocatalysis is a particularly attractive method for the environmental detoxification of polluted waters.

Finally, in the case of radiolysis, a high energy electron beam is used to irradiate wastewater. Radicals such as •OH, •H and hydrated electrons are generated, which then stimulate the degradation of the water pollutant.

Recent technology developments and growing experience with the full-scale application of AOPs have brought these technologies to the stage at which, in some cases, AOPs are technically viable, reliable, and economical in many applications replacing traditional technologies such as carbon adsorption and air stripping. Depending on the case (site and specific characteristics), AOPs may offer a superior solution because of the nature of their complete pollutant destruction.

However, as with any technology, careful attention must be given during the technology selection process as to its appropriate use and application. Many factors must be evaluated and compared to other potentially applicable technologies during this

screening analysis. In general, AOPs use sources of UV light of different wavelengths to produce the ·OH radicals. Moreover, there are several AOP designs that may achieve the same goal; thus AOPs have to be compared and scrutinized in terms of energy efficiency and ability to achieve the same goal with minimum cost and with complete pollutant degradation.

The importance of the AOPs is growing and the expectations about these processes have stimulated several international meetings in Canada: The AOP Symposium in Toronto, Canada (1990), the TiO_2 Conference, London, Ontario, Canada (1993); the AOT Conference, London, Ontario, (1994) and a new larger conference (World Environmental Congress) is being planned for 1995, also in London, Ontario.

I.4 HETEROGENEOUS PHOTOCATALYSIS

I.4.1. HISTORICAL BACKGROUND

The photoactivity of the TiO_2 has been known for at least 70 years. However, interest in the photochemistry on TiO_2 was stimulated by the work of Fujishima and Honda (1972), who used TiO_2 (rutile) as photoanode, irradiated with near UV light, and a platinum cathode. These researchers carried out the photoelectrolysis of water into gaseous oxygen and hydrogen. This method was proposed as a potential route for the generation of hydrogen. The cited study, and the numerous papers that followed highlighted the importance of semiconductor photoelectrochemistry and the potential use of solar energy to produce fuels such as hydrogen.

Carey et al. (1976), from the Canada Centre for Inland Waters in Burlington, Ontario were amongst the first to recognize the potential of TiO_2 for the photocatalytic degradation of organic pollutants. These authors found that by using a light beam with a wavelength of 365 nm it was possible to achieve complete mineralization of chloro-organic molecules.

During the early 1980s, Ollis and coworkers (Pruden and Ollis, 1980) demonstrated that in the presence of near-UV and TiO_2, common chlorinated aliphatic hydrocarbons in water were completely mineralized. As a follow-up to this research, a series of contributions by Pelizzetti and Serpone (1985) and Matthews (1988a) showed that under near-UV irradiation TiO_2 can degrade a wide range of compounds, such as

phenols, cathecol, naphthol, chlorophenols, fluorophenols, pesticides, PCBs, benzene, benzoic acid, and salicylic acid. Using these experiments, mineralization rates and product formation rates (Cl^-,CO_2) were assessed. As well, various kinetic models were proposed. Moreover, Matthews (1989) showed that under similar conditions, not only are chlorinated aliphatic compounds converted to carbon dioxide, but also a whole range of contaminants, including some aromatic compounds that are normally very resistant to oxidation. On this basis, it became clear that near-UV illuminated TiO_2 provides a powerful wet oxidation method of general applicability.

Another very interesting area of research concerns the use of sunlight as a light source for TiO_2 irradiation. It was shown by Ahmed and Ollis (1984) that the reaction could be solar powered. This finding introduced a significant additional incentive for implementation of the photocatalysis process, given the free energy cost of using solar photons.

Regarding the specific kinetics for photocatalytic conversion on TiO_2, Serpone and Al-Ekabi (1988) suggested a Langmuir-Hinselwood type mechanism, which implies the existence of strong reactant adsorption on the TiO_2 surface.

TiO_2 and ZnO were proposed as potential photocatalysts (Barbeni et al. 1985). It was apparent, however, that TiO_2 in the anatase crystalline form represented the catalyst with potentially higher prospects. In fact, under the proper reaction conditions, illuminated TiO_2 or supported TiO_2 can bring about complete mineralization for a significant range of pollutants (Ollis, 1983). While the areas of TiO_2 photocatalytic activity and the basic kinetics are, as stated above, already established, photocatalyst development is still evolving. For example, Bockelmann et al. (1993) considered the use of TiO_2 doped with Fe.

There have also been significant research efforts concerning the fundamental aspects of photocatalysis. Typical examples are the contributions of Valladares and Bolton (1993) and Sun and Bolton, (1995) who consider various aspects of quantum yields for assessing photocatalytic efficiency.

Moreover, there have also been valuable contributions to clarify photocatalytic reaction mechanisms. To this end, reaction intermediates were studied in detail by Glaze et al. (1993) and by Pelizzetti and Serpone (1993) providing the establishment of

potential reaction pathways. Given important financial incentives and possible applications in remote areas, the use of solar energy is now actively investigated. In this respect Blanco and Malato (1993) and Turchi et al. (1993) represent valuable contributions. Thus, extensive research and new advancements can be expected in this crucial area of photocatalysis application.

Furthermore, the fascinating chemistry of TiO_2 has stimulated researchers around the world to explore other decontamination applications. For instance, Ollis (1993) and Weedon (1994) have recently proposed TiO_2 as a photocatalyst for the photoconversion of gas phase pollutants, such as trichloroethylene and other organic chemicals.

While some of the physicochemical principles of the photocatalytic conversion process are relatively well understood, the reactor design and reactor engineering of the photocatalytic units still require major attention. In this respect, Yue (1985 a) was among the first to stress the importance of the comprehensive design of the photocatalytic units. It is in this particular area where the present study seeks to [illegible]vate with a novel comprehensive photocatalytic design. This design is well supported in various kinetic principles and transport phenomena considerations which add particular value to the proposed unit.

As reported in recently reviews by Bahnemann et al. (1994), Serpone (1994), Matthews (1993) and Fox and Dulay (1993), photocatalysis is an area of technical and scientific opportunity. In fact, there are increasing concerns about water contamination and as a result a pressing need for viable solutions for the purification of drinking waters. All this provides important incentives for advanced photocatalytic units, such as the one considered in the present thesis work.

I.4.2 MECHANISM OF THE PHOTOCATALYTIC PROCESS

The basic mechanism of heterogeneous photocatalysis is related to the "excitation" of TiO_2 or other metal oxide in suspension or immobilized on a transparent matrix under irradiation from either natural sunlight or artificial low energy UV light. It is now generally agreed that this "excitation" promotes an electron from a level in the valence band of the solid to a highly delocalized level in the conduction band, creating a localized oxidizing site (a "hole") and a reducing site (an "electron") Serpone (1994).

$$TiO_2 + h\nu \text{ --------> } h^+ + e^- \quad (1)$$

This photogenerated electron-hole-pair can then be captured by reagents that are adsorbed on the photocatalyst surface. For example, the hole can be filled by electron transfer, either from an adsorbed pollutant molecule or from an adsorbed water molecule. In the later case, a hydroxyl radical is formed. Alternatively, the photogenerated electron can be captured by oxygen adsorbed onto the particle surface forming a superoxide radical anion, hydroperoxide radical, hydrogen peroxide and finally a hydroxyl radical.

$$h^+ + OH^- \rightarrow \cdot OH \quad (2)$$

$$e^- + O_2 \rightarrow \cdot O_2^- \quad (3a)$$

$$\cdot O_2^- + H^+ \rightarrow \cdot O_2H \quad (3b)$$

$$H^+ + \cdot O_2^- + \cdot O_2H \rightarrow H_2O_2 + O_2 \quad (3c)$$

$$H_2O_2 + h\nu \rightarrow 2 \cdot OH \quad (3d)$$

Subsequent chemical reactions by any of these species lead to the oxidative degradation of the organic pollutant and finally to mineralization. A general stoichiometric expression for the mineralization of a chlorinated organic pollutant is the following:

$$C_nH_mO_zCl_y + x\ O_2 \rightarrow n\ CO_2 + y\ HCl + w\ H_2O \quad (4)$$

where $w = (m-y)/2$ and $x = n + (m - y)/4 - z/2$

Fox and Dulay (1993) indicated that mechanistic work on heterogeneous photocatalysis, conducted for a suspension of TiO_2 in a non aqueous solvent, has clearly shown that photoexcitation of the solid photocatalyst results in interfacial electron transfer, producing surface-bound intermediates which undergo a sequence of secondary chemical reactions. Furthermore, most organic compounds can be oxidized directly by direct bandgap photoexcitation of these particles. While information exists concerning the relative reactivity in oxygenation steps and oxidative cleavage to predict the course of photocatalytic reactions, there are major uncertainties for the prediction of quantum

efficiencies.

It has to be stressed that, both in aqueous and non-aqueous suspensions, the key issue governing the efficiency of photocatalytic oxidative degradation is the minimization of electron-hole recombination by maximizing the rate of interfacial electron transfer to capture the photogenerated electron and/or hole. In turn, Fox and Dulay (1993) state that these rates are significantly influenced by the densities of Lewis acid and base sites on the surface of the photocatalyst, the state of hydration of active $^{\cdot}OH$ groups on the surface and the hydrophobic-hydrophilic character of the surface. These variables, in turn, are influenced by reaction conditions and the method used in the preparation of the photocatalyst.

It is important to mention that conduction band electrons have also been considered in the mechanism of photocatalytic reductions of precious and/or toxic metals such as Au, $P^{\cdot}$ Ag, Rh, Hg, Pb and in the photoconversion of CN^{-} and H_2S in less toxic materials (Serpone et al., 1991).

I.4.3 PHOTOCATALYTIC REACTORS

As stated above, the design of photocatalytic reactors is an area that still offers major challenges, particularly in the context of scaled reactors operated with high energy utilization.

It is apparent that selection of the proper illumination for a given geometrical configuration, adequate flow and mixing characteristics inside the reactor and the interaction with photocatalyst are essential subjects to consider in optimizing the operation of these units. The importance of these topics, as reported by Yue (1985a), points toward the significance of the reactor design to achieve maximum photoconversion performance.

A review of the literature demonstrates that there are various possible heterogeneous photoreactor designs. These designs may be classified as follows:

a) **Slurry Reactors:** suspended TiO_2 particles in intimate contact with the water irradiated stream (Blake et al., 1990) or slurry reactors (Ollis et al., 1984). In this option, a suspension of TiO_2 particles in vertical units or horizontal ducts

offers a number of problems which are summarized as follows:

1. Limited propagation of light in water suspensions with low-medium TiO_2 particle loading (Yue, 1985c).
2. Difficulties of TiO_2 particle recovery ($< 1\ \mu m$) (Bolton, 1990), a major issue while the objective of the waste water treatment process is to obtain drinking waters "free of extraneous suspended particles".
3. The difficulty of maintaining a sufficient concentration of molecular oxygen throughout the reactor is considered to be one of the major engineering problems (Bahnemann et al., 1993).
4. Settling of the solid in horizontal lines providing uncontrolled holdups of TiO_2 in the reactor.

Because of the above described facts, slurry reactors still have major problems for commercial implementation and scale-up.

b) **Spiral and Falling Film Reactors:** TiO_2 immobilized on surfaces (interface) contacting partially (at the interface) an irradiated water stream or falling film.

The use of immobilized TiO_2 attached to transparent and irradiated surfaces (interfaces) contacting only partially (at the interface) a water stream such as in case of the spiral photoreactor (Matthews 1989) or in the falling film reactor (Bahnemann, 1993), may offer disadvantages in terms of ineffective access of all water fluid elements to the irradiated TiO_2 particles. Application of this technique is limited to small scale apparatus, where the wall area (holding the TiO_2) per unit volume is still reasonable. However, commercial scale units, where the wall area per unit volume is much lower, may find this method severely inadequate.

c) **Glass Mesh Enwrapped Reactor:** TiO_2 entrapped in a glass mesh (Nulite's type reactor) (Al Ekabi and Amiri, 1990).

Finally, the third of the three alternatives considered, TiO_2 embedded in a glass mesh, is the one which was considered to offer the greatest potential and was consequently selected for the present study. It was judged that a photocatalytic reactor

with immobilized titanium dioxide supported on a glass mesh matrix was the most attractive approach for an efficient mineralization of organic pollutants. Good propagation of light in the media with no difficulties with TiO_2 particle recovery from drinking waters are considered to be the most relevant advantages.

However, the implementation of a photocatalytic reactor at the commercial scale with immobilized TiO_2 on glass mesh has many relevant issues still to be solved:

a. Manufacture of glass mesh with high TiO_2 loadings to facilitate maximum utilization of the light source,
b. Manufacture of glass mesh holding TiO_2 particles strongly attached to the glass fibers with minimum structural changes of the anatase photocatalyst,
c. Design of a unit with an adequate water flow distribution allowing for intimate contact between the polluted water and the TiO_2 particles,
d. Design of a unit with adequate and maximum utilization of the light source input provided.

Efforts in the context of the present study were directed toward overcoming these problems and developing a new design. Thus, the major outcome of this research was the development of a novel heterogeneous photoreactor that can carry out photodegradation of chemical pollutants efficiently and can be used easily, either to clean waste waters or drinking waters by destroying dangerous chemicals.

I.4.4 POTENTIAL APPLICATIONS OF ARTIFICIAL AND SOLAP PHOTOCATALYSIS

One of the most attractive features of photocatalytic oxidation is that this technique can be applied using either sunlight or artificial low energy UV light. Some of the potential applications, as pointed out by Matthews (1993), are as follows:

1. Decontamination of wastewaters.
2. Decontamination of groundwater.
3. Preparation of ultrapure water.
4. Purification of domestic water.

5. Purification of the water supplies of cities.

The use of sunlight is now being tested at the pilot plant level in several installations around the world, such as the Plataforma Solar in Almeria (PSA), Spain, the National Re: ewable Energy Laboratory in Golden, Colorado, USA and Sandia National Laboratories in New Mexico, USA. Concentrated sunlight from solar collectors is directed toward a TiO_2 slurry suspension flowing in horizontal pipes. The system has been tested for a wide number of industrial and ground water pollutants (Blanco and Malato, 1993; Turchi et al., 1993)

This method faces, however, significant limitations. First, it is difficult to secure good light transmission and adequate irradiation of a suspension in a milky media, where the TiO_2 loading cannot be controlled accurately. As well, adequate TiO_2 suspensions in horizontal pipes may produce solid sedimentation. Secondly, at the end of the treatment, fine TiO_2 particles (0.1-0.5 μm) have to be separated from the water. Drinking waters that cannot be freed of fine TiO_2 suspended solids will face major resistance from the public. All this involves additional expense in a continuous treatment process, where the final product should be clear drinking water.

Most of these problems can, nevertheless, be avoided if the TiO_2 can be strongly attached to a stationary support illuminated with sunlight and water circulated in contact with the immobilized catalyst bed. In this type of system, there are various ways and methods to immobilize the TiO_2 photocatalyst. One of them considers TiO_2 held on the reactor walls while a falling water film circulates through the photoreactor. The disadvantage of this system is that it provides only partial contact between the phases involved (water-light-TiO_2), contacting at the interface and consequently should yield low efficiencies of photoconversion. For this reason this system could only be adopted for small scale units.

While solar energy may become an energy source of choice, particularly in countries with abundant solar light, electrically powered photoreactors are still a potential option. For example, the use of multilamp systems for the decontamination of industrial wastewaters and groundwater have started to be commercialized by companies such as Matrix Photocatalytic Inc. Given that these systems employ a costly energy source, the energy efficiency indexes become a major consideration and determining factor for large

industrial scale adoption and implementation.

I.4.5 ADVANTAGES AND LIMITATIONS OF TiO_2 PHOTOCATALYSIS

The advantages of photocatalytic oxidation over conventional or other photochemical methods can be outlined as follows:

a. There is no consumption of expensive oxidizing chemicals. In conventional oxidizing processes, costly oxidizing chemicals such as $KMnO_4$, H_2O_2, O_3 are employed. In the case of heterogeneous photocatalysis, there is no need for special oxidants, given that oxygen from air is used.

b. TiO_2 is a common chemical, non-toxic and insoluble in water.

c. The light required to activate the TiO_2 is long wave UV and is transmitted well by glass. To carry out the process, even a low power tube (e.g., 15 W in this study) is enough to degrade organic pollutants.

d. The photocatalytic reaction may be driven by the natural UV component of sunlight.

e. The oxidation is powerful and indiscriminate leading, with the exception of only few pollutants (carbon tetrachloride, atrazine), to complete mineralization.

Another recently reported difficulty with the TiO_2 photocatalytic route is the intrinsic limitation of the process given the low quantum yield (~5%) as reported by Valladares and Bolton (1993), Sun and Bolton (1995). This low quantum yield and its effect on water decontamination costs, particularly when using artificial light, highlights the importance of the overall energy efficiencies of different designs, whether they are homogeneous or heterogeneous reactors.

Thus, in order to succeed with this technology, there are still a number of important issues to be clarified. An outstanding one is the design of the photocatalytic reactor with a maximum energy efficiency, which will secure optimum performance. Also of critical importance is the ability to understand how high energy efficiencies may be achieved and how they are influenced by various chemical species to be photoconverted.

I.5 SCOPE OF THE THESIS AND OBJECTIVES

The review presented in the previous sections demonstrates that there is significant need for more efficient photocatalytic reactor systems. It is particularly relevant to mention that this need applies to photocatalytic reactors that can show high energy photoconversion efficiencies, within the inherent limitations of the catalyst and may be easily scalable. The successful development of such a photoreactor could make photocatalytic technology more economical and viable.

Based on these facts the following objectives for this research were proposed as follows:

I. To develop at the conceptual level and to build a novel design for a photocatalytic reactor involving supported TiO_2 on a glass mesh with specific features: controlled fluid dynamics conditions, optimum TiO_2 loading on the mesh and reactor illumination.

II. To study the following physicochemical characteristics of the designed system: adsorption, kinetics, quantum yield and mass transfer in connection with the degradation of a model pollutant in the designed photocatalytic reactor.

III. To test the new design, develop kinetic modelling with the model pollutant to confirm the characteristics of the proposed design and to establish a photochemical thermodynamic efficiency factor which may provide some insights of the photocatalytic reaction.

IV. To compare, using the energy efficiency factor, the performance of this reactor with other photocatalytic reactor designs.

V. To operate the prototype unit under conditions such that the results of this research will provide a good basis for future photocatalytic reactor development.

CHAPTER II

PHOTOCATALYTIC REACTOR DESIGN

II.1. INTRODUCTION

The design of heterogeneous photocatalytic reactors has received increasing attention. While photocatalytic processes have already been demonstrated at the laboratory scale, there is a general consensus that the systems available, both at the commercial or demonstration scale, are facing inherent limitations concerning overall efficiencies due to poor illumination, quantum yield or mass transfer problems. While problem of low quantum yield cannot be addressed in reactor design, the other two factors can be improved in a good design.

Thus, there is a need for new and scalable designs, mainly for the photocatalytic destruction of water contaminants in industrial wastewaters and in the treatment of drinking waters. These systems could be employed for the treatment of waters contaminated with organic pollutants, as well as for the removal of heavy metals from wastewater streams.

While the photocatalyst with the best prospects is titanium dioxide (TiO_2) in the anatase form, other types of photocatalysts (e.g., TiO_2/Fe) or different ways in which the TiO_2 contacts the water stream (e.g., immobilized, slurry) could eventually be considered for future designs.

In heterogeneous systems [liquid (water)-solid (TiO_2) or liquid (water)-gas(air)-solid (TiO_2)] phases can coexist in the photoreactor. Given that the oxygenation of the system can be carried out separately (e.g., in the water reservoir), the challenge appears to be in how to optimize the contact between the water-solid phases (pollutant, photocatalyst), while keeping maximum light energy source utilization. It is important as well to have fundamental criteria for comparising of different reactor designs, taking into account the different key parameters, such as reactor volume, initial concentration of pollutant, power of the lamp and rate of reaction.

In this chapter, the characteristics of a newly designed "PHOTO-CREC" reactor, relevant to the above mentioned matters, are reviewed. This novel design optimizes

crucial factors for maximum efficiency, such as mass transfer and photocatalyst loading.

II.2. NEW PHOTOREACTOR: PHOTO-CREC I

There are a number of factors to be considered in the design of a heterogeneous photoreactor. The importance of these factors, and the means by which they were considered in the design for the PHOTO-CREC reactor concept, are reviewed in the following sections. Figure II.1, shows a diagram of PHOTO-CREC I reactor.

II.2.1. LIGHT SOURCE

The performance of a photoreactor is directly affected by the irradiation source. The type of light source to be chosen should be determined by the photodegradation method to be used. The choice should be made considering lamp specifications, energy and intensity requirements. In the case of using TiO_2 as a photocatalyst, it is necessary to use light sources with a wavelength output in the range 320 to 380 nm (near UV range).

On the other hand, if solar light is the selected energy source and TiO_2 the chosen photocatalyst, it is important to consider that the fraction of sunlight, which is able to excite the TiO_2, represents only about 3% of the total solar irradiation. Moreover, concentrated sunlight sources, instead of direct unconcentrated irradiation have also been adopted.

In the PHOTO-CREC I reactor, a 15 W blacklight blue lamp (BLB), with a peak intensity at 365 nm, was used. This lamp provides the TiO_2 bandgap energy required to produce electrons and holes, which are necessary to produce the $\cdot OH$ radicals and initiate the photodegradation of the water pollutants.

The effect of light intensity is also another important consideration that has to be carefully considered, given the known dependence of the photodegradation rate on light irradiation and the economical factors involved. While at high light intensities photoconversion rates are proportional to a fraction%' 0 ^^r of the irradiance, at moderate intensities these rates are directly proportional (Ollis, 1990). Thus, it is usually convenient to design a high perfomance unit with a lamp of low to moderate intensity, such that the photoreactor operates in the region where the rates of photoconversion are directly proportional to the light irradiance. This significant design criterion was adopted

Figure II.1 Diagram showing the cross section of PHOTO-CREC I reactor with details of one basket and of the flanges used for fixing the basket in the desired position.

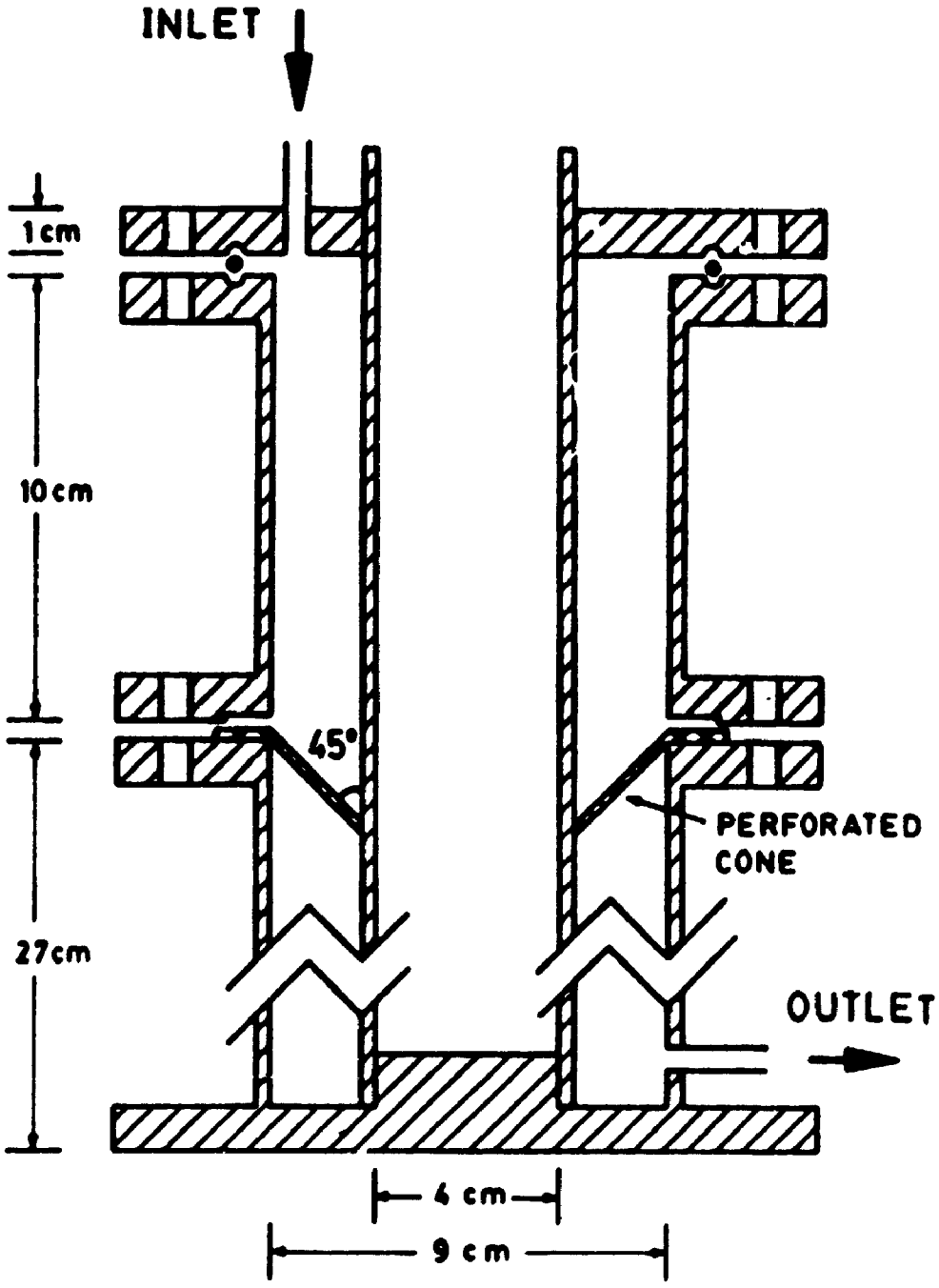
INLET
1cm
10cm
27cm
45°
PERFORATED
CONE
OUTLET
4 cm
9 cm

in the selection of the lamp source for the PHOTO-CREC prototype.

II.2.2. PHOTOREACTOR GEOMETRY

Regarding the photoreactor geometry, the spatial relation between reactor and light source is of paramount importance. Usually in electrically powered photoreactors, the light source is mounted within a glass tube connected to the fixture to give a certain pattern of irradiation. The geometrical configuration of the reactor is usually chosen so as to get the maximum benefit from the pattern of irradiation. This means that the photocatalyst has to be placed at strategic locations in the system, with optimum orientation, to ensure that essentially all the photocatalyst is in the view angle of the source, or in other words the emitted light is "seen" by the photocatalyst.

In the case of the PHOTO-CREC I design, an annular geometry was chosen. With this configuration, the lamp was placed inside a central tube, while the immobilized photocatalyst was located in the annular channel between the inner and outer tubes. This type of configuration was chosen to provide an effective illumination of the mesh and containment of the emitted light inside the photoreactor.

Regarding the PHOTO-CREC reactor, it was designed in such a way that at least 50% of "skin" fiber glass mesh, holding the immobilized TiO_2, was directly exposed to the light source irradiation. The other 50% of the "skin" fiber glass area (back of the mesh) and the internal mesh fibers was also exposed directly to the light source (given the high transmitance of the light through the mesh) and to the internal reflection and scattering of the light. Thus, this design assured that a high degree of the mesh area containing the immobilized TiO_2 was irradiated and could eventually be excited for the generation of $\cdot OH$ radicals.

II.2.3. MATERIALS OF CONSTRUCTION

Once a given photoreactor configuration is chosen, it is necessary to provide for adequate materials of construction. For example, in some selected parts of the unit the only material requirements are to have a good heat transfer, good thermal behaviour for temperatures in the 20-50 °C range, good resistance from low to moderate pressures (130-300 kPa) and good resistance to corrosion (pH > 3). However, in other sections

of the photoreactor, materials requirements are more specific and stringent. In addition, some materials having the above mentioned properties also require good light transmission. Regarding materials with specific optical properties, various glasses could be selected: optical glass, pyrex glass, vycor glass and quartz. Quartz usually gives the best light transmission, but with a higher material cost.

In the case of using titanium dioxide as a catalyst, transmission in the 320 to 380 nm wavelength range is required. Under these conditions, pyrex glass provides 80% transmission and can be considered as adequate. Pyrex glass was selected for the central tube of the annular configuration of PHOTO-CREC II.

II.2.4. HEAT TRANSFER

Efficient means of heat removal often must be introduced in a photoreactor design to keep the temperature close to the desired ambient temperature. This problem may be even more acute in homogeneous systems requiring higher intensity lamps.

In the case of PHOTO-CREC I, the concept adopted was to power the unit with a low intensity lamp. Given the high energy efficiencies expected, it was anticipated that temperature fluctuations would be no more than a few degrees. As will be described later, once the unit was operated it was found that maximum deviations were about $\pm$ 5°C, and consequently it was confirmed that special heat transfer devices (e.g., cooling coils, heat exchanger) were not needed in the case of the PHOTO-CREC I design.

II.2.5. MODE OF OPERATION

The mode of operation (batch, semibatch or continuous) is a relevant matter to decide for a new design. In general, in the case of photoreactors at the laboratory scale, it is convenient to use recirculating batch reactors. Low photoconversion rates may yield, in the exploratory phases of a particular design, partially converted pollutants that cannot be easily disposed.

Moreover, considering state-of-the-art photocatalytic technology, operation of single pass reactors in the field for decontamination of relatively large flow of water appears still to be too cumbersome. It requires large reactors, as in the case of the flow

through solar reactor used at NREL in Colorado, or several dozens of reactors in series as in the case of the unit designed by the Matrix Photocatalytic Company. Thus, there is a significant challenge to develop a simple unit operating in a single pass mode. This unit should be viable in the context of its high efficiencies resulting from the optimized selection of various design parameters.

PHOTO-CREC I was operated in the CREC laboratories in the batch mode given various safety considerations. However, this unit was conceptualized with the general view of being scalable and transformable in a single pass system suitable for processing large volumes of water with good photoconversion efficiency.

II.2.6. MIXING, PHASE CONTACTING AND FLOW CHARACTERISTICS.

Mixing, phase contact and flow patterns are critical matters in any heterogeneous photoreactor design to secure adequate interaction among pollutants, photons and photocatalyst.

Phase contacting depends on mixing and flow patterns within the photoreactor. Phase contact efficiency results in differences in rates of photoconversion and efficiency of light energy utilization. These crucial matters, characteristic of each specific design, create an incentive for new photoreactor designs, where various contacting factors are optimized.

While the problem is certainly complex and should be evaluated in the context of the type of reactor geometry adopted, the design should be such as to ensure intimate contact of the water stream with the TiO_2 particles under conditions of high photocatalyast irradiation. High and uniform water flow through the mesh, with proper positioning (orientation) of the mesh-light source, should lead to optimum operation. With this approach, mass transfer limitations can be circumvented.

The PHOTO-CREC I photoreactor (Fig. II.1) was envisioned considering the various critical contacting phenomena described above. PHOTO-CREC was thus conceived with the expectation of providing a high rate of photoconversion with high photoconversion efficiencies.

In the PHOTO-CREC I system, the principal components to achieve these goals were a series of so-called "baskets". These baskets, to be described in detail in the

following sections of this thesis, hold the glass mesh with the immobilized TiO_2. To yield the optimal operation conditions, preventing possible movement of the glass mesh inside the reactor, water downflow circulation was selected. This direction of the water flow, downflow instead upflow, secured minimum displacement of the mesh, even for large variations of the water flow rate.

II.2.7. OXYGEN SUPPLY

Concerning oxygen supply some calculations, based on the overall reaction stoichiometry for the model compound (methylene blue) were conducted as follows:

$$C_{16}H_{18}N_3SCl + 25.5\ O_2 \rightarrow 16\ CO_2 + 6\ H_2O + HCl + H_2SO_4 + 3\ HNO_3$$

where $C_{16}H_{18}N_3SCl$ = methylene blue= MeB.

Thus, for 12 μM of methylene blue, about 276 μM of oxygen will be required.

Then, under conditions close to oxygen saturation, as assessed using a Hysim computer package (an advanced program for process simulation) (Hypotec Ltd., 1993) about 300 μM of oxygen are dissolved in the 2.2 L of water at 15° C used during the experimental runs.

However, given that the PHOTO-CREC I system has a water reservoir open to the laboratory atmosphere, and given that this reservoir was subject to intense water mixing with recirculation and agitation, it is expected there was ample opportunity during all experiments for oxygen re-absorption, and consequently an adequate oxygen supply for complete photoconversion. The MeB photoconversion was in all cases above 90%. In conclusion, limitation of the oxygen supply should not have affected the experimental results of this research.

In summary, the first unit conceptualized in the context of this study named as PHOTO-CREC I, had the following characteristics and dimensions:

- Concentric Unit
- Down flow water circulation,
- Light Source: 15W , blacklight tube with a maximum output at 365 nm.
- Maximum number of baskets used: 3
- Internal unit diameter: 4.0 cm
- External unit diameter: 9.0 cm
- Height: 38.0 cm

The described unit, was manufactured in the Mechanical Shop of the University of Western Ontario and represented the first prototype of a PHOTO-CREC reactor. The experimental results using this unit are discussed in Section IV.1.

II.3. INTERNAL COMPONENTS OF THE PHOTO-CREC I REACTOR

As stated above, one essential internal component of PHOTO-CREC I reactor was the so-called "basket system". The basket system was constituted by a canister holding the glass mesh with the immobilized TiO_2. In order to secure a good and controlled contact of water circulating through the glass mesh, the TiO_2 impregnated mesh was held in canisters of a funnel shape, made out of perforated stainless steel metal screens, with 41% open area, with about 25 holes of 3 mm diameter. The inclination of the stainless steel screens was carefully selected to be at a 45 degree angle. Thus, this design assured that a high degree of the total mesh area with immobilized TiO_2 was irradiated and could be excited for the formation of $\cdot OH$ radicals.

Another significant design consideration in PHOTO-CREC I relates to water flow patterns in the vicinity of the mesh. In order to secure uniform water distribution, enough pressure drop in the combined, mesh and basket system, has to be imposed on the circulation stream. This is a frequent criterion adopted for the same purpose in the case of liquid distributors in liquid-solid reactors and gas distributors in gas-solid reactors.

It can be shown that for typical velocities of 7.0 cm/s in the orifice plate and 15.0 cm/s in the glass mesh, a combined pressure drop can be calculated as follows:

$$\Delta p_{plate} = 0.02 \text{ kPa}$$

$$\Delta p_{mesh} = 0.04 \text{ kPa}$$

$$\Delta p_{total} = \Delta p_{mesh} + \Delta p_{plate} = 0.06 \text{ kPa}$$

The standard requirement for uniform distribution of water or uniform fluid velocity requires a minimum total pressure drop per plate in the range of 5-10% of the total hydraulic head.

Several of these baskets, all of them having very similar dimensions as the ones previously described, were employed placing them at different annular positions. The basket positions, as illustrated in Fig. II.2, were carefully selected to prevent basket overlapping causing partial illumination: all baskets and glass mesh were included in the view angle of the light source.

To prevent water leakage and to avoid preferential water circulation through the sides of the baskets, the baskets mountings were manufactured with O-ring housings in the upper and lower sections. The rubber O-rings, once installed under controlled pressure, effectively prevent water leakage through the basket sides.

Thus, the selected design of the screen plate, with a significant pressure drop and sealing with O-rings, assured controlled contact of the water flow circulation through the mesh. This design consideration was critical for good water-mesh contact and flow redirection, as needed by the 45 degree basket orientation.

To achieve maximum efficiency, a high loading of uniformly distributed and strongly bonded TiO_2 particles (Degussa, P-25) on the fiber glass was employed. TiO_2 immobilized on glass mesh, using techniques to be described in Chapter 3 of this study, reached loadings as high as 8.5% (wt). TiO_2 particles were strongly bonded ("anchored") to the fiber glass mesh while impregnating the mesh in a methanol-water solution.

II.4 THE PHOTO-CREC II REACTOR

After a first series of experiments, the PHOTO-CREC I reactor was modified in order to have a more efficient unit (see PHOTO-CREC II in Fig.II.2). In addition to an increase in the number of baskets from 3 to 15, the photoreactor was modified as follows:

1. An internal pyrex glass tube to house the UV lamp.

During the first series of experiments (1 and 3 baskets) a plexiglass tube to house the UV lamp was used. This plexiglass tube was replaced before the second series of experiments with a pyrex glass tube. This change circumvented the reduction of the light

Figure II.2 Diagram showing the PHOTO-CREC II reactor with details about the annular channel, baskets and water flow circulation.

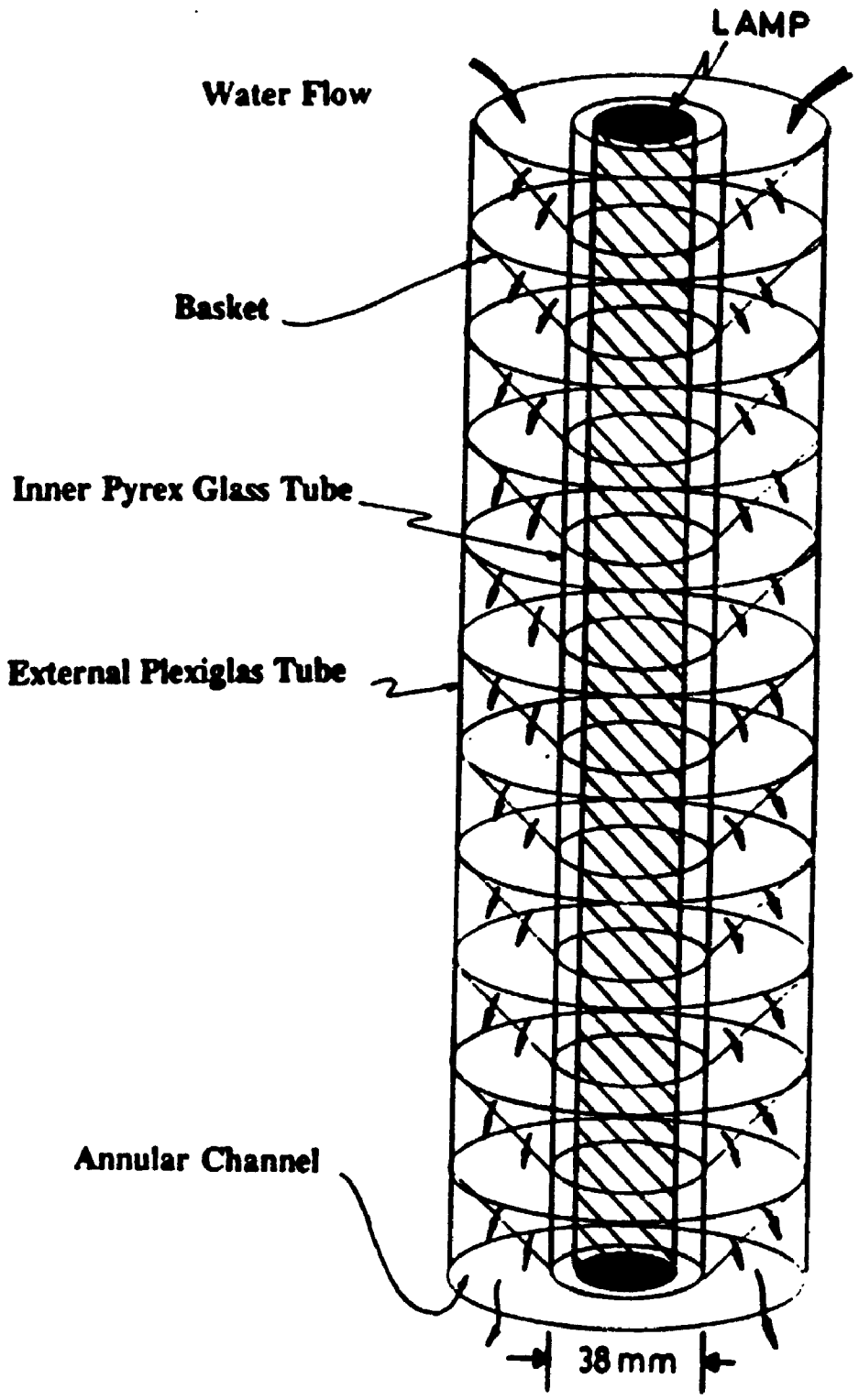
LAMP
Water Flow
Basket
Inner Pyrex Glass Tube
External Plexiglas Tube
Annular Channel
38 mm

Figure II.3 Diagram showing the top, side and bottom view of the basket. The top view of the basket shows the impregnated glass mesh while the bottom view shows the perforated plate.

TOP VIEW

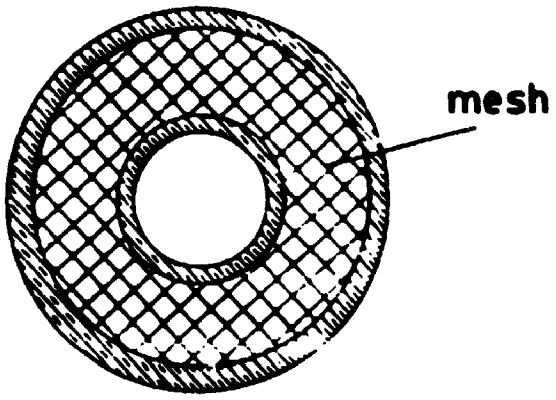

SIDE VIEW

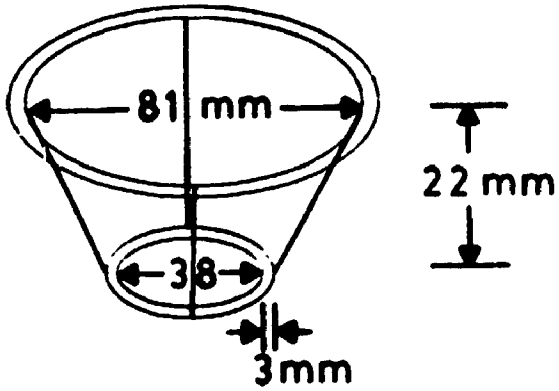

BOTTOM VIEW

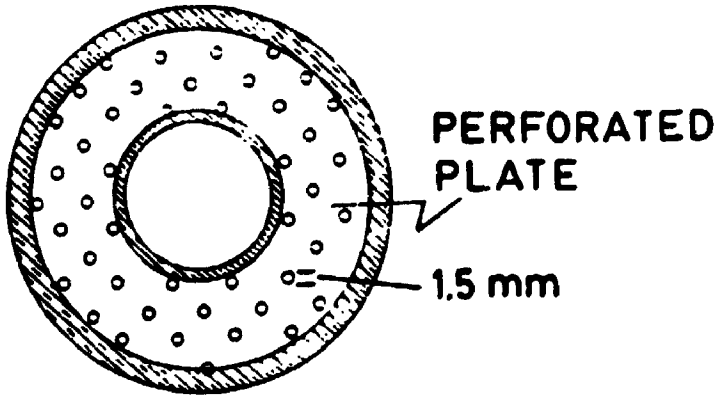

absorption in the plexiglass tube (UV lamp peaking at 365 nm). It is important to point out that the Pyrex glass, being more transparent to the UV than plexiglass, provided a higher efficiency of light utilization and consequently was beneficial for an optimized unit.

2. Three external sections made of plexiglass.

The PHOTO-CREC II (with 15 baskets) was built with a modular configuration consisting of three sections each 14 cm long. These three sections were built in such a way that they could be easily assembled and disassembled. Furthermore, this modified configuration of the photoreactor allowed easy loading of the baskets and quick replacement of the glass mesh in the photoreactor unit. Each section held 5 baskets with a total of 15 baskets in the unit. This resulted in a total photoreactor length of 42 cm. This geometry and number of baskets gave the best utilization of the concentric space of the PHOTO-CREC II unit, as well as of the light source. Furthermore, this approach of easy assembly and disassembly and modular design was, during this project, explored extensively given the potential prospects for scaling-up of the PHOTO-CREC II unit. It was hoped that once the concept of PHOTO-CREC II was confirmed, the present project could also provide strategies for constructing low cost PHOTO-CREC II units. It was expected that the capacity of these units could be changed quite easily and that these units could be maintained with minimum cost. In this sense, it can be concluded that the proposed design and the characteristics of the set up, fulfil these various requirements. In fact, the materials selected for the PHOTO-CREC II unit are quite inexpensive and the glass mesh maintenance is easy to handle, given easy access to the various baskets.

3. The unit covered externally with a stainless steel sheet cover.

Regarding the characteristics of the external tube, it was also designed to minimize losses of the light emitted. With this end in mind, the unit was covered externally with a stainless steel metal sheet. This additional feature of the set-up allowed most of the emitted light to be kept inside the reactor, reflecting back most of the light that did not originally reach the glass mesh of the basket, thus minimizing light losses and optimizing the photoconversion.

4. Basket with Spacers

Spacers were provided to the system in such a way that baskets could be slid easily bringing them into a fixed position with minimum effort, and thus accurately achieving needed source view angles and preventing basket overlapping. Different views of the basket are presented in Fig.II.3.

The PHOTO-CREC II unit with 15 baskets was used in most of the experiments (discussed in Chapter VI) carried out in this Thesis.

II.5 CONCLUSIONS

The present chapter described the contribution of this Thesis to the design and conceptualization of a new photocatalytic reactor (PHOTO-CREC II). While developing these activities, careful consideration was given to the main factors that should be involved in an optimum design: reactor geometry, materials of construction, contacting between phases, heat transfer, light source view angles, TiO_2 loading, oxygen supply and internal components. The result should be an optimized design where several factors are combined satisfactorily.

CHAPTER III

PHOTOCATALYST PREPARATION AND CHARACTERIZATION

III.1. INTRODUCTION

High efficiency operation of a photocatalytic reactor requires TiO_2 immobilization with a high and uniform distribution of TiO_2 on the matrix. It is also required that the TiO_2 be strongly bonded onto the matrix surface with the anatase crystals remaining in their original crystalline form. Thus calcination or other thermal treatments should be avoided. These considerations are of crucial importance in order to get the maximum advantage of the surface provided by the matrix as well as requirements to prevent TiO_2 particles from being washed off during operation of the photoreactor.

III.2. PREPARATION OF TiO_2 SUPPORTED ON GLASS MESH

The impregnation of a glass mesh with titanium dioxide (TiO_2-anatase) was accomplished using different TiO_2 suspensions in water-methanol mixtures. TiO_2 (P-25 from Degussa) was selected considering its high anatase content and small particle size. The anatase crystalline form of TiO_2 has been reported to be much more active than the rutile crystalline form. The glass mesh was pretreated with concentrated nitric acid to remove any type of material held on the surface. The mesh was kept in contact with the impregnating solution for six hours in a specially designed system that allowed permanent contact of the TiO_2 slurry with the glass mesh. The impregnation cell, illustrated in Fig. III.1, included a glass vessel containing the impregnating suspension (TiO_2 in a water-methanol mixture), a plexiglass cylindrical section with 4 half moons symmetrically carved into the bottom and a magnetic stirrer to provide radial and axial mixing. The glass mesh was supported on the upper surface of the cylindrical plexiglass section. This design helped considerably by forcing the TiO_2 suspension flow in an upward direction in the central zone and in a downward direction in the peripheral zone of the impregnating cell. Thus uniform and controlled particle-mesh contact was achieved with minimum TiO_2 settling in the corners of the impregnation cell.

Figure III.1 Schematic of the mesh impregnation system with details of the cylindrical ring supporting the mesh and the slurry recirculation.

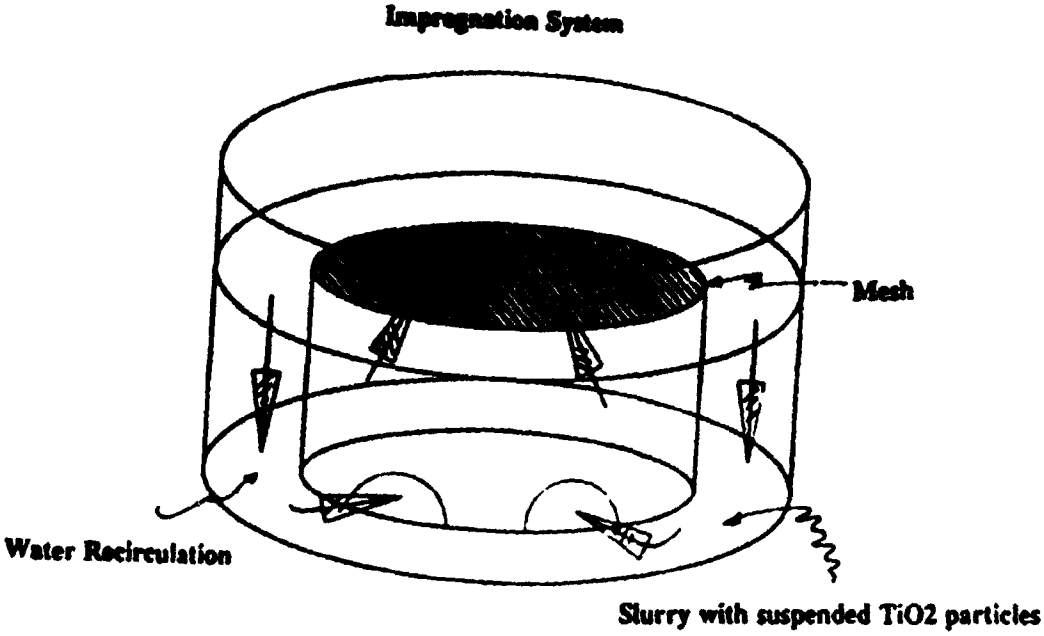
Impregnation System
Mesh
Water Recirculation
Slurry with suspended TiO2 particles

After the impregnation, the samples were washed with distilled water and dried for four hours at 110°C. The mesh samples were then analyzed using Scanning Electron Microscopy and Energy Dispersive X-Ray Microanalysis (SEM-EDX). This allowed for an analysis of the TiO_2 particle distribution (monolayer, aggregates) and the TiO_2 loading.

The impregnation tests revealed that when the glass mesh was contacted with just an aqueous dispersion of TiO_2 (Anatase, Aldrich, with an average particle size of 0.55 μm), a poor heterogeneous dispersion of small particles and large aggregates of particles was obtained. The dispersed smaller particles (< 1 μm) were strongly bonded onto the glass mesh and the large aggregates of particles (> 1 μm) were very loosely bonded and easily removed, as was demonstrated by SEM analysis. Both types of particles can be seen in the SEM micrographs shown in Fig. III.2.

However, when a dispersant such as methanol was added to the water-TiO_2 suspension, the quantity of small particles held by the glass mesh fibers sharply increased, exhibiting a very even distribution of TiO_2 particles on the surface of the glass fibers. In this case, the ratio of aggregates of particles formed was much smaller, as shown in the second set of SEM micrographs (Fig. III.3). This means that the dispersion of particles on the fiber is higher when methanol solutions are used to prepare the TiO_2 dispersion. It was also demonstrated that when dispersant fluids, such as methanol, are used during impregnation, the dispersant helps to enhance particle collection by the surface and consequently to increase the final loading of TiO_2. In these experiments, TiO_2 (anatase) particles from both Degussa and Aldrich were used and similar results were obtained.

III.3. STRENGTH OF THE TIO_2-GLASS FIBER BONDING AND THE EFFECT OF PARTICLE SIZE

An "anchoring" test using the originally designed photoreactor PHOTO-CREC I apparatus, was carried out to assess the strength of particle bonding to the mesh. Water was recirculated at different flow rates from 100 to 1000 mL/min for over 2 hours. These fluid dynamic conditions are similar to those expected in the operation of the

Figure III.2 SEM micrographs showing small (0.5 μm) and large (5-15 μm) agglomerates on the surface of the glass mesh fibers. The impregnated mesh was prepared using TiO_2 suspended in water.

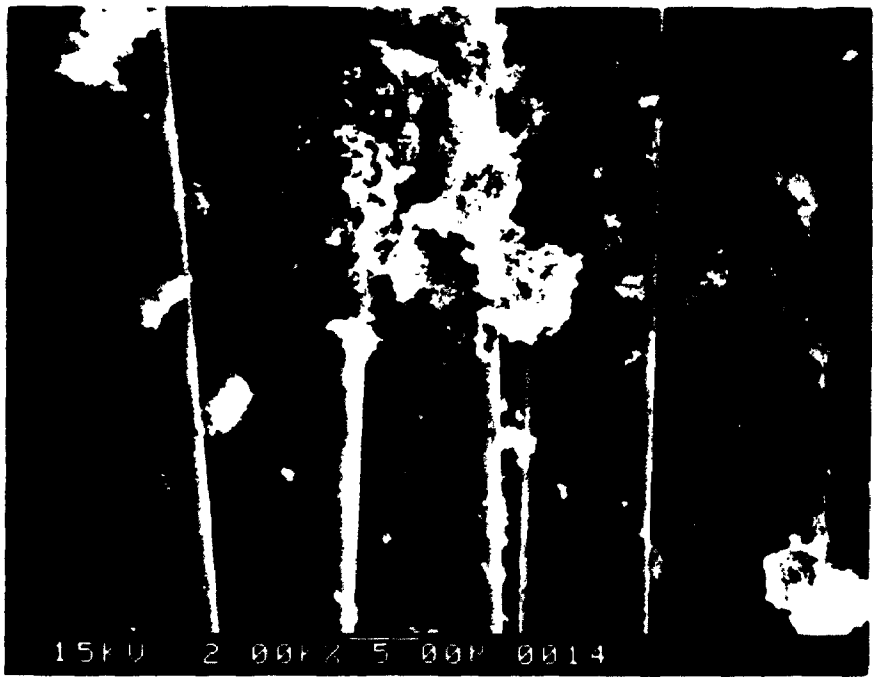
15kV 2 00kX 5 00µ 0014

PHOTO-CREC I unit.

The results obtained did not show any significant loss in the TiO_2 loading, as was demonstrated by SEM-EDX analysis. This is also illustrated by comparing micrographs Fig. III.4 with those of Fig. III.3, where it is seen that there is no significant change in the particle loading after the mesh was subjected to two hours of operation.

In addition, and in order to check the effect of TiO_2 particle size on "anchoring", Degussa P-25 (20 nm) TiO_2 particles were used for impregnation under the same conditions as those for Aldrich TiO_2 particles (500 nm) described above. It was demonstrated that similar results and similar loadings (8%) could be obtained. Thus, it appears that the TiO_2 particle size, in the 20 - 500 nm range of particle size, does not significantly influence the particle bonding to the surface.

III.4. CHARACTERIZATION OF THE GLASS MESH SUPPORTED PHOTOCATALYSTS USING (SEM-EDX)

One important characteristic of mesh preparation effectiveness relates to the TiO_2 loading. In order to examine the loading characteristics of the TiO_2 photocatalyst, analysis of the different samples prepared was carried out by using Scanning Electron Microscope-Energy Dispersive X-ray Microanalysis (SEM-EDX) of TiO_2 on different regions of the samples. A characteristic analysis of the sample is shown in Fig. III.5. The bared glass-mesh used as the support was also examined showing its composition as a Si-Ca-Al oxide matrix, with very small amounts of the oxides of Cr and Zn.

III.5. OPTIMIZATION OF THE TIO_2 LOADING ON THE GLASS MESH.

The critical factors in the preparation of the TiO_2 loaded mesh that need to be considered for an optimized TiO_2 immobilized photocatalyst are:

1. Concentration of methanol in the impregnating solution.
2. Impregnation time.
3. loading of the TiO_2 in the impregnating suspension.

Figure III.3 SEM micrograph showing small TiO_2 particles deposited on glass mesh prepared from TiO_2 suspended in a solution of 25 % (v/v) of methanol in water. (Magnification 2000 and 1000 times).

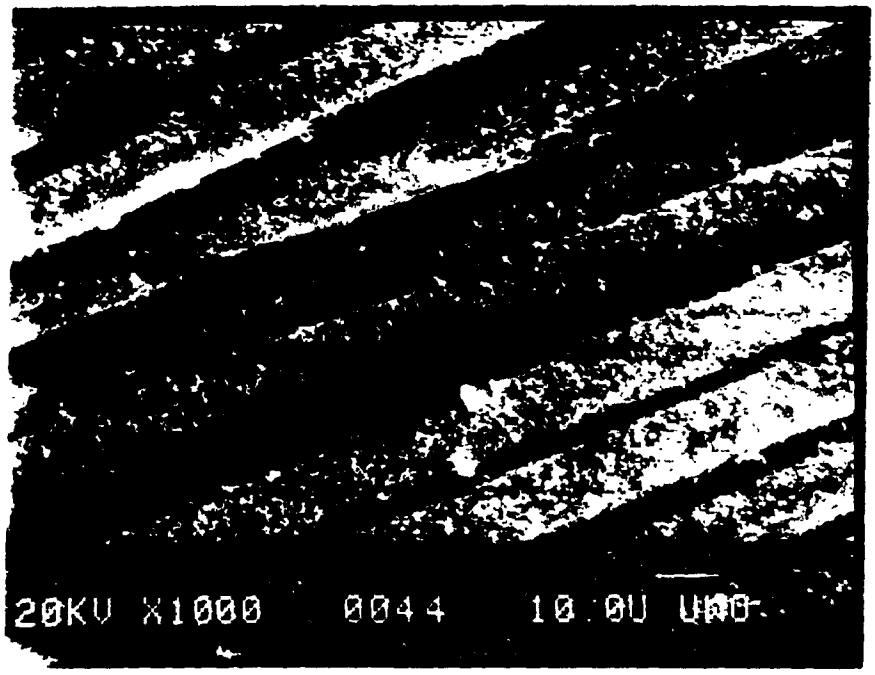
20KV X1000 0044 10.0U UWO


20KV X2000 0044 10.0U UWO

Figure III.4 SEM micrograph showing the distribution of small TiO_2 agglomerates following the completion of the test for checking the strength of bonding ("anchoring test").

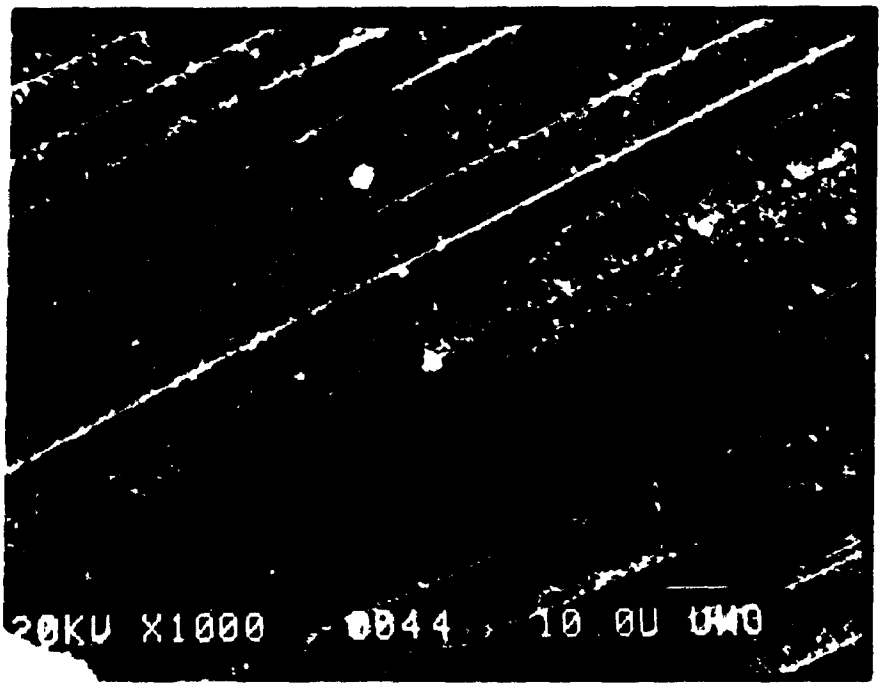
20KV X1000 0044 10 0U UWO

Figure III.5 A typical SEM-EDX analysis report of a TiO_2-glass mesh sample. The Ti peak is used to track the TiO_2 on the glass mesh.

SURFACE SCIENCE WESTERN -5 00 WED 24-JUL-91 14:01
Cursor: 0.000keV = 0 ROI (S) 0.000: 0.000

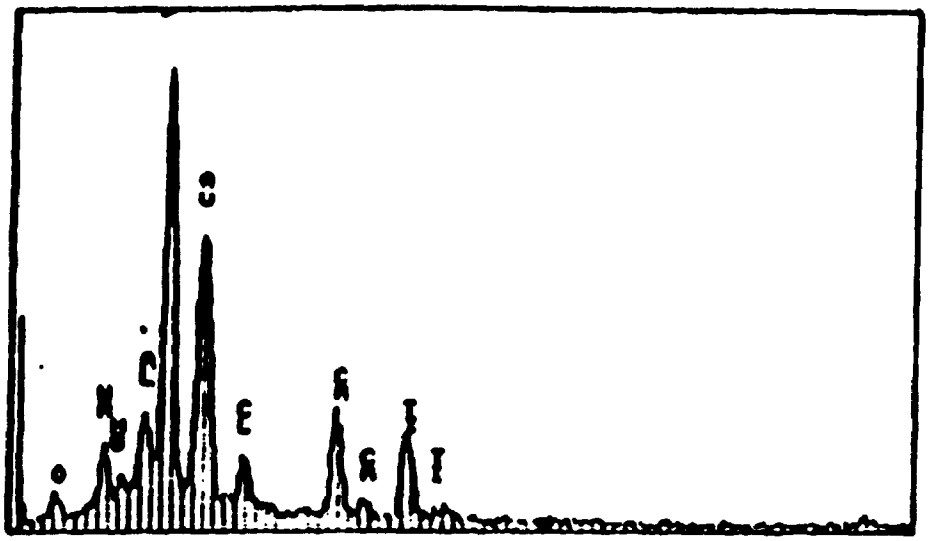

0.000 VFS = 512 10.240
00 MESH 2

SQ. QUANTIFY

MESH 2
Standardless Analysis
15.0 KV 34.4 Degrees

Chi-sqd = 1.6:

Element	Rel. K-ratio	Net Counts
Au-L	0.36457 +/- 0.07612	259 +/- 54
Au-M	0.36895 +/- 0.00731	6295 +/- 153
Al-K	0.02425 +/- 0.00464	1086 +/- 269
Si-K	0.11848 +/- 0.00424	5304 +/- 200
Ca-K	0.06477 +/- 0.00349	1969 +/- 106
Ti-K	0.04354 +/- 0.00303	1309 +/- 91
Na-K	0.03953 +/- 0.00596	614 +/- 93
Mg-K	0.00465 +/- 0.00302	105 +/- 152
Cl-K	0.01923 +/- 0.00237	730 +/- 91

ZAF Correction 15.00 KV 34.40 deg
No.of Iterations = 3

Element	K-ratio	Z	A	F	Atom%	Wt%	Formula	Compound%
Al-K	0.032	1.034	1.443	0.993	3.84	4.67	Al2O3	8.83
Si-K	0.154	1.006	1.315	0.998	16.05	20.36	SiO2	43.55
-K	0.084	1.037	1.047	0.989	5.88	9.86	CaO	12.67
Ti-K	0.083	1.139	1.038	1.000	4.52	9.70	TiO2	16.31
Na-K	0.051	1.026	1.947	0.998	9.00	10.26	Na2O	13.03
Mg-K	0.006	1.002	1.754	0.996	0.96	1.06	MgO	1.76
Cl-K	0.025	1.063	1.159	0.993	1.91	3.06	Cl	3.06
O -K	0.119	0.937	3.668	1.000	57.82	41.76 S	---	---
					Total=	100.00%	Total=	100.00%

Many experiments were carried out to optimize the photocatalyst preparation. Solutions of methanol-water from 5 to 50% containing 5.0 g/L of TiO_2 were tested and the TiO_2 impregnated on the meshes analyzed using SEM-EDX. The results are shown in Fig. III.6. The amount of TiO_2 loaded on the mesh increased when mixtures with higher proportions of methanol were used. At 25% of methanol in water, a plateau was reached, where a maximum weight loading of 8.5% weight percent of TiO_2 was achieved.

III.6. STRENGTH OF ADHESION OF TIO_2 ON THE GLASS MESH

The TiO_2 particle collection exhibits an interesting phenomenon (sizes smaller than 1 μM are held very strongly on the fiber surface). It appears that this collection effect may arise from strong electrostatic forces between the mesh surface and the TiO_2 particles. Once bonded, particles are "anchored" on the fiber surface and very difficult to remove.

III.7. CONCLUSIONS

It has been demonstrated that TiO_2 immobilization can be achieved with high (up to 8%) and uniform TiO_2 distribution on a glass mesh matrix. With the impregnation method used, involving the use of a particle dispersant (methanol-water solutions), TiO_2 is strongly bonded onto the glass mesh. The impregnated mesh, holding the TiO_2, is stable for several hours under typical water flows with no detectable washing off of TiO_2 particles. Moreover, by following the approach proposed, thermal treatments (calcination), or other methods affecting the anatase crystal structure, are completely avoided.

These findings are of importance in order to take advantage of the available mesh surface as well as requirements to capture as much light as possible from the light source into the TiO_2 particles.

Figure III.6 Weight percent of TiO_2 loading on glass mesh as a function of the concentration of methanol in methanol-water dispersant solution.

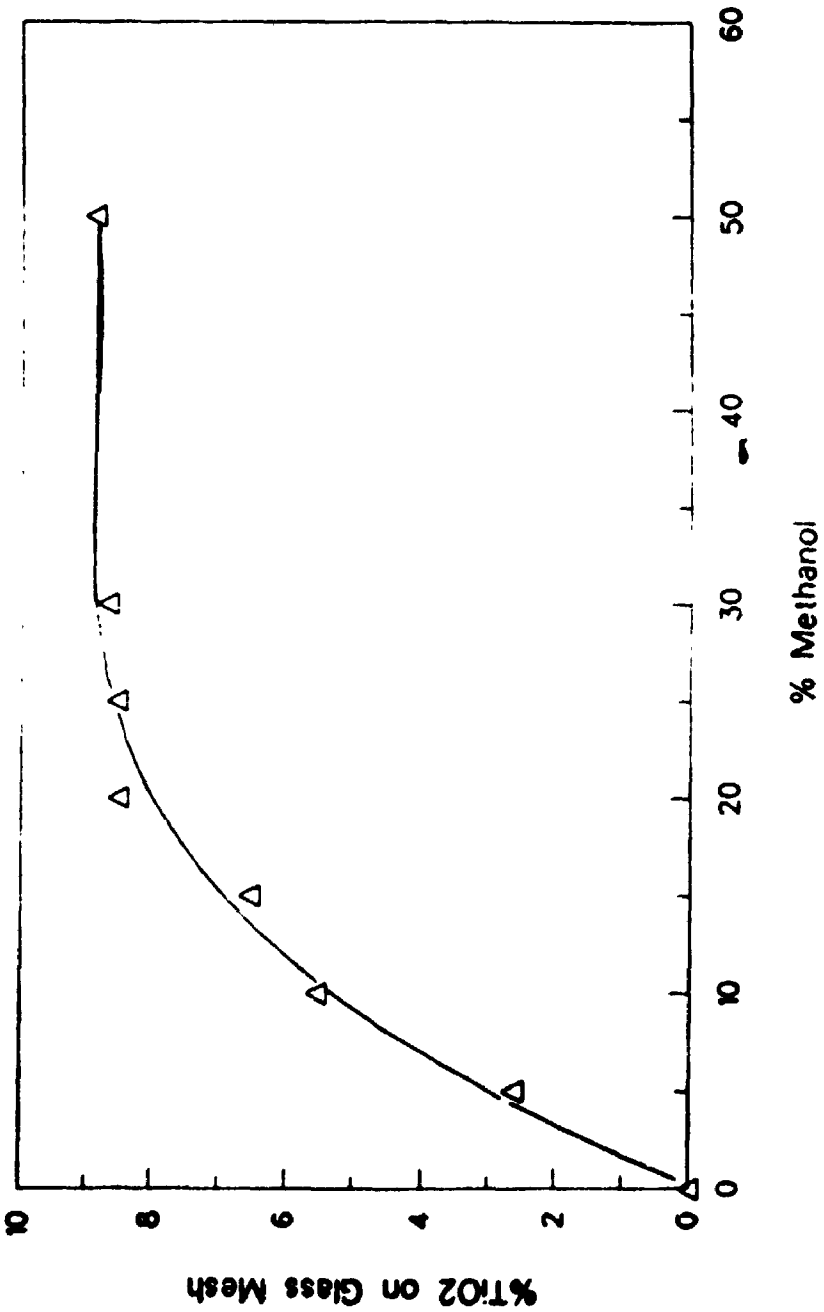
%TiO2 on Glass Mesh
0
2
4
6
8
10
0
10
20
30
40
50
60
% Methanol

CHAPTER IV

ENERGY EFFICIENCY FACTORS FOR HETEROGENEOUS PHOTOCATALYTIC REACTORS

IV.I INTRODUCTION

Given the need for criteria that can be used to compare different reactor systems, based on the efficiency of the electrical energy used to operate the unit and consequently directly related with the economics of the system, two factors have already been proposed: "The Electrical Energy per Order" (EE/O) introduced by Bolton et al.(1992) and the "Photon Efficiency" (Φ) introduced by Bockelmann et al.(1993). In this chapter these factors are discussed and a new factor "The Photochemical-Thermodynamic Efficiency Factor" is introduced.

IV.2 ELECTRICAL ENERGY PER ORDER

Bolton (1992) [see also Bolton and Cater, 1994] proposed that the energy efficiency of the photocatalytic process can be evaluated using the Electrical Energy per Order (EE/O). The EE/O contains the implicit assumption of first order kinetics and is defined as the electrical energy required to reduce the concentration of a pollutant by one order of magnitude in 1000 US gallons (3785 L) of water. Smaller values of EE/O are considered to indicate a more efficient process, because less light energy is needed. For batch operation the EE/O values are calculated from the equation:

$$EE/O = \frac{P.(t/60).3785}{V.\log[C_i/C_f]} \qquad (IV.1)$$

where P is the lamp emitted power (kW), t is the irradiation time (min), V is the total volume (L) and C_i and C_f are the initial and final pollutant concentrations (μM).

IV.3 THE PHOTON EFFICIENCY FACTOR

Bockelmann et al. (1992) suggested an alternative equation for assessing the efficiency of solar powered reactors using the following relation:

$$\Phi = (C_i - C_f)\, v / \epsilon_{abs} \qquad (IV.2)$$

where ϵ_{abs} is the absorbed molar photon flux (einstein s^{-1}), v is the volumetric flow of treated water (L s^{-1}) and C_i and C_f(μM) are the entry and exit pollutant concentrations.

While Eq (IV.2) is not constrained to any specific kinetic model, it postulates that the photocatalytic reactor can be modelled as a continuous stirred unit (CSTR). Thus, the Φ factor of Bockelmann et al. (1992) is limited to CSTRs and should be applied with caution when dealing with batch, close to plug flow or non-ideal CSTR photocatalytic units.

Moreover, concerning limitations of the above described efficiency factors, the following can also be stated:

1. The proposed efficiencies are not dimensionless as required by consistent thermodynamic definitions,
2. Problems arise when applying these relationships to model pollutants. Photocatalytic efficiencies based on the C_i/C_f ratio (e.g., the EE/O factor) or $(C_i - C_f)$ (e.g., the Φ factor) neglect the light energy used to photoconvert intermediate chemical species and consequently underestimate photocatalytic efficiency.

IV.4. THE PHOTOCHEMICAL THERMODYNAMIC EFFICIENCY FACTOR

As was mentioned in Section IV.2, valuable contributions have been developed in recent years by Bolton et al. (1992) and Bockelmann et al. (199_), emphasizing the importance of energy efficiency factors for photodegradation processes. However, in spite of this progress, there is a need to establish criteria to compare photoreactor efficiencies on the basis of known photochemical and thermodynamic principles.

This efficiency criteria should be applicable to the kinetic model and/or reactor type used and provide a basis for positive photoreactor performance evaluation. This topic is addressed in the present thesis work through the derivation of a so-called "*Photochemical-Thermodynamic Efficiency Factor*" (PTEF).

In order to derive the PTEF, let us consider a photocatalytic reactor under source irradiation and quasi-isothermal conditions. In this unit, as it occurs in many other

chemical processes, an energy rate input Q_{in} is supplied with only a fraction of this energy rate Q_{used} utilised for the desired goal of $\cdot OH$ radical formation. As a result, there is a second fraction of the total light energy input, so-called Q_{lost}, that will be unused and dissipated as thermal energy without achieving any useful conversion.

Accordingly, the total energy input Q_{input} to the photochemical unit can be represented as the addition of two terms, Q_{used} and Q_{lost}:

$$Q_{input} = Q_{used} + Q_{lost} \qquad (IV.3)$$

Thus, the exercise of designing a superior photocatalytic reactor will be one of striking the best combination of reactor design parameters which increases as much as possible Q_{used} and minimizes Q_{lost}.

Given the relevance of Q_{used} and Q_{lost} and their relative importance, it is significant to introduce a PTEF η based on the Q_{used}/Q_{input} ratio. Thus, this PTEF provides a dimensionless number basis of comparison for assessing photocatalytic reactor efficiency.

$$\eta = Q_{used} / Q_{input} \qquad (IV.4)$$

It is significant that the above mentioned criterion is of general applicability and is not restricted to a specific photoconversion process, be this process homogenous or heterogeneous.

Consequently, in order to assess η it is necessary to provide means for calculation of both Q_{input} and Q_{used}. Q_{input} is directly related to the electrical power of the lamp, P (W) and expressed in J s^{-1} with the following relation:

With respect to Q_{used}, leading to the formation of $^{\cdot}OH$ radicals, there may be different representations of this term as follows:

$$Q_{input}(J\ s^{-1}) = P(W) \qquad (IV.5)$$

(a) For a homogeneous process:

$$Q_{used} = r_{OH}\, \Delta H_{OH}\, V \qquad (IV.6)$$

or

$$\eta = r_{OH}\, \Delta H_{OH}\, V/P \qquad (IV.7)$$

where r_{OH} (mol L^{-1} s^{-1}), ΔH_{OH} (J mol^{-1}) and V (L) represent, respectively, the rate of ·OH radical formation, the enthalpy involved in the ·OH radical formation in a homogenous process and the total water hold up.

(b) For a photocatalytic process:

$$Q_{used} = r_{OH}\, \Delta H^{*}_{OH}\, w \qquad (IV.8)$$

or

$$\eta = r^{*}_{OH}\, \Delta H^{*}_{OH}\, w/P \qquad (IV.9)$$

where r_{OH}^{*} is in mol $gcat^{-1}$ s^{-1}, ΔH_{OH}^{*} in J mol^{-1} and w in gcat represent respectively the rate of ·OH formation, the enthalpy of ·OH radical formation in a photocatalytic reaction and the total amount of photocatalyst.

In practice, many researchers working with TiO_2 like to picture the photocatalytic reaction as a pseudohomogeneous process. In this case the PTEF can be written as

$$\eta = r_{OH}\, \Delta H^{*}_{OH}\, V/P \qquad (IV.10)$$

where $r_{OH} = r_{OH}^{*}\, w/V$

Regarding Eqs (IV.7) and (IV.10), they contemplate that PTEFs are not only a function of ·OH radical formation rates but also are related to enthalpies of generation of the critical ·OH radical. Furthermore, these equations point towards the fact that both r_{OH} and ΔH_{OH}^{*} must be carefully assessed if accurate values for η are going to be measured.

Once the PTEFs are introduced and their importance acknowledged, a key issue is how to calculate or evaluate the parameters involved. One important matter is how to assess the r_{OH} formation. While the model pollutant consumption rate is directly measurable, a simple relationship to r_{OH} cannot be invoked. In fact, the pollutant consumption rate is somewhat related to the rate of ·OH radical formation. However, the proper evaluation of the ·OH radical formation rate from pollutant consumption rates requires that important distinctions be made.

First, an ·OH radical balance can be established involving the rate r_{OH} of formation of ·OH radicals with the rate $r_{OH,c}$ of ·OH radicals consumed and the rate $r_{OH,acc}$ of ·OH radicals "accumulated":

$$r_{OH} = - r_{OH,c} + r_{OH,acc} \qquad \text{(IV.11)}$$

Moreover, the $r_{OH,c}$ rate can be equated with $\Sigma\ \nu_p r_p$, which represents the summation of all rates of pollutant photodegradation, including not only pollutants in untreated water (model pollutant initially in the system), but also all intermediate chemical species. Thus, the following equation results:

$$r_{OH} = \sum \nu_p r_p + r_{OH,acc} \qquad \text{(IV.12)}$$

For example, in cases where the untreated water contains a model pollutant and a number of other chemical intermediate species ($t > 0$), such as in the case of methylene blue and phenol studied in this Thesis, r_{OH} cannot be directly equated with the rate of disappearance of the model compound. In other words, ·OH radicals are also consumed for the photoconversion of intermediate chemical species and by other scavengers in the system.

Furthermore, the reaction stoichiometry or stoichiometric numbers for each of these initial and intermediate steps are not known. It is important to emphasise that only at the very beginning of the photoconversion, when the concentration of all chemical species equals the concentration of the model pollutant can the following be advanced:

$$r_{OH} = \nu r_{mp,c} + r_{OH,acc} \qquad \text{(IV.13)}$$

where $r_{mp,o}$ represents the rate of disappearance of the model compound at time t=0.

Nevertheless, there are still some pending problems before one can take advantage of the proposed relations: for a given initial concentration C_i of model pollutant, ν and the $r_{OH,acc}$ are unknown and consequently r_{OH} still cannot be calculated.

$r_{OH,c}$ can be assessed, however, by increasing the concentration of model pollutant C_i. When the model pollutant concentration with respect to other scavangers is very high (in large excess), the stoichiometric number ν become presumably close to -1. Given there is no certainty about ν value, it can be stated that, under these conditions, $r_{OH} = \nu\, r_{mp,o}$ with $r_{OH,acc}$ equal to 0 and $r_{mp,o}$ maximum. Thus,

$$r_{OH} = \nu\, [r_{mp,o}]_{max} \qquad \text{(IV.14)}$$

In summary, under those conditions the PTEF factor becomes

$$\eta = \nu\, [r_{mp,o}]_{max}\, \Delta H^{*}_{OH}\, V/P \qquad \text{(IV.15)}$$

From Eq (IV.15), it can be observed that both the $[r_{mp,o}]_{max}$ and ΔH_{OH}^{*} values are key parameters to assess the PTEF. Moreover, thermodynamic and kinetic considerations presented in this section point toward the following conclusions:

1) A PTEF of general applicability can be established for assessing photocatalytic reactor performance. The expression for PTEF is not affected by unit configuration. Thus, various photocatalytic reactor configurations using anatase TiO_2 crystals, which should have the same ΔH_{OH}^{*}, can be compared with the same equation.

2) The PTEF can be based on the maximum reaction rate of model pollutant disappearance. The PTEF equation is valid at high enough model pollutant concentrations, that is, at conditions where a zero order reaction model prevails. Thus, experiments where the concentration of pollutant is increased progressively until a $[r_{mp,o}]_{max}$ is identified, are advised.

3) The PTEF also points towards the significance of some key parameters which require careful evaluation, such as the ΔH_{OH}^{*}, the enthalpy of $\cdot OH$ radical formation.

4) Given that the PTEF at high initial model pollutant concentration becomes essentially equal to the rate of $\cdot OH$ radical formation suggests that the PTEF should be independent or weakly dependent on the pollutant chemical structure and should only be a characteristic of the specific photocatalytic reactor used. Thus, experiments with, for example, methylene blue or phenol, case of this study, can be performed in a given photocatalytic unit and the behaviour of other compounds, in terms of PTEF, can be advanced without the need of performing experiments.

Even acknowledging that future work is highly recommended to evaluate ΔH_{OH}^{*} and to calculate the PTEF parameter, it can still be used for comparison of various photocatalytic reactors. Given that photocatalytic reactors use TiO_2 anatase catalysts in various designs, they should display the same ΔH_{OH}^{*}. Thus, Eq (IV.15) can be rearranged to:

$$\eta / (-\nu \Delta H_{OH}^{*}) = -[r_{mp,o}]_{max} V/P \qquad (IV.16)$$

An interesting approach applicable for monochromatic lamp irradiance is that of de Lasa and Valladares (1993), where most of the lamp output is near 365 nm. Here one can rewrite the PTEF with the lamp light power output, P_{light}, as follows:

$$P_{light} = N_o \, h \, c / \lambda \qquad (IV.17)$$

where

N_o is the incident photon flux (photon s^{-1}); hc/λ is the photon energy (J $photon^{-1}$) of wavelength λ. Alternatively

or

$$P_{light} = N_A \, e_o \, h \, c / \lambda \qquad (IV.18)$$

where

N_A is the Avogadro Number (6.023×10^{23}) and ϵ_o the incident light flux (einstein s^{-1}).

Substitution of Eq (IV.18) into the expression for the PTEF, as defined in Eq (IV.15), yields the following relation:

$$\eta = \theta \phi \chi \eta_{OH} \qquad \text{(IV.19)}$$

where: $\theta = \epsilon_{abs}/\epsilon_o$ represents the fraction of photon flux absorbed by the photocatalyst in polluted water, where ϵ_{abs} = the photon flux absorbed in the photocatalyst.

$\phi = \nu[r_{mp,o}]_{max} V/\epsilon_{abs}$ is a quantum yield which provides the fraction of photons absorbed by the photocatalyst resulting in the generation of $\cdot$OH radicals.

$\chi = P_{light}/P$ represents the light power efficiency of the lamp.

$\eta_{OH} = \Delta H_{OH}^* /[N_A hc/\lambda]$ represents the fraction of photon energy used in creating $\cdot$OH radicals.

Given that η_{OH} should be a constant for the anatase form of TiO_2 and that the ratio η/η_{OH} is proportional to the ratio $\eta/\Delta H_{OH}^*$, it can be observed that $\eta/\Delta H_{OH}^*$ is a function of ϕ,θ and χ only. On this basis an estimate of the maximum value of $\eta/\Delta H_{OH}^*$ can be derived by noting from Eqs (IV.19) and (IV.16) that

$$\eta/\Delta H_{OH}^* = \phi\theta\chi/[N_A hc/\lambda] \qquad \text{(IV.20)}$$

If the ideal case is considered, ϕ, Θ and $\chi = 1$, for $\lambda = 365$ nm then, the $\{\eta/[\Delta H_{OH}^*]\}_{ideal} = 3 \times 10^{-6}$ mol J^{-1}. One should note that lamp light power efficiencies χ are 0.30 or less.

Thus, rewriting PTEF in terms of ϕ, θ and χ shows that the PTEF is a combined result of three parameters. An optimum combination of them may lead to the best photoreactor designs. As will be shown later for existing photocatalytic reactors, $\eta/[-\nu\Delta H_{OH}^*]$ values are about three orders of magnitude below the ideal level.

In summary, various thermodynamic and kinetic considerations allow us to propose a PTEF which provides a valuable reference for unit performance comparison. This relationship, as presented in Eq (IV.16) will be employed extensively for the evaluation of photocatalytic reactors and in the various discussions that follow.

IV.5 Conclusions

Given the need of assessing this design in the context of other alternatives already presented in the technical literature, a new photochemical-thermodynamic efficiency factor (PTEF) for photocatalytic reactors is introduced. This factor stresses the importance of new research directions, provides mechanistic insights and holds significant potential interest for the development and assessment of various photocatalytic reactor designs.

CHAPTER V

EXPERIMENTAL METHODS

V.1 MATERIALS

Titanium dioxide, Degussa P25 (mostly anatase) was used as the photocatalyst. As reported by the manufacturer this material has a BET surface area of 50 $m^2 g^{-1}$ and a mean particle size of 30 nm. The photocatalyst was impregnated on a "glossy" type glass mesh. Methylene blue (BDH indicator) and Phenol (Caledon laboratories Ltd., reagent grade), were used in this experiment without further purification. Deionized double distilled water was used throughout this study.

V.2 INSTRUMENTATION

Experimental runs were carried out in the PHOTO-CREC I (original design with one and three baskets) and PHOTO-CREC II (modified design, with 15 baskets), using a black light blue (BLB) lamp of 15 W.

The model compounds used, methylene blue and phenol, were analyzed spectrophotometrically using a Hewlett Packard Model 8450 Diode Array spectrophotometer.

The analysis of the TiO_2 supported on glass mesh was carried out using a Scanning Electron Microscope (ISI, DS-130) and Energy dispersive X-ray analyzer system (PGT), (SEM-EDX), from The Surface Science Laboratory, at the University of Western Ontario.

A peristaltic Pump master flex (Cole Palmer) was used to recirculate the water through the photoreactor using different flow rates.

Experiments to determine the total organic carbon (TOC) were carried out with a TOC-5050 Analyzer Shimadzu Model.

V.3 PREPARATION OF TEST SOLUTIONS WITH MODEL POLLUTANTS

0.200 g of methylene blue (MeB) was dissolved completely in distilled water in a 1000 mL volumetric flask, making up a 6.26×10^{-4} M stock solution. In a typical experiment at an initial concentration of 12 μM, 48 mL of this stock solution was transferred to a flask to which distilled water was added to a total volume of 2500 mL. From this flask, 2200 mL were used to fill the reactor and the external tank. The solution was then circulated through the system. Samples for analysis were taken every 15 min over a five hour period of circulation, the first hour with the light off. After one hour, the MeB adsorption on the glass mesh reached equilibrium and the light was turned on, producing the MeB degradation. The same procedure was carried out with phenol using two different initial concentrations (42 and 557 μM).

V.4 ANALYSIS OF SAMPLES

The samples were analyzed using a Hewlett Packard E Model 8450 Diode Array spectrophotometer for quantitative analysis. The photocatalyzed reaction was followed by the disappearance of a methylene blue absorption band at 664 nm. A calibration curve of known concentration of MeB was previously determined. The results were subjected to regression analysis and the extinction coefficient was determined ($\epsilon = 60000 \pm 2300$ M^{-1} cm^{-1}) using Beer's law. In the experiments of TOC determination the analysis was carried out simultaneously with the spectrophotometric determination using the same samples.

Systematic experimental runs at different initial concentrations (from 3 to 50 μM), flow rates (from 100 to 1000 mL/min) and relative light intensities were run. In the experiments with different light intensities, stainless steel meshes with different aperture sizes were used with the same BLB 15 W lamp.

In the experiments with phenol as a model, it was determined quantitatively by using UV spectrophotometry. The decay in the concentration of phenol was followed by the disappearance of its strong absorption band at 270 nm. A calibration curve with known concentrations of phenol was previously prepared. The extinction coefficient determined was determined to be $\epsilon = 1400 \pm 50$ M^{-1} cm^{-1}

V.5. POTASSIUM FERRIOXALATE ACTINOMETRY

This standard actinometry method is based on the photochemical conversion of Fe(III) to the Fe (II) ion and has been described by Calvert and Pitts (1966). The standard actinometric solution used was a 0.0060 M potassium ferrioxalate solution. The solution was irradiated for 15 seconds each time with the solution recirculating through the PHOTO-CREC I reactor. Then, the concentration of ferrous ion was analyzed in a UV-Vis spectrophotometer using phenanthroline as the complexing reagent. The entire sampling procedure was conducted in a dark room to minimize errors introduced by room light, and all experiments were compared with a blank reference.

The absorbance of the solution was measured at 510 nm and the concentration of ferrous ion determined from a calibration graph of the absorbance of prepared samples of known concentration of Fe(II). The results were subjected to a regression analysis, and the number of photons absorbed was calculated using Beer's Law. The known standard value of the quantum yield for this reaction is 1.26 ± 0.01 at 365 nm and 0.0060 M potassium ferrioxalate solution (Murov et al., 1989).

CHAPTER VI
PHYSICOCHEMICAL STUDIES

VI.1 INTRODUCTION

Given the prospects of good perfomance of the PHOTO-CREC reactor, a series of reaction tests with model compounds (methylene blue and phenol) were carried out. The goals for these experimental runs were to determine the physicochemical and efficiency parameters of the reactor. The following physicochemical parameters were determined: adsorption constants in the combined glass mesh-TiO_2 system, the effect of the initial concentration of the model compound, water flow rate and light intensity on the kinetic constants. The following efficiency factors were also determined: quantum yield (ϕ), electrical energy per order (EE/O) and the photochemical-thermodynamic efficiency factor (PTEF). These factors were then compared with other reactor systems. Finally, the effect of mass transfer and chemical reaction was studied and a kinetic model proposed.

VI.2. PRELIMINARY EXPERIMENTS WITH METHYLENE BLUE AS A MODEL POLLUTANT. KINETICS CALCULATIONS.

The first series of experiments with the PHOTO-CREC I photoreactor were carried out with the aim of exploring the photocatalytic activity of the mesh and the performance of the photoreactor. The dye Methylene Blue (MeB) was used as a model pollutant because it presents several advantages: (1) a well defined optical absorption maximum at 664 nm (see Fig.VI.1), (2) good resistance to light degradation in the absence of the photocatalyst, (3) optically transparent at the wavelength range of the lamp (365 nm), (4) its bleaching can easily be followed using spectrophotometric techniques.

The decrease of the Methylene Blue concentration was measured by using a Hewelett Packard model 8450 diode array spectrophotometer. Calibration curves were prepared using a MeB solution of known concentration and measured at 664 nm. The photoactivity of the glass mesh with immobilized TiO_2 in one basket was confirmed and is described as curve A in Fig. VI.2. 20% of MeB was converted after two hours of

Figure VI.1 Absorbance Spectra (200-800 nm) of a Methylene Blue Solution.

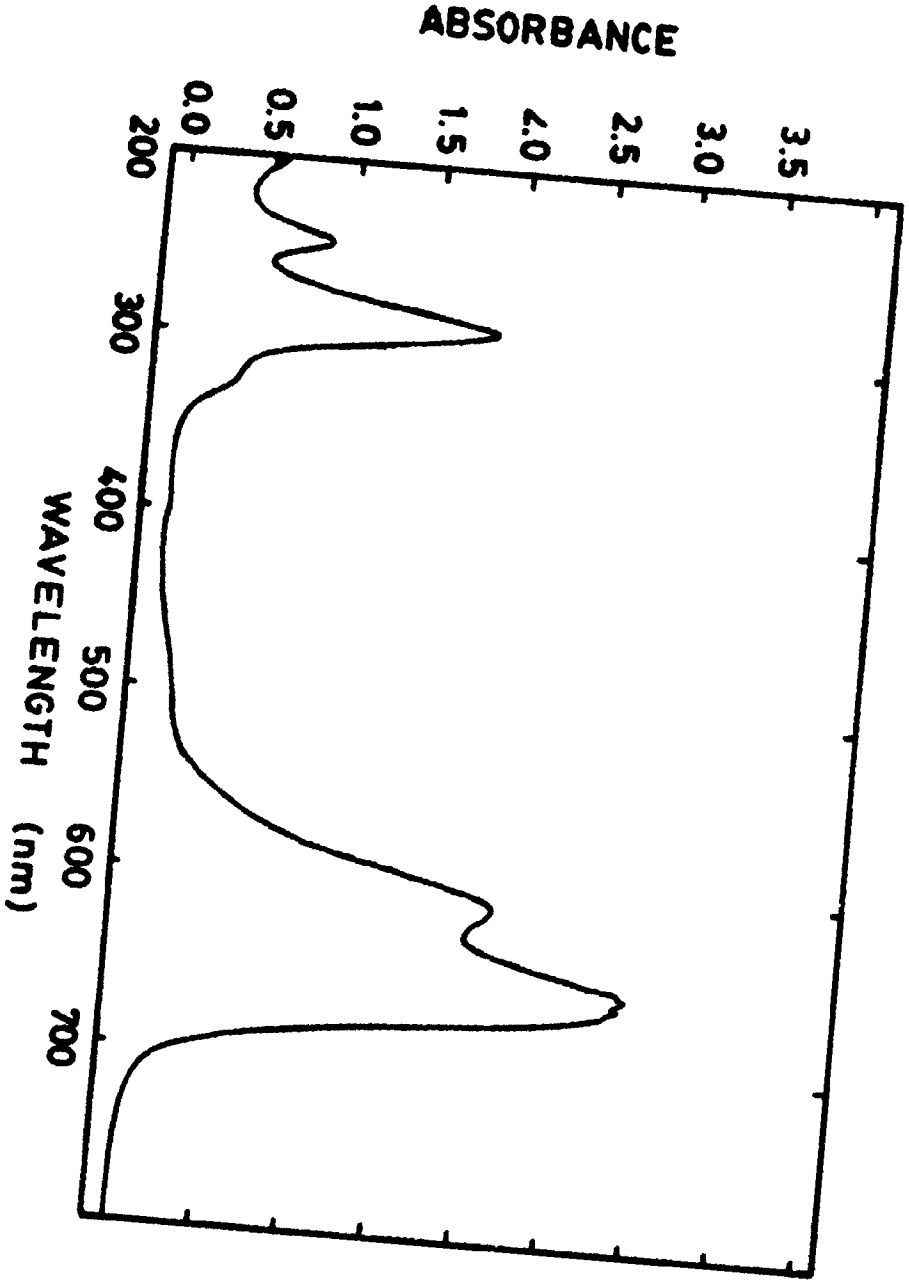
ABSORBANCE
0.0
0.5
1.0
1.5
2.0
2.5
3.0
3.5
200
300
400
500
600
700
WAVELENGTH (nm)

operation using the 15 W blacklight blue tube.

The number of experiments was then extended using three baskets and similar conditions as before, obtaining in this case a conversion of 58% after 2 hours of operation, as is shown in curve B in Fig. VI.2.

The results obtained were also plotted in a semi-log graph showing a straight line typical of first-order kinetics. The kinetic parameters were then calculated. The results obtained are given in Table VI.1.

TABLE VI.1 KINETIC PARAMETERS IN PHOTO-CREC I

No. of Baskets	Aparent Kinetic Constant, k_{app} (min^{-1})	Half life (min)
1	0.0015 ± 0.0002	462
3	0.0066 ± 0.0003	105

With these initial results, it was possible to evaluate the performance of the unit with a few baskets and introduce the modifications to the photoreactor, as was explained in Chapter II. The modified unit is called PHOTO-CREC II. A better performance of the photoreactor was expected with a larger number of baskets.

VI.3 REACTOR OPERATION CONDITIONS

In the continuation of this research, systematic runs were carried out using the PHOTO-CREC II using MeB as the model pollutant and 15 baskets.

In general the experiments were carried out under the following experimental conditions:

1. *Initial concentration of MeB*: The range of concentrations was from 3 to 50 μM. This is the range often found for organic pollutants in drinking water or contaminated groundwaters. 12 μM was taken as a standard for several experiments.

Figure VI.2: Degradation of Methylene Blue using the PHOTO-CREC I reactor unit with one basket, curve A (--X--) and three baskets, curve B (--Δ--). These experiments were conducted under the following conditions: solution volume, 1.6 L; flow rate: 150 mL/min; lamp power, 15 W; initial MeB concentration, 4.0 μM.

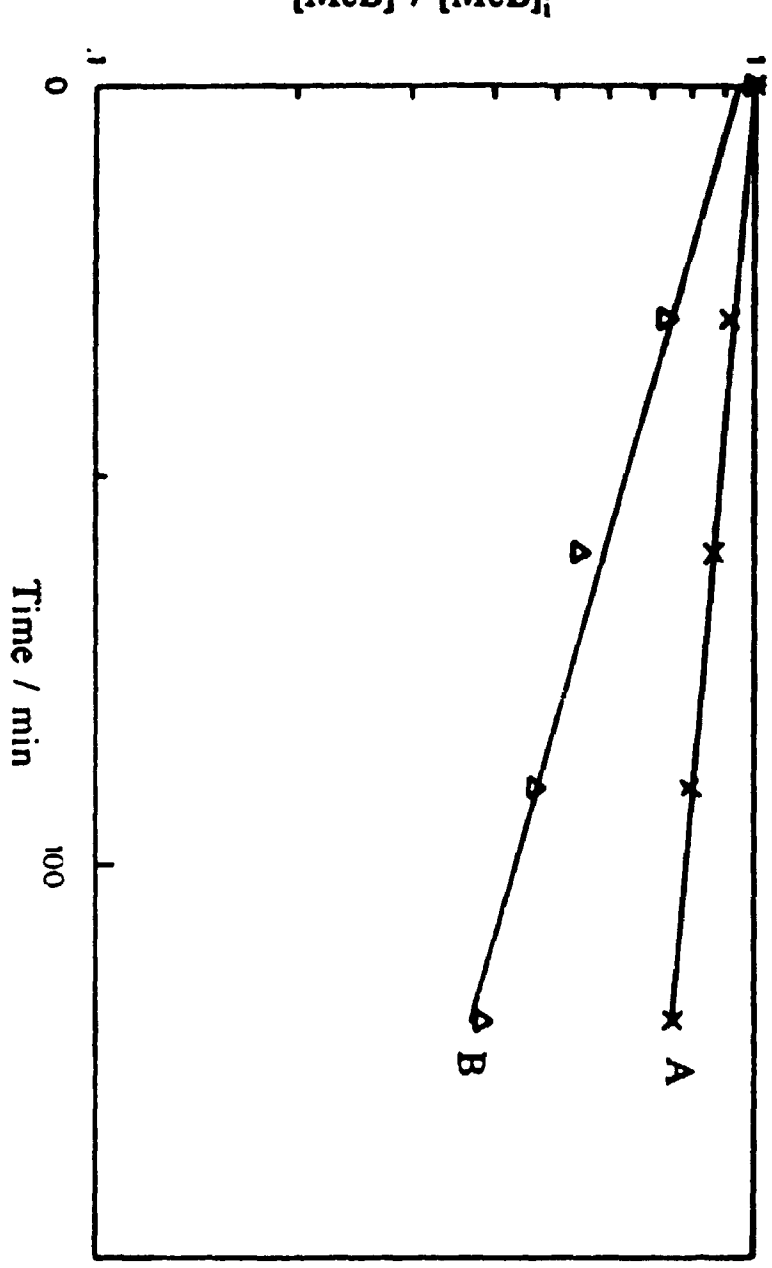
[MeB] / [MeB]i
0
1
Time / min
100
A
B

2. *Oxygen concentration*: it was considered that the oxygen concentration was near saturation and in equilibrium in the system. The water reservoir was open to the atmosphere and continuously agitated, permitting oxygen from the air to be reabsorbed, regenerating the oxygen consumed in the photocatalytic reaction. A calculation using Hysim simulation program (Hyprotec Ltd., 1993) of the oxygen dissolved in the working conditions of the PHOTO-CREC I was carried out, obtaining a value of 300 μM.

3. *Total Volume*: the total volume used was 2.2 L in the experiments with the final reactor design and using 15 baskets.

4. *Flow Rate*: the flow rate for most of the experiments was 150 mL/min. But in the experiments on the effect of flow rate, runs from 100 to 1000 mL/min were carried out.

5. *Light Source Used*: the lamp used in all the experiments was a 15 W black light blue tube that produced radiation peaking at 365 nm with a radiation output of 800 $\mu W/cm^2$ at a distance of 12 inches as described by the manufacturer.

6. pH: The pH used was the "natural" pH of the MeB solution. The average value of pH obtained was 5.4 $\pm$ 0.5

7. *Temperature*: the average temperature conditions of the water solution of model pollutant MeB was 18 $\pm$ 2 °C

VI. 4. ADSORPTION OF MEB ON THE TIO_2 IMPREGNATED GLASS MESH

For this experiment the MeB solution was recirculated through the reactor with the light source off. Samples were taken every 15 min over 90 min. It was found that the MeB concentration initially dropped but then became relatively constant after 15 min indicating that the system (mesh-MeB solution) approached adsorption equilibrium (see the first part of Fig. VI.3). Several adsorption experiments for the system mesh-MeB solution were carried out for different initial concentration of MeB. The results obtained are shown in Fig. VI.4. An initial steeply rising curve that gradually flattens off was obtained. The initial rise is related to the strong tendency of the TiO_2/mesh surface to bind the MeB molecules and the levelling off can be attributed to the saturation of the surface adsorption sites. The MeB adsorbed on the TiO_2 loaded mesh approaches

Figure VI.3: Typical experiment showing the photodegradation of Methylene Blue in PHOTO-CREC II reactor showing the adsorption of MeB on TiO_2 supported glass mesh ("Dark Reaction") and the switching on of the UV lamp, starting the photocatalysis reaction period. The run was conducted under the following conditions: solution volume, 2.2 L; flow rate, 150 mL/min; lamp power, 15 W; initial MeB conc, 12 μM.

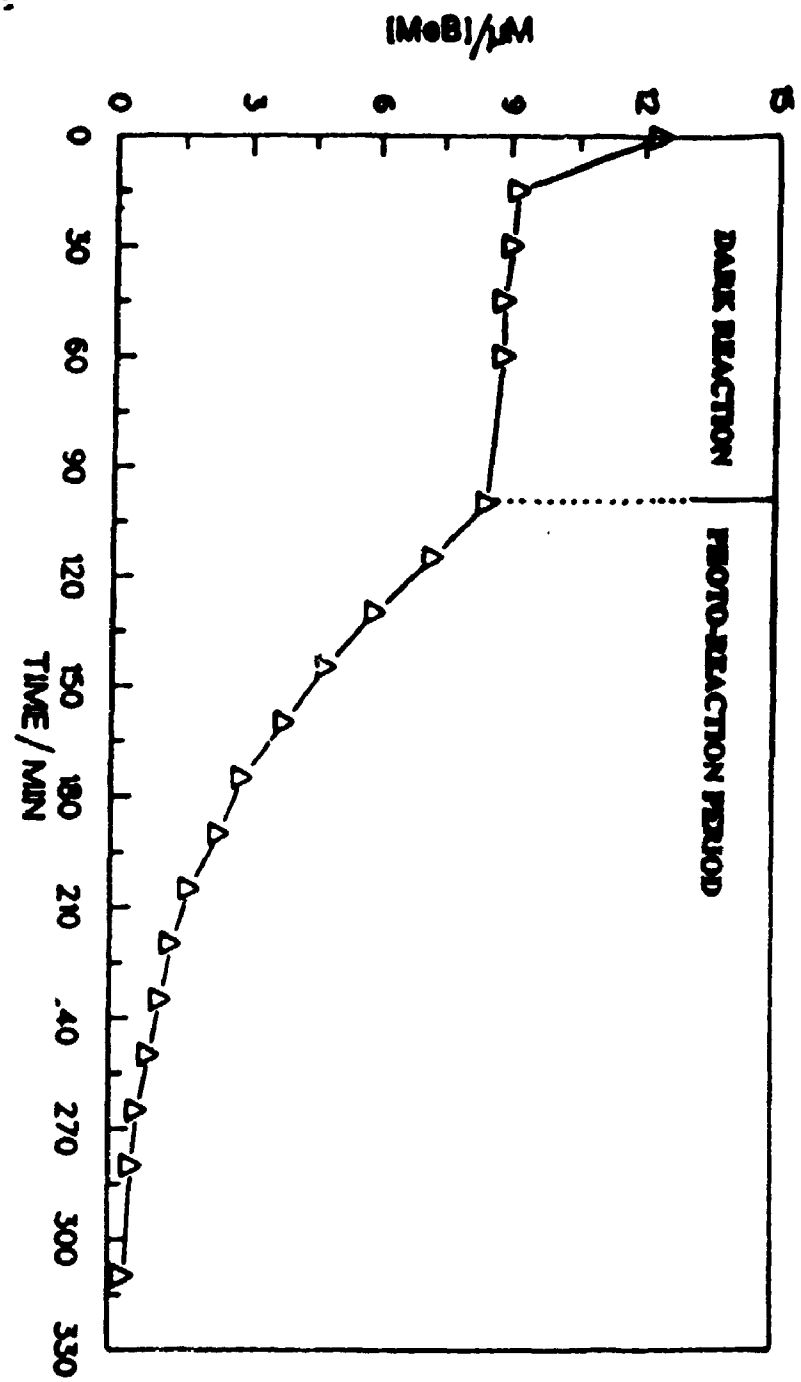
[MeB]/μM
0
3
6
9
12
15
0
30
60
90
120
150
180
210
240
270
300
330
TIME / MIN
DARK REACTION
PHOTO-REACTION PERIOD

Figure VI.4: Methylene Blue adsorbed per gram of mesh at different initial MeB concentrations, showing that the surface saturation is reached at $[MeB]_{Eq}$ of $\sim 25\ \mu M$.

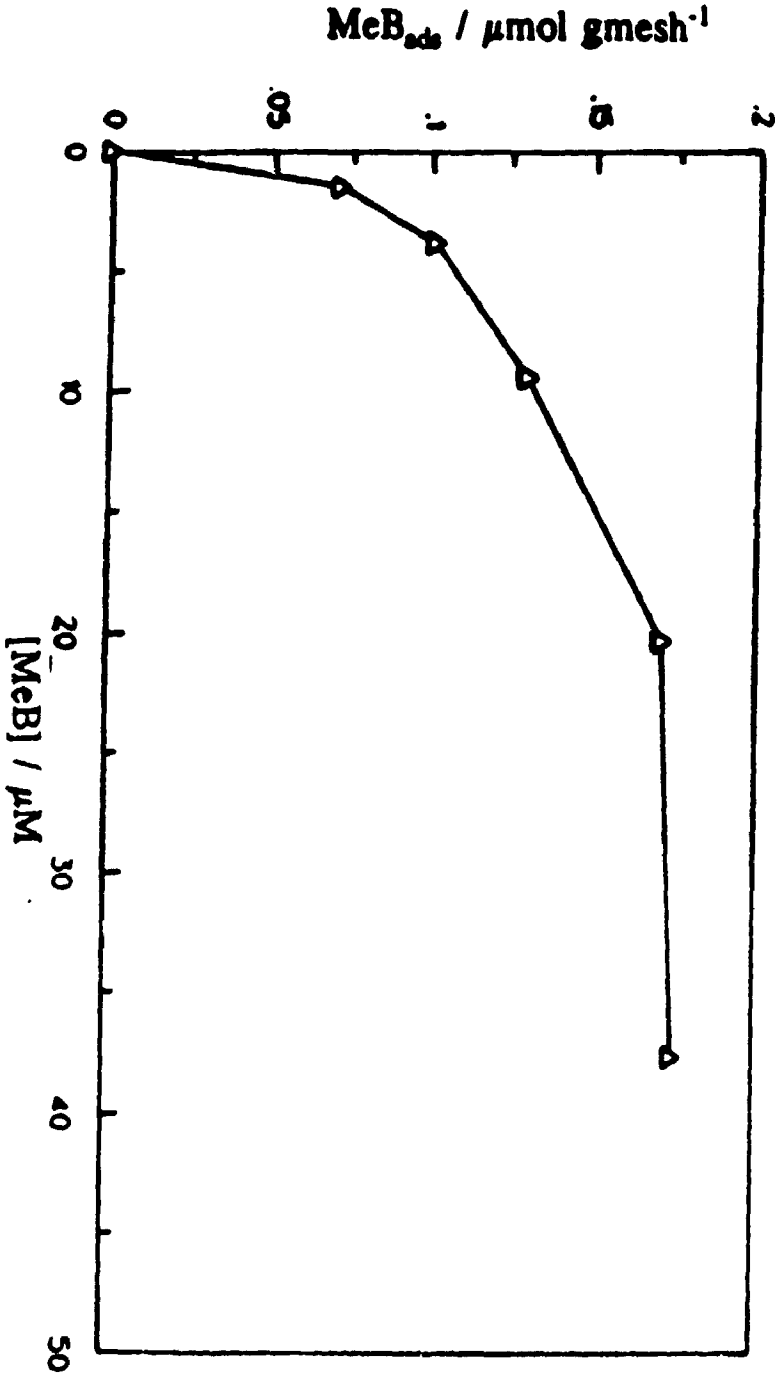
MeB$_{ads}$ / μmol gmesh^{-1}
0
0.5
1
1.5
2
0
10
20
30
40
50
[MeB] / μM

saturation when a value of the equilibrium concentration of MeB of 20 μM is reached. The graph has the typical shape of an adsorption isotherm. The expression that might describe the MeB adsorption behavior on the TiO_2 glass mesh is the Langmuir Adsorption Isotherm:

$$[MeB]_{ads} = \frac{K_1 K_2 [MeB]_{Eq}}{1 + K_1 [MeB]_{Eq}} \qquad \text{(VI.1)}$$

Where $[MeB]_{ads}$ is the moles of MeB adsorbed per gram of mesh and $[MeB]_{Eq}$ is the equilibrium concentration of MeB in the solution; K_1 and K_2 are constants for the given system. If the reciprocal of the above expression (Eq. VI.2) is plotted, a straight line is obtained from which it is possible to obtain K_1 and K_2.

$$\frac{1}{[MeB]_{ads}} = \frac{1}{K_1 K_2 [MeB]_{eq}} + \frac{1}{K_2} \qquad \text{(VI.2)}$$

The reciprocal plot is shown in Fig. VI.5 and the parameters obtained are:

$K_1 = 0.471 \pm 0.065\ \mu M^{-1}$ $\qquad$ $K_2 = 0.167 \pm 0.024\ \mu mol\ gmesh^{-1}$

Concerning these parameters, Matthews (1989) states that K_1 is related to the adsorption affinity while K_2 is related to saturation coverage of the surface.

VI.5 Typical Kinetic Response in the Light

A typical experiment can be seen in Fig. VI.3 and is described as follows: The solution containing MeB was recirculated through the reactor with the light source off. Samples for spectrophotometric analysis were taken every 15 min over a 5 h period. There was an initial rapid decrease of the MeB concentration, arising from its adsorption on the TiO_2 supported glass mesh. This decrease of MeB concentration from the solution

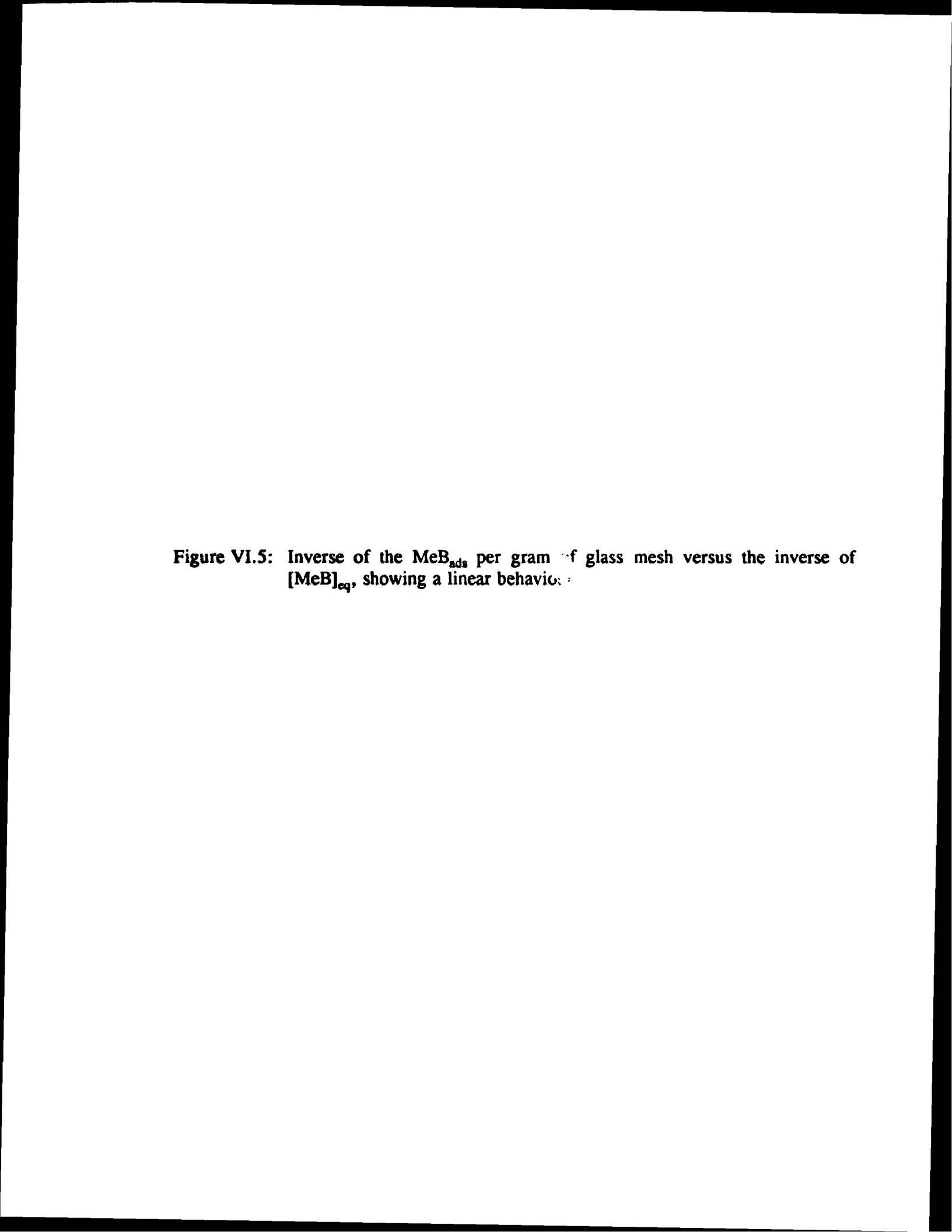

Figure VI.5: Inverse of the MeB_{ads} per gram of glass mesh versus the inverse of $[MeB]_{eq}$, showing a linear behavior.

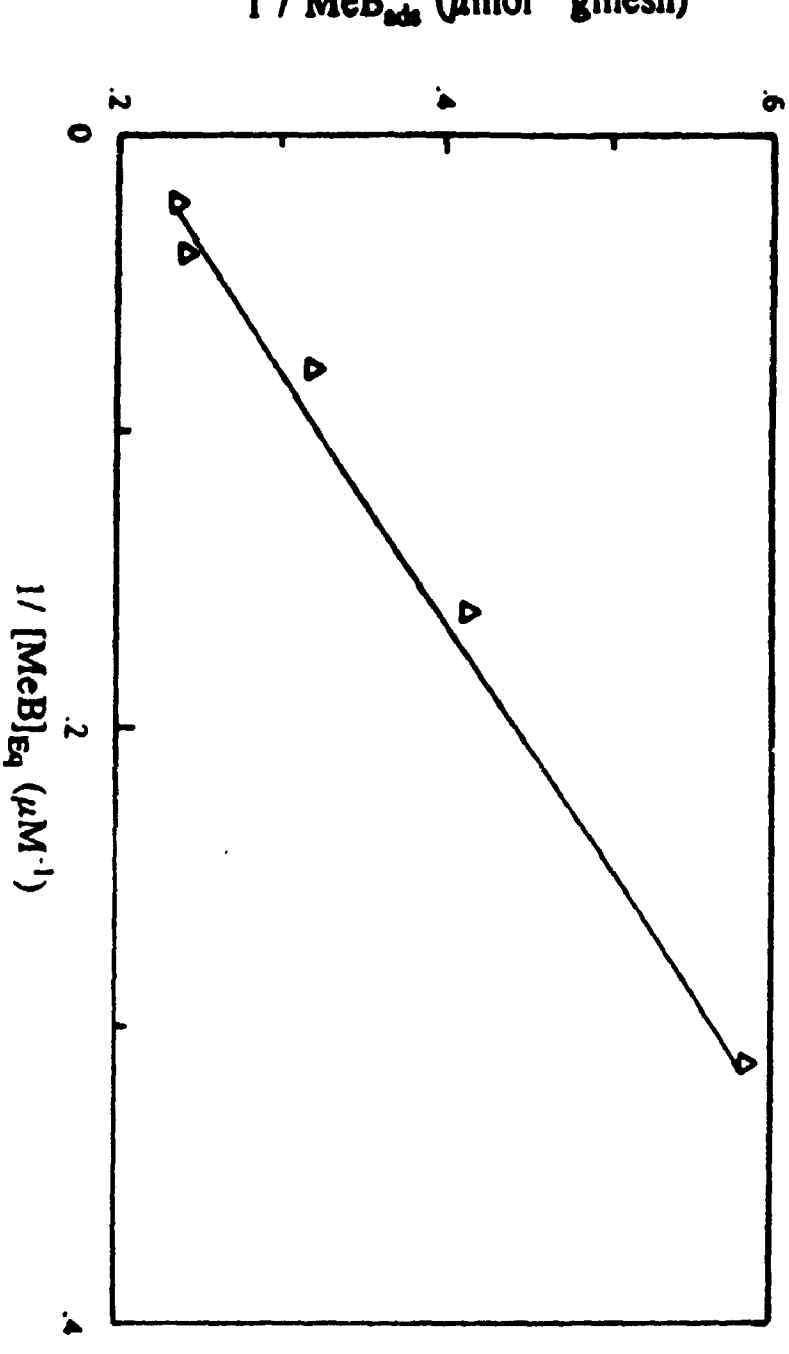
1 / MeB$_{ads}$ (μmol^{-1} gmesh)
.2
.4
.6
0
.2
.4
1/ [MeBl]$_{Eq}$ (μM^{-1})

(called the "dark reaction") occurred before the light was switched on. After 15 min the MeB adsorption on glass mesh surface achieved equilibrium. Once the MeB concentration reached a plateau, the light source was switched on and samples were taken every 15 min. An exponential decrease of the MeB concentration occurred thereafter. During the reaction period 90% bleaching was reached in 2.0 h for 2.2 L of a 12 μM solution of MeB at a flow rate of 150 mL/min.

VI.6. DETERMINATION OF THE KINETIC PARAMETERS

The results described in Fig. VI.3 were plotted on a semilog graph for the photocatalyzed reaction period after the light was switched on. As shown in Fig. VI.6, the data fit a straight line, which confirms apparent first-order reaction kinetics for the degradation of MeB. The kinetic results show an increase of ~10 in the apparent rate constant between the PHOTO-CREC I reactor with one basket and the PHOTO-CREC II reactor with 15 baskets, as was expected. The results obtained were: $k_{app} = 0.017 \pm 0.002$ min^{-1} and $t_{1/2} = 41$ min; 90% of the MeB was bleached after 2 h.

VI.7. EFFECT OF INITIAL CONCENTRATION OF MeB

The effect of the initial concentration of MeB on the rate of disappearance from the solution was studied using different concentrations ranging from 6 to 50 μM (before adsorption). The experimental conditions were as follows: flow rate, 150 mL/min; total volume, 2.2 L; lamp power, 15 W, BLB tube. The experimental results are described in a semilog graph in Fig. VI.7 and Table VI.2

The results show that when MeB initial concentration increases, the apparent first-order rate constant k_{app} decreases, suggesting that at higher concentrations there is an increasing limitation of the reaction rate, depending on the number of available sites on the TiO_2/glass mesh system. These results demonstrate first order kinetics for all the concentrations presented in Fig. VI.6. The kinetic constants and half lives, at different initial concentrations, are given in Table VI.2.

VI.8. EFFECT OF FLOW RATE OF THE RECIRCULATED SOLUTION.

Experiments to determine the effect of the recirculation flow rate in the

Figure VI.6: Semilog plot of experimental conversion of Methylene Blue versus reaction times in the PHOTO-CREC II reactor.

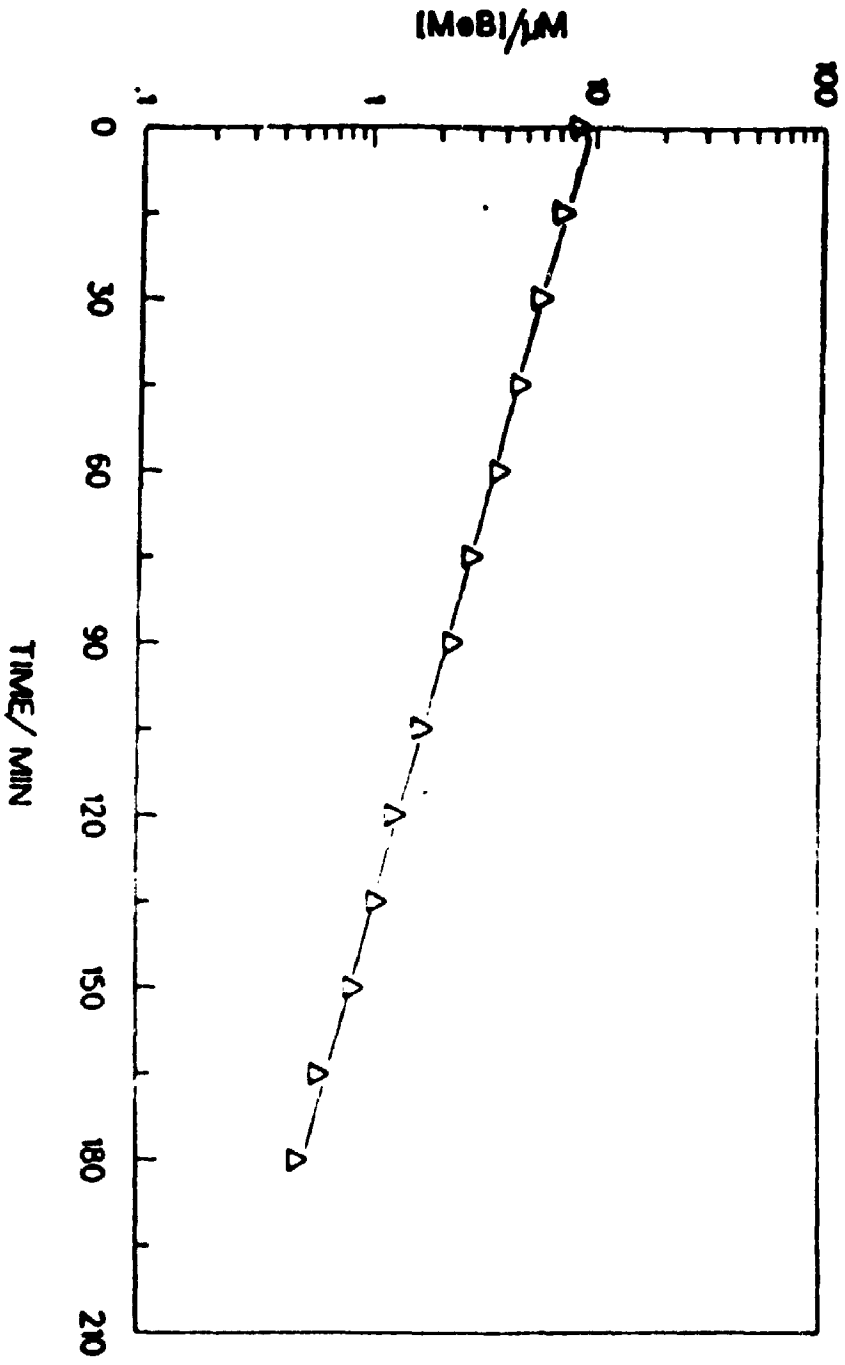
[MoB]/μM
TIME/ MIN
0
30
60
90
120
150
180
210

Figure VI.7: Experimental MeB concentrations for various times of reaction showing the effect of initial MeB concentration in the PHOTO-CREC II unit. The experimental runs were conducted under the following conditions: solution volume, 2.2 L; flow rate, 150 mL/min; lamp power, 15 W; -- -- 39.4 μM; -- -- 20.4 μM; -- -- 9.4 μM; -- Δ -- 3.8 μM

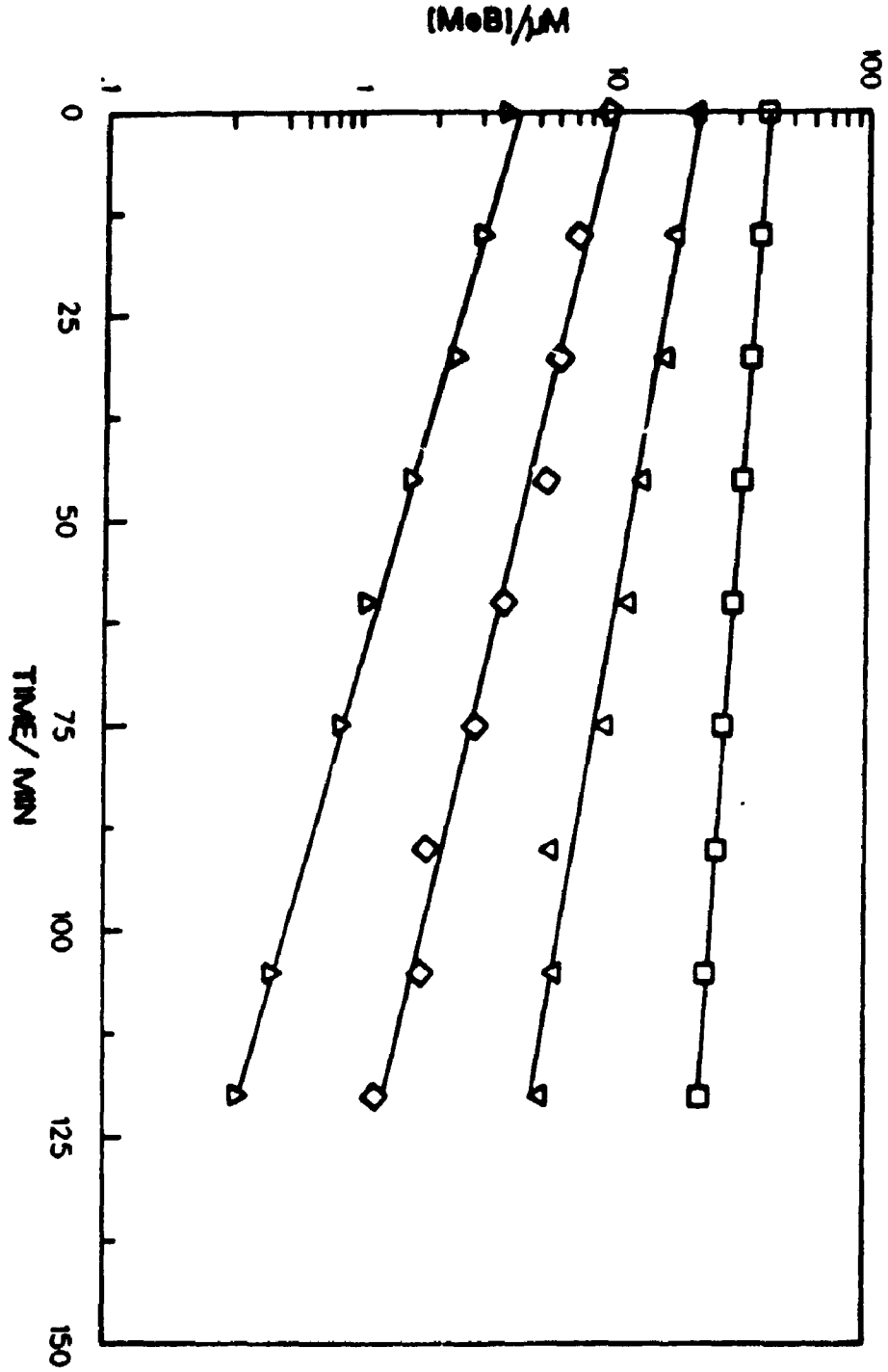
[MoBl]/μM
.1
1
10
100
0
25
50
75
100
125
150
TIME/ MIN

TABLE VI.2. EFFECT OF INITIAL CONCENTRATION OF MeB

Solution volume, 2.2 L; Flow rate, 150 mL/min; Lamp power, 15 W

$[MeB]_o$ (μM)	Apparent kinetic rate constant (min^{-1})	Half life $t_{1/2}$ (min)
3.8	0.021 ± 0.002	34
9.4	0.017 ± 0.001	40
20.4	0.012 ± 0.001	56
39.4	0.005 ± 0.001	133

photoreactor and the related mass transfer controls were carried out in a range of 100 to 1000 mL/min under the following conditions: total volume, 2.2 L; initial MeB concentration, 12 μM; lamp power, 15 W BLB lamp.

The experiments were typically run for 4 h including 1 h for the dark reaction. The results of the experiments show that when the flow rate increases, the apparent kinetic constant increases reaching a plateau at a flow rate of 500 mL/min. The results are described in Fig. VI.8 and Table VI.3.

Given the increase of fluid velocity in the proximity of the fiber mesh when the water flow rate increases, a reduction in the mass transfer boundary layer can be expected. Thus there will be an overall increase in mass transfer rates, with a corresponding reduction of mass transfer limitations and higher apparent kinetic rate constants. When a limit is reached, such that further flow rate increases do not yield higher apparent kinetic rate constants, it can be argued that the overall rate of photoconversion is controlled only by chemical reaction at the surface of the TiO_2 particles. This is an optimized operating condition for a given design. In the case of PHOTO-CREC II, this condition is reached for flows higher than 500 mL/min. Chapter VI, section VI.14 deals further with the modelling aspects of these experiments.

VI.9. EFFECT OF LIGHT INTENSITY

Experiments to determine the effect of the light intensity on the reaction rate were carried out in the PHOTO-CREC II unit. The lamp was wrapped with a stainless steel mesh, having different aperture sizes, allowing different fractions of the light source to pass into the reaction chamber of the photoreactor. The meshes used had the following open areas: 50%, 40% and 36%. The results are presented in Fig. VI.9.

The experiments were carried out using a 12 μM solution of MeB and a flow rate of 500 mL/min, showing a linear dependence of the light intensity with the reaction rates. This result was expected due the low power (15 W) of the lamp used. This is a desirable condition for the optimization of energy utilization in the unit designed.

Figure VI.8: Experimental MeB concentrations for various times of reaction showing the effect of the water flow rate. The experimental runs were conducted under the following conditions: solution volume, 2.2 L; lamp power, 15 W; initial MeB concentration, 12 μM. -- -- 322 mL/min; --Δ-- 237 mL/min; -- -- 110 mL/min; -- -- 500 mL/min; -- + -- 750 mL/min.

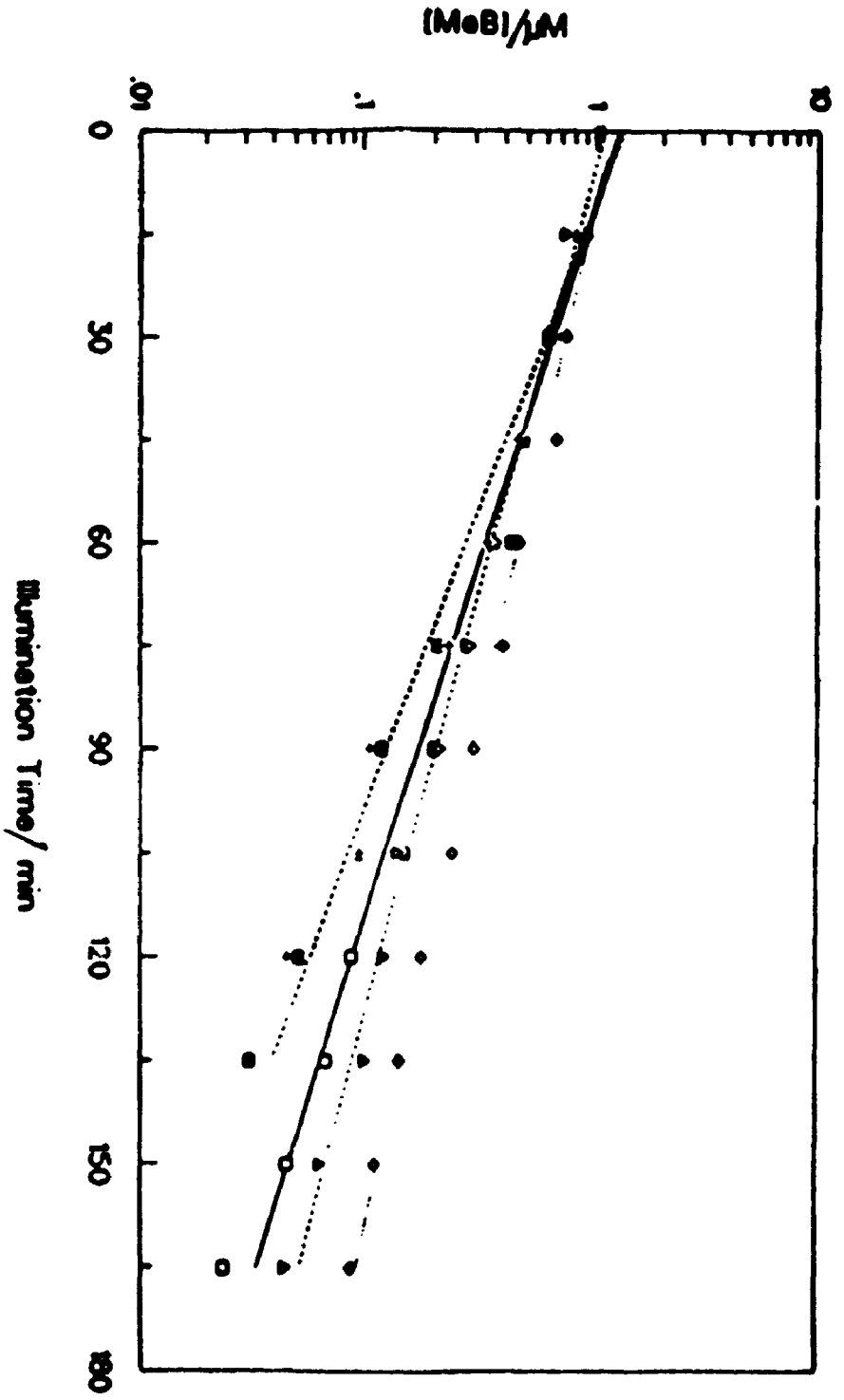
[MoBl]/μM
0.0
1
2
3
0
30
60
90
120
150
180
Illumination Time/ min

TABLE VI.3. EFFECT OF FLOW RATE

Solution volume : 2.2 L; Initial MeB concentration: 12 μM; La: p power: 15 W.

Flow Rate (mL/min)	Apparent kinetic rate constant, k_{app} (min^{-1})	Half life, $t_{1/2}$ (min)
110	0.015 ± 0.002	47
150	0.017 ± 0.002	40
237	0.019 ± 0.002	37
322	0.022 ± 0.002	32
500	0.0263 ± 0.001	26
750	0.0262 ± 0.002	26

Figure VI.9: Change of the apparent reaction rate constant with different light intensities

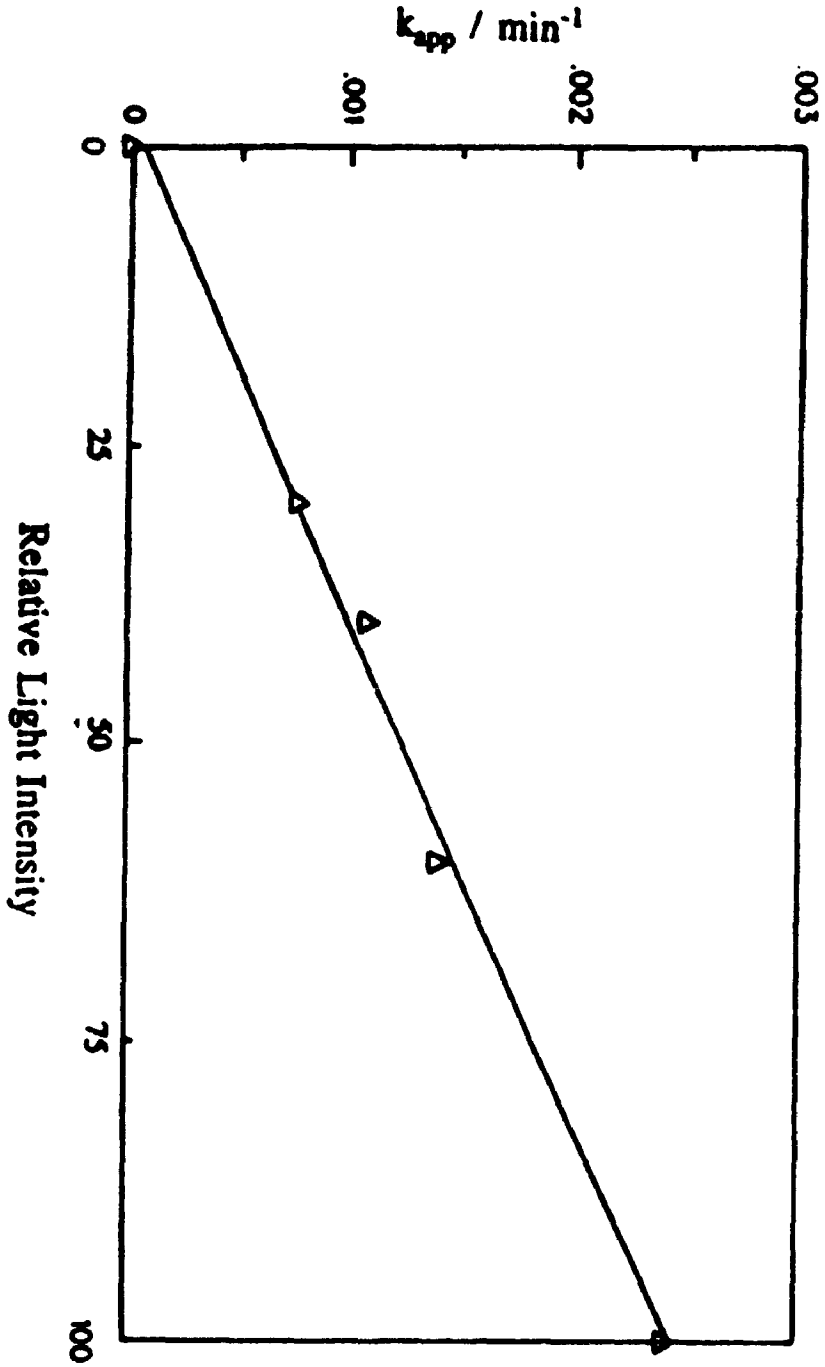
k_{app} / min^{-1}
0
.001
.002
.003
0
25
50
75
100
Relative Light Intensity

VI.10. QUANTUM YIELD OF THE BLEACHING OF MeB

The quantum yield of the bleaching of MeB in the PHOTO-CREC II unit should be determined by assessing the number of photons emitted by the lamp that reach the surface of the TiO_2 supported on the glass mesh and the fraction of this light that is adsorbed by the TiO_2. The number of photons emitted by the lamp that enter the reaction chamber was measured by using potassium ferrioxalate actinometry. The fraction of light absorbed was determined by measuring the light absorbed by the mesh and the photocatalyst using an integrating sphere.

The actinometry of the lamp and the photoreactor was carried out by recirculating a 6.0×10^{-3} M solution of potassium ferrioxalate through the photoreactor from the reservoir. The method of Calvert and Pitts (1966) was used to measure the rate of ferrous ion formation. The results are shown in curve A in Fig. VI.10. The slope, calculated by regression analysis was, slope = 0.072 ± 0.001 min^{-1}. Using this result, the photon flux entering the reactor was calculated to be $\epsilon_o = (2.7 \pm 0.2) \times 10^{-4}$ Einstein/min (see Appendix 1). However, it is not possible to assume that the same number of photons/min were absorbed by the photocatalyst because part of this light was absorbed by the glass mesh and other components of the unit and part was transmitted through the mesh. To quantify part of this phenomenon, an experiment was conducted to measure the fraction of light absorbed by the photocatalyst. The experiment consisted in determining the light absorbed by the bare glass mesh and that by the supported TiO_2 photocatalyst, by taking a UV diffuse reflectance spectrum at 365 nm (using an integrating sphere) for both the TiO_2 supported on glass mesh and the bare mesh. The result of this experiment showed that the fraction absorbed by the mesh is 0.29, by the TiO_2 is 0.39 and 0.32 of the light was transmitted through the mesh. Thus, the photon rate absorbed by the TiO_2 and in the mesh system was calculated to be $\epsilon_{abs} = (1.05 \pm 0.05) \times 10^{-4}$ Einstein/min.

The results obtained for the effect of MeB concentration on the quantum yield are shown in Fig. VI.11. They indicate that the quantum yield increases with the MeB concentration, reaching a plateau with a maximum quantum yield of $\phi = 0.0063$.

The results obtained for the effect of water flow rate on the quantum yield are shown in Fig. VI.12. They indicate that the quantum yield increases when the flow rate

Figure VI.10: Absorbance at 510 nm of Fe^{2+} complex produced when light of 365 nm was irradiated to the potassium ferrioxalate actinometry solution in the PHOTO-CREC II reactor.

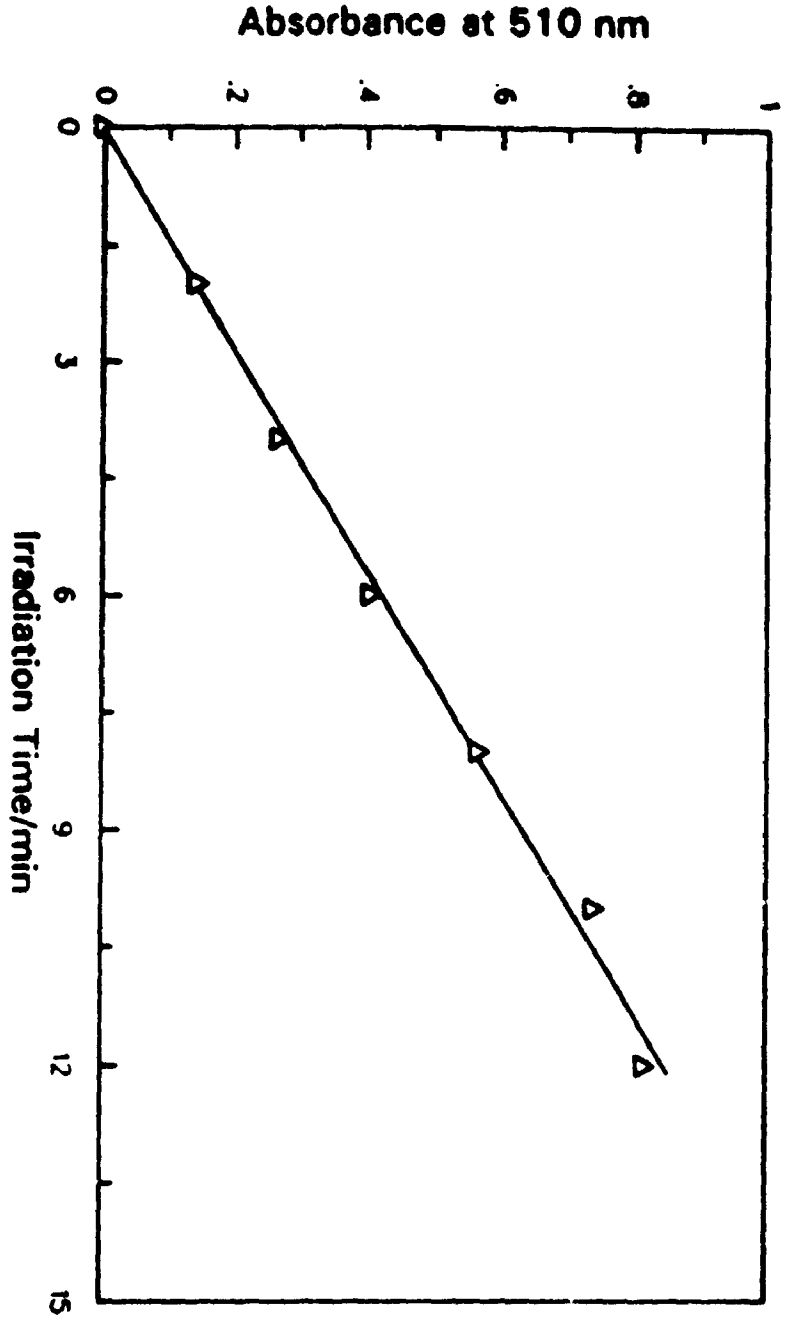
Absorbance at 510 nm
0
2
4
6
8
1
0
3
6
9
12
15
Irradiation Time/min

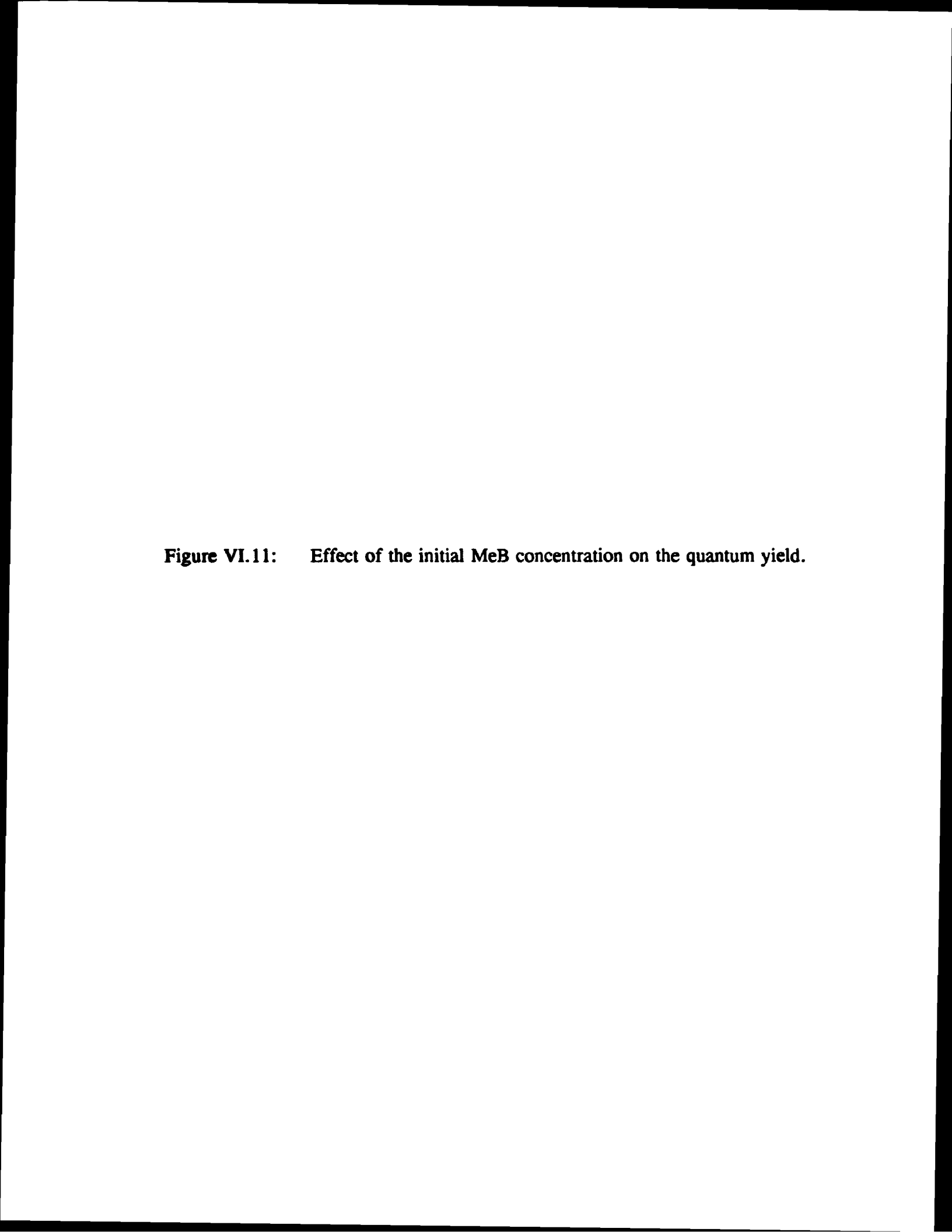

Figure VI.11: Effect of the initial MeB concentration on the quantum yield.

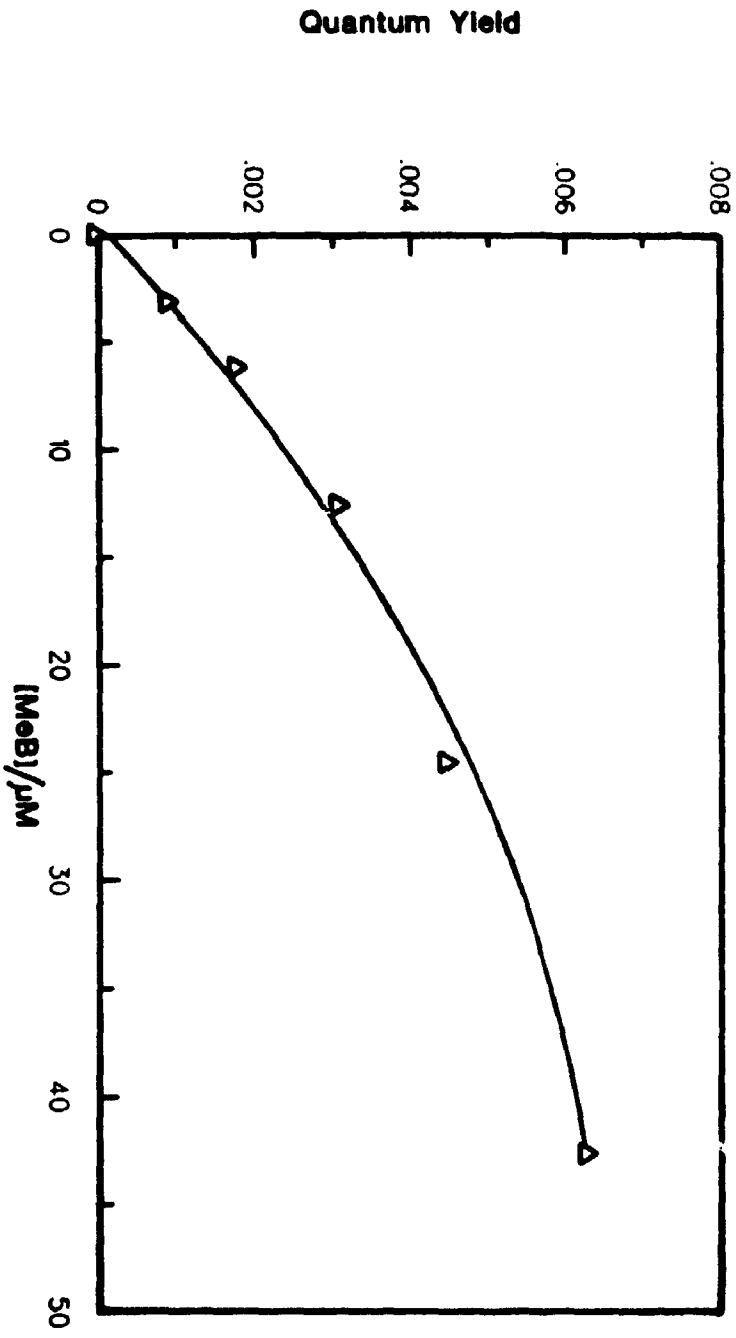
Quantum Yield
0
.002
.004
.006
.008
0
10
20
30
40
50
[MeBI]/μM

Figure VI.12: Effect of the flow rate on the quantum yield.

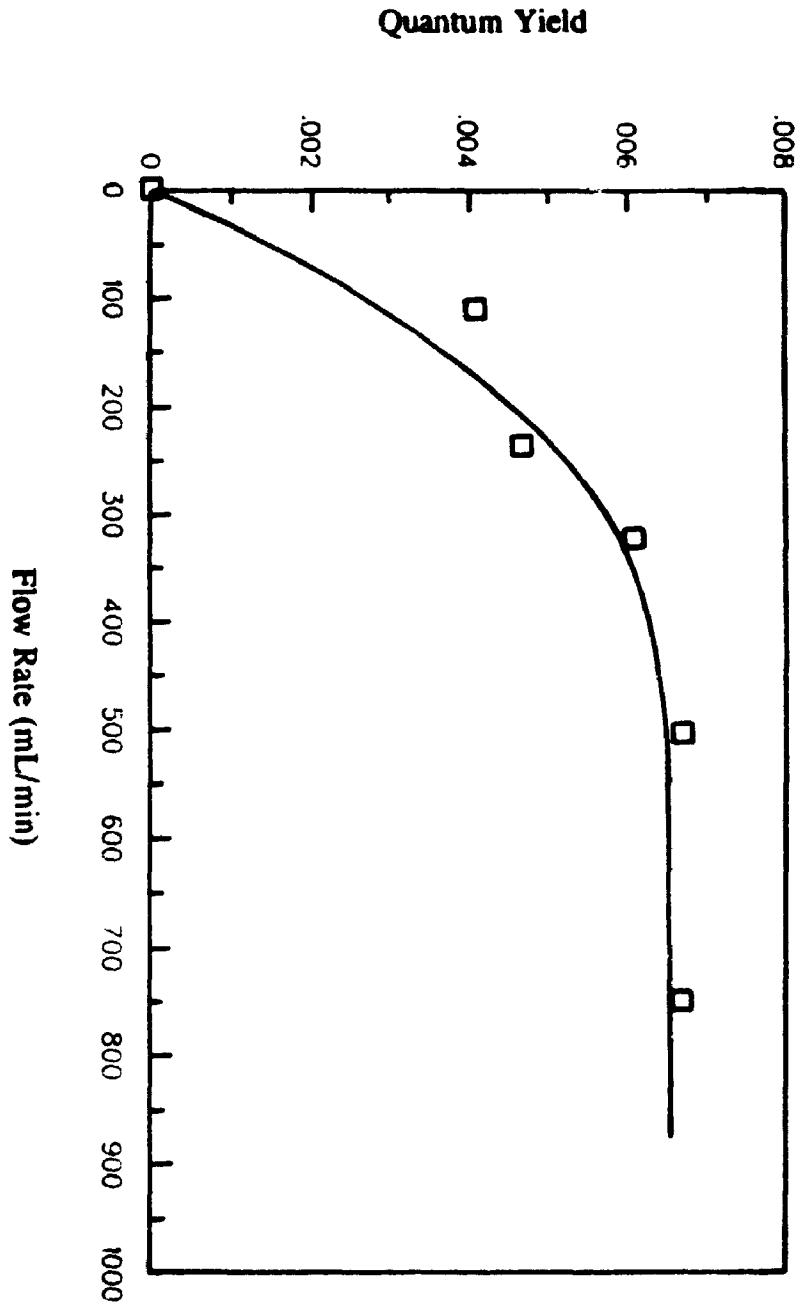
Quantum Yield
.008
.006
.004
.002
0
0
100
200
300
400
500
600
700
800
900
1000
Flow Rate (mL/min)

is increased from 150 mL/min to 500 mL/min, where a constant value is reached at $\phi = 0.0067$.

These results can be compared with those reported before using a slurry system (Valladares and Bolton, 1993). Those results show that the quantum yield $\phi = 0.033$ for a slurry system is ~5 times higher than in the immobilized system.

In summary, the quantum yield values evaluated in this study represent a minimum quantum yield of the system and should only be considered as a general reference.

VI.11. MINERALIZATION OF MeB-TOTAL ORGANIC CARBON ANALYSIS

Studies concerning photocatalytic conversion of MeB and possible intermediates were carried out by the simultaneous determination of the total organic carbon (TOC) and the bleaching of the MeB solution. The results show (Fig. VI.13) an initial TOC lag period with respect to the MeB bleaching. This was followed by a fast disappearance of TOC. In the first hour of illumination, 27% of MeB was bleached and 9% of the TOC was mineralized. In the following two hours of illumination, MeB was bleached and mineralized at almost the same rate. However after 3 hours, there was a decrease in the mineralization rate. Furthermore, after 5 hours of illumination the Me^{n} was 85% bleached and 72% mineralized. Reviewing the results obtained, it is suggested that after 3 hours of illumination, an intermediate is formed that appears to be slow to degrade. Complete mineralization was found after 20 hours. In summary, the overall MeB bleaching was observed to take place at a rate approximately four times faster than that of complete mineralization. This result agrees well with a study previously reported by Matthews (1989) using MeB as model reactant and a glass spiral reactor system.

VI.12. KINETICS AND EFFICIENCY WITH A SECOND MODEL POLLUTANT: PHENOL

Experiments using PHOTO-CREC II photoreactor were carried out using phenol as a second model pollutant. The disappearance of the phenol was followed by spectrophotometry and the results fit first-order kinetics. The experiments were carried

Figure VI.13 Decrease of % MeB concentration ( ) and Total Organic Carbon (TOC) ( ) with irradiation time.

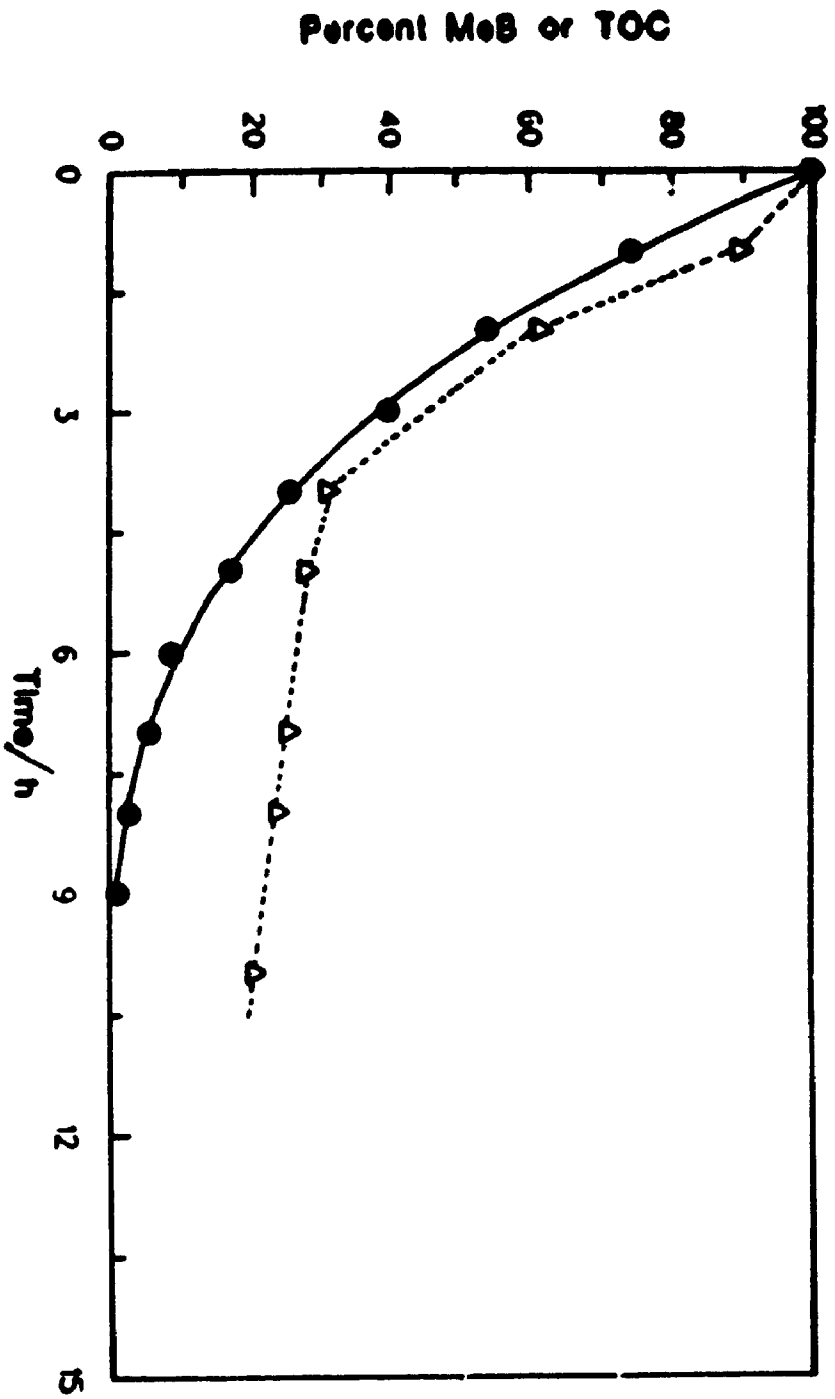
Percent MoB or TOC
0
20
40
60
80
100
0
3
6
9
12
15
Time/h

Figure VI.14: Degradation of phenol in tne PHOTC -CREC II reactor with 15 baskets. The experimental runs were conducted under the following conditions: solution volume, 2.2 L; lamp power 15 W, initial phenol concentration, 42 μM ( ) and 557 μM ( ); flow rate: 150 mL/min.

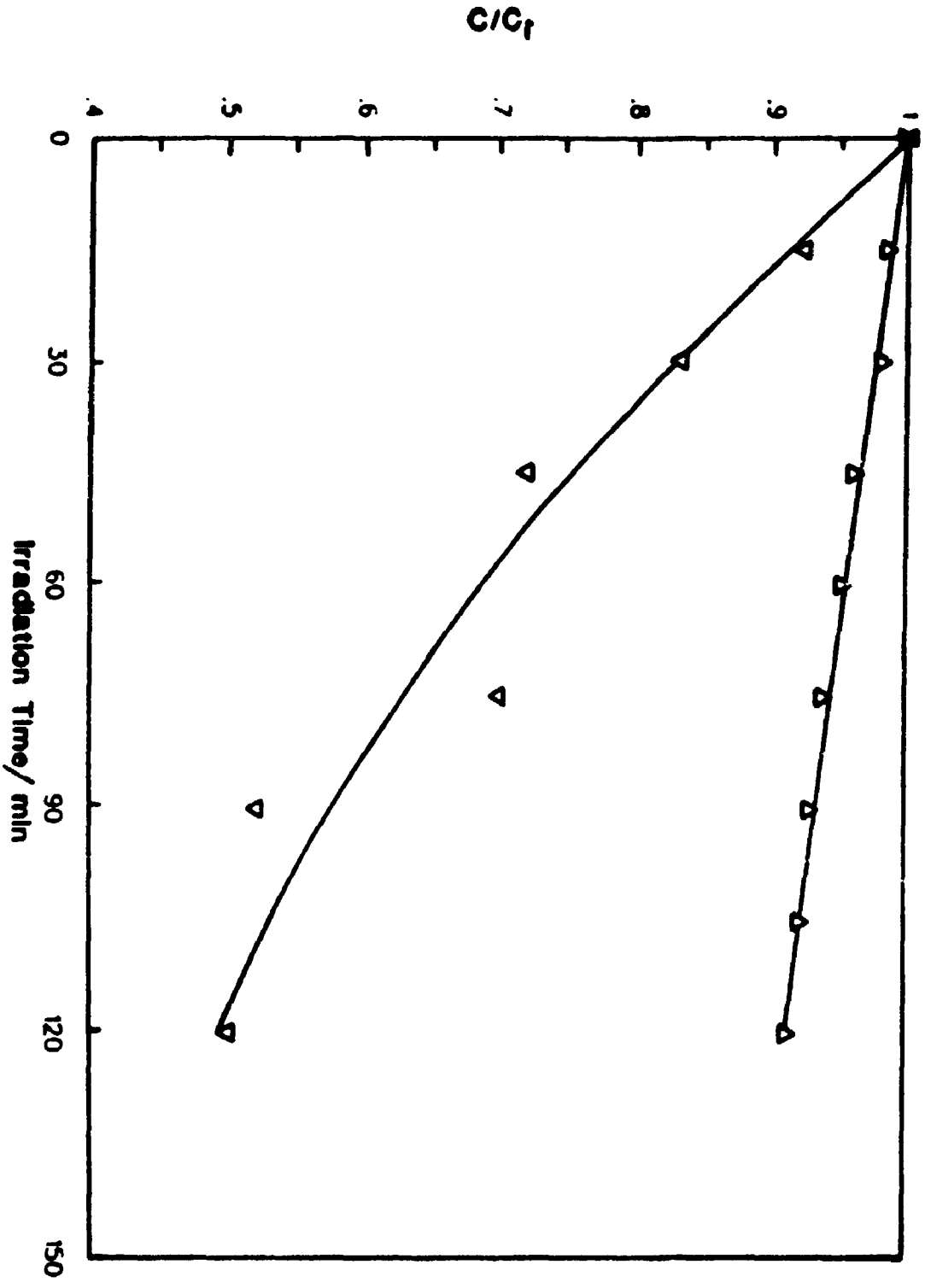
C/C0
.4
.5
.6
.7
.8
.9
1
0
30
60
90
120
150
Irradiation Time/ min

TABLE VI.4. PHENOL DEGRADATION KINETICS AND EFFICIENCY PARAMETERS

Solution volume, 2.2 L; Lamp power, 15 W; flow rate 150 mL/min

[Phenol] (μM)	Apparent kinetic constant k_{APP} (h^{-1})	Half life $t_{1/2}$ (h0)	Quantum Yield (ϕ)
557	0.046	15.2	0.0063
42	0.35	1.9	0.0038

out at two different concentrations: 42 and 557 μM, at "natural" pH (4.5) using 2.2 L of solution at a flow rate of 150 mL/min, obtaining conversions in one hour operation from 4.6% at 556 μM to 26.0% at 42.1 μM. Changes in the normalized phenol concentration (C/C_i) as a function of the illumination time for two different initial concentrations are shown in Fig. VI.14. Kinetic and quantum yield parameters were obtained and are presented in Table VI.4.

The values obtained for the quantum yield were 0.0021 ± 0.0005 and 0.0035 ± 0.0005. These values are similar to those obtained for MeB. The efficiency factors EE/O and PTEF for the photodegradation of phenol are discussed in the next section.

VI.13. ENERGY EFFICIENCY OF THE PHOTOCATALYTIC PROCESS IN THE NOVEL PHOTOREACTOR, PHOTO-CREC II

VI.13.1 ELECTRICAL ENERGY PER ORDER (EE/O)

Energy efficiency of the photocatalytic process was evaluated in the present thesis using the Electrical Energy per Order (EE/O), as defined and explained in Chapter IV and the Photochemical Thermodynamic Efficiency Factor (PTEF), developed in the present study and defined as well in Chapter IV.

Since the photocatalytic degradation rate of the model pollutant in the systems tested follows first-order kinetics, it is possible to calculate the electrical efficiency of the photocatalytic process by using the figure-of-merit "Electrical Energy per Order" (EE/O) that was introduced by Bolton et al. (1992) and discussed in Section IV.1.
The EE/O values were calculated from the equation that relates EE/O with the k_{app} :

$$EE/O = \frac{145.25P}{V.k_{app}} \qquad \text{(VI.4)}$$

Where P is the lamp power (kW), V is the total volume (L) and k_{app} is the apparent kinetic constant. The results obtained are shown in Figs. VI.14 and VI.15.

These results show that at a flow rate of 150 mL/min, the EE/O varies from 50 at $[MeB]_i = 6$ μM; to 145 at $[MeB]_i = 45$ μM. The best values are obtained at lower

Figure VI.15: Effect of initial concentration of MeB on the electric energy per order (EE/O). Experimental runs were conducted using the PHOTO-CREC II reactor under the following conditions: solution volume, 2.2 L; lamp power, 15 W; flow rate, 150 mL/min.

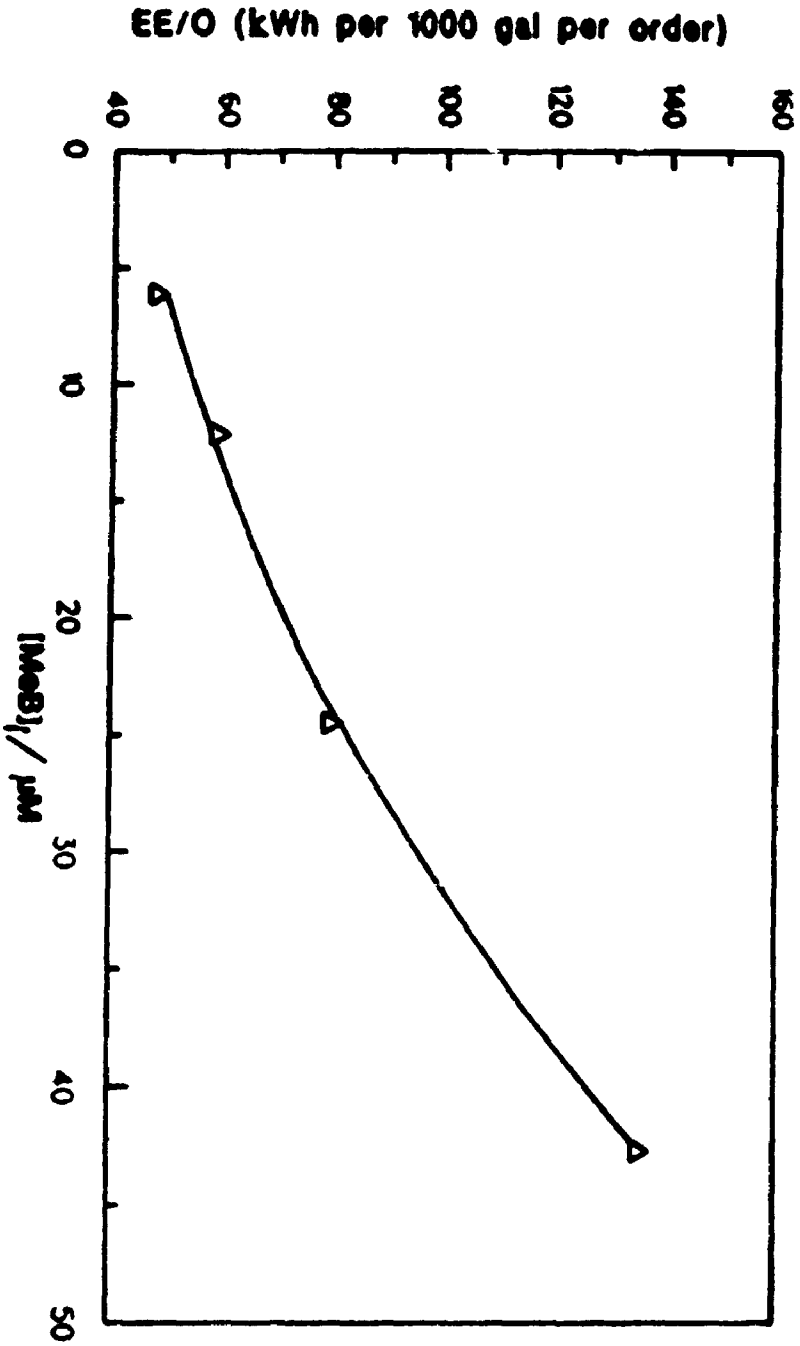
EE/O (kWh per 1000 gal per order)
40
60
80
100
120
140
160
0
10
20
30
40
50
MWBI, /mM

Figure VI.16: Effect of flow rate on the electric energy per order (EE/O). Experimental runs were conducted using the PHOTO-CREC II unit under the following conditions: solution volume, 2.2 L ; lamp power, 15 W; initial MeB concentration, 12 μM.

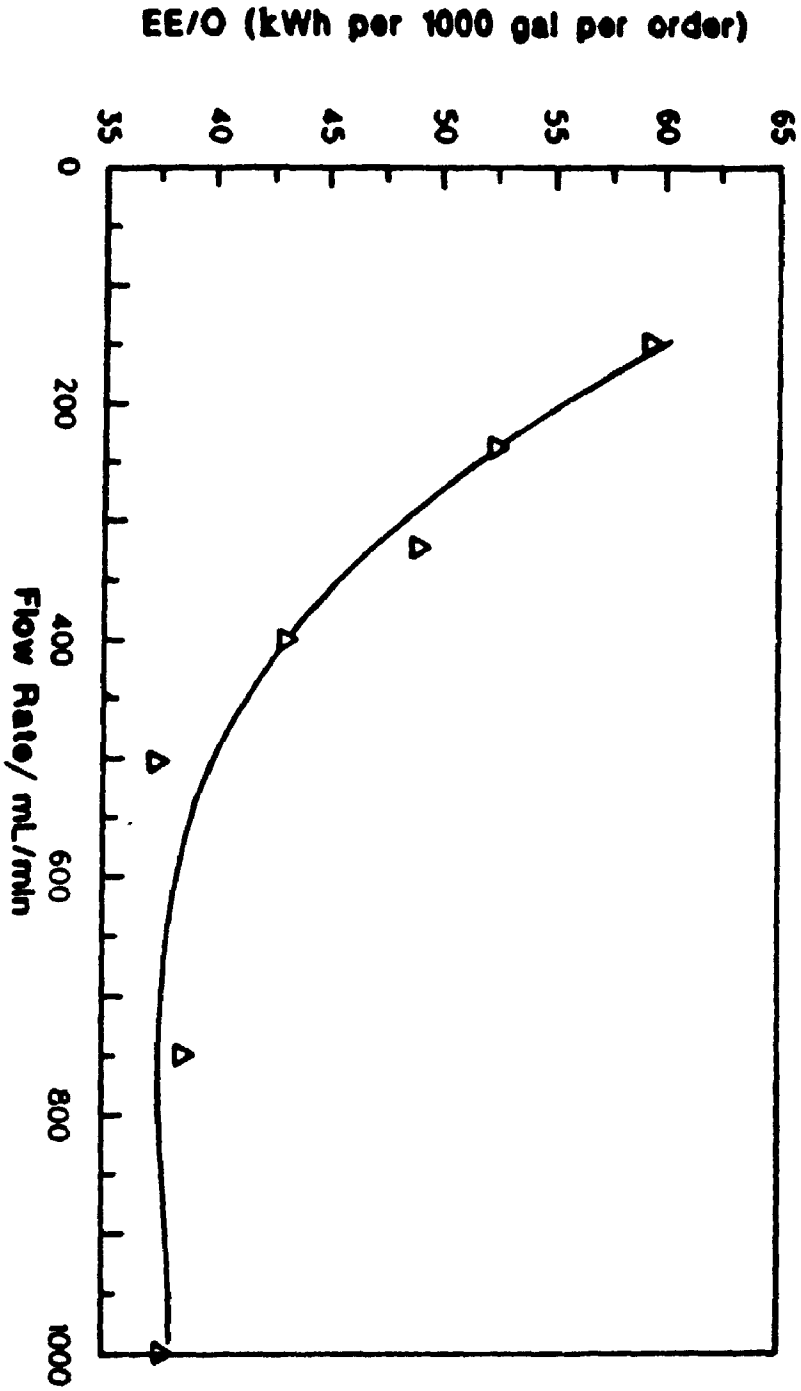
EE/O (kWh per 1000 gal per order)
35
40
45
50
55
60
65
0
200
400
600
800
1000
Flow Rate/ mL/min

TABLE VI.5 EFFICIENCY FACTOR

ELECTRICAL ENERGY PER ORDER (EE/O)

Concentration of MeB (μM)	Flow rate (mL/min)	EE/O (kW/h per 1000 gal per order)
6.2	150	48.3
12.0	150	59.5
24.5	150	80.5
42.7	150	135.7
12.0	237	52.6
12.0	322	49.1
12.0	503	37.6

TABLE VI.6

ELECTRICAL ENERGY PER ORDER (EE/O) FOR SEVERAL REACTOR SYSTEMS

MODEL POLLUTANT	TYPE OF TiO_2 SYSTEM	INITIAL CONCENTRATION (μM)	EE/O	REF.
Methylene Blue	Inmobilized PHOTO-CREC II Reactor	12	38	This Thesis
Methylene Blue	Inmobilized Spiral, Tin Film Reactor	10	83	Matthews (1989)
Methylene Blue	Slurry	12	4888	Valladares (1993)
Phenol	Inmobilized PHOTO-CREC II Reactor	42	160	This Thesis
Mix of Phenols	Inmobilized, Nulite Reactor	63	2725	Al Ekabi et al. (1990)
Phenol	Slurry	100	552	Okamoto et al. (1985)
Phenol	Slurry	1000	17251	Wei et al. (1990)

concentrations of the model pollutant. This result is due to k_{app} decrease with the initial concentration as was explained in Section VI. 7.

With experiments at an initial concentration of MeB of 12.0 μM and different flow rates, there is an increase in the photocatalytic efficiency (low EE/O) when the flow rate increases. The best value obtained for the EE/O was 38 at 500 mL/min. It is important to note that the PHOTO-CREC II, with these experimental results obtained in a prototype unit (150 hours of operation) and even without final optimization, the EE/O as low as 38. This is clearly encouraging and supports the innovations introduced with PHOTO-CREC II. Several EE/O values have been calculated from different publications for different photocatalytic reactor systems and are shown in Table VI.6. As can be seen some the EE/O values reported are very high. What makes the PHOTO-CREC II system to have low EE/O values is the fact that using such a weak lamp (15 W) the reaction rates are relatively high. The reason for that is a design that allows an optimum contact between the pollutant in the solution with the illuminated TiO_2 supported on the glass mesh, eliminating the problems of mass transfer and other inefficiencies that are present in other designs.

VI.13.2 PHOTOCHEMICAL THERMODYNAMIC EFFICIENCY FACTOR (PTEF)

As stated in Section IV.4 of this thesis, the PTEF index $\eta/[-\nu\Delta H_{OH}^{\circ}]$, provides a sound methodology for assessing photocatalytic efficiency as well as for comparing the relative efficiencies of different photochemical reactors. It is important to mention, as discussed in Chapter II, that to apply this analysis the following data are required: initial photoconversion rates of model pollutants at different pollutant concentrations, lamp power and total volume of the water treated.

While the volume of the technical literature regarding photocatalysis of organic pollutants with TiO_2 is profuse, there is only a relatively small number of publications reporting all the data needed to calculate PTEFs for several organic pollutants. In this context and through the review of the technical literature, the following cases were considered for PTEF calculations:

Figure. VI.17 $\{\eta/[-\nu\Delta H_{OH^*}]\}$ for different initial concentrations of model pollutant calculated from the data of Terzian et al. (1991) for *m*-cresol.

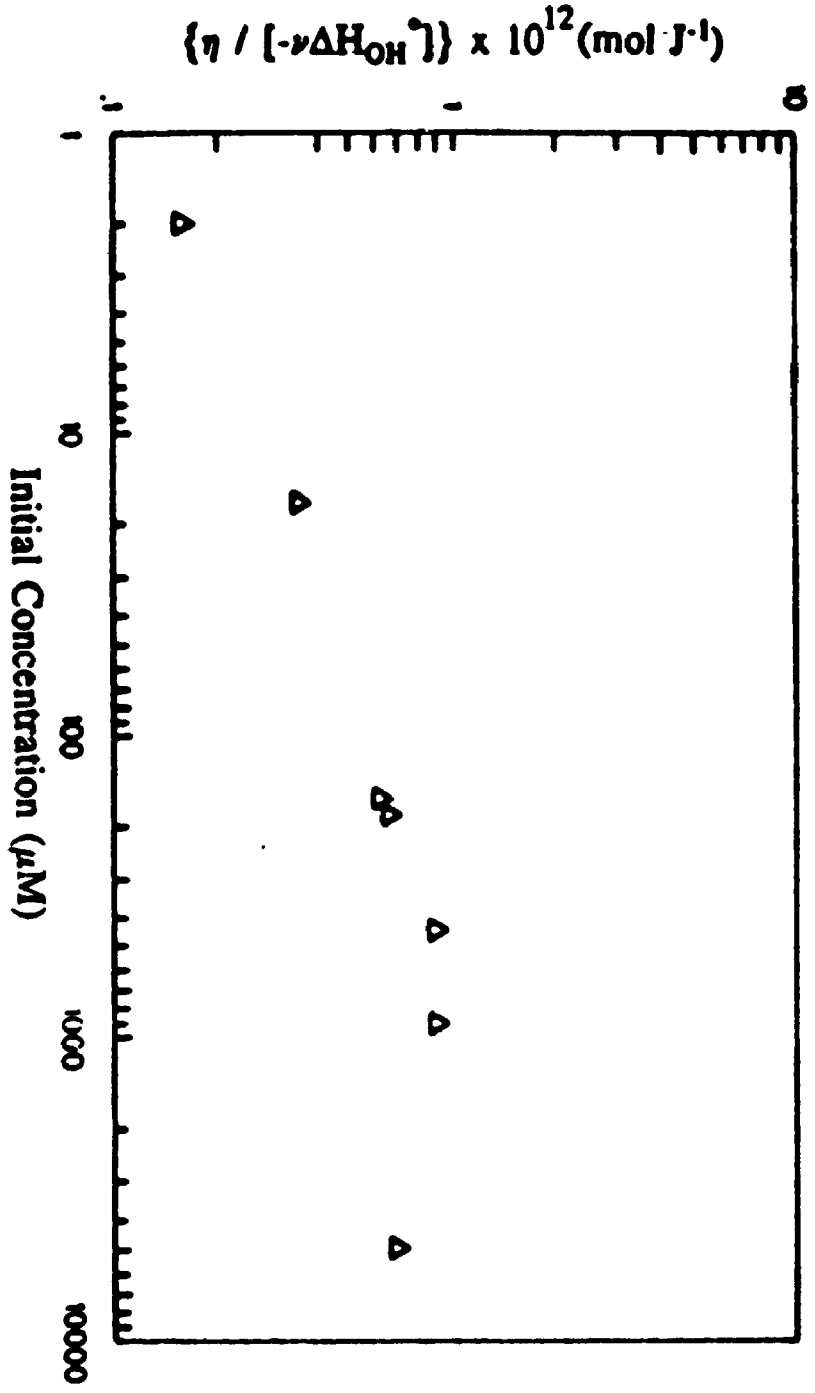
{η / [-νΔH_OH•]} x 10^12 (mol J^-1)
Initial Concentration (μM)
10000
1000
100
10
1

1) Case 1: Data from Terzian (1991).

Terzian et al. (1991) developed a comparative study of the initial photocatalytic conversion rates of *m*-cresol, *o*-cresol and *p*-cresol using TiO_2 in the anatase form from Degussa (P-25). Experiments were carried out in a 50 mL pyrex glass reactor with 100 mg of catalyst and a Hg/Xe, 900 W lamp.

The *m*-cresol results (Figure VI.16), clearly display a steady increase of $\eta/[-\nu\Delta H_{OH}^{\circ}]$ with initial concentrations. This trend continues until an approximate plateau value of 1×10^{-12} mol J^{-1} is achieved. Although, as will be discussed later, PTFEs are in the low range, data from this study helps to demonstrate that $\eta/[-\nu\Delta H_{OH}^{\circ}]$ increases with the initial concentration of pollutant, with a plateau reached at high initial concentrations. It can be argued that under these conditions the pollutant photoconversion rate equals the rate of •OH radical formation. This upper value of $\eta/[-\nu\Delta H_{OH}^{\circ}]$ represents the maximum efficiency or maximum PTEF achievable with this particular design.

2) Case 2: Data from Matthews (1988)

Matthews (1988), carried out an extensive study of the initial photocatalytic conversion rates of 22 organic solutes over a UV irradiated film of TiO_2 from Degussa (P-25). 75 mg of TiO_2 were employed to coat a 7 m long 65 turn spiral of borosilicate glass tube with a spiral volume of 90 cm^3. A 20 W black light blue fluorescent tube and a 40 mL water pollutant solution was used in the experiments.

$\eta/[-\nu\Delta H_{OH}^{\circ}]$ results for five of these compounds (benzoic acid, phenol, acetone, chloroform, salicylic acid, 2-chlorophenol, 4-chlorophenol and chlorobenzene at various initial concentrations (Figure VI.17), show, as in the case of Terzian et al., a steady increase with C_i to a plateau value of 2.0×10^{-9} mol J^{-1}.

While this limiting $\eta/[-\nu\Delta H_{OH}^{\circ}]$ value is higher than that obtained from the data of Terzian et al., a striking result is the relative independence of the PTEF with the particular model compound used. Thus, the analysis of Matthews' data in the context of the PTEFs points toward two important conclusions:

Figure. VI.18 $\{\eta / [-\nu\Delta H_{OH}^{\bullet}]\}$ for different initial concentrations of model pollutant calculated from de data of Matthews (1988). Acetone; Chloroform; Phenol; 2-Chlorophenol; Chlorobenzene.

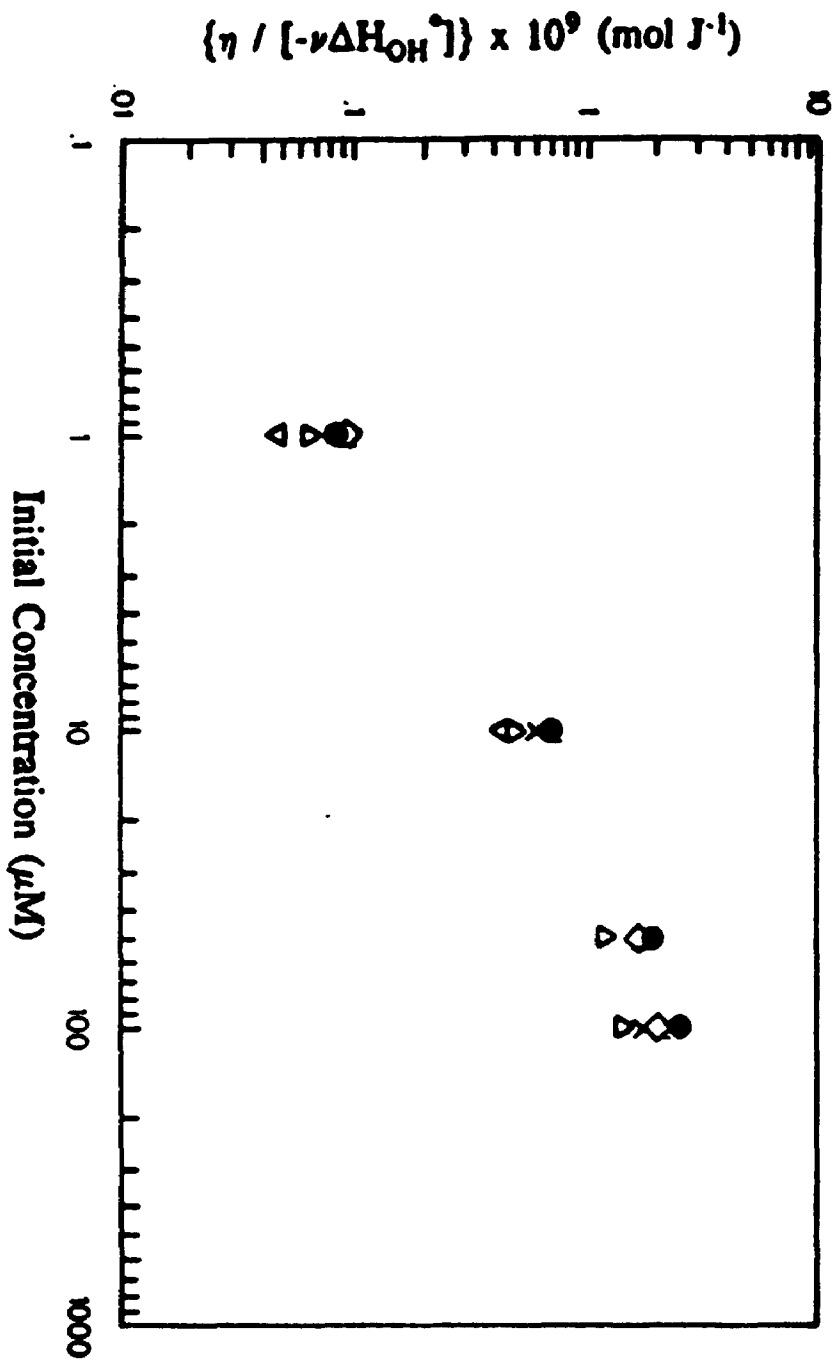
{η / [-νΔH_OH•]} x 10^9 (mol J^-1)
Initial Concentration (μM)
1
10
100
1000

a) PTEFs can be used effectively to rank efficiency in photocatalytic reactors,

b) PTEFs at higher concentrations are a weak function of the specific molecule photoconverted and this implies a correlation of the photoconversion pollutant rates with ·OH radical formation rate.

3) Case 3: Data from Ollis (1985)

Ollis (1985) conducted photocatalytic experiments using a slurry reactor with a loading of 1 g/L TiO_2 in water. The slurry unit had volume a 600 mL volume and was equipped with a 105 W lamp. Ollis tested 12 halogenated hydrocarbons. With the exception only of perchloroethylene, all the other compounds tended to yield a maximum $\eta/\Delta H$ of (0.4-0.6) x 10^{-9} mol J^{-1}, as is shown in Fig. VI.19. This allows the following conclusions:

a) Maxima observed for $\eta/[-\nu\Delta H_{OH}^{*}]$ with the Ollis data are at high level being however, smaller than those from the data of Matthews ($2x10^{-9}$ mol J^{-1}). It should be pointed out that the volume of Ollis' reactor was 600 mL or 15 times the unit of Matthews with a volume of 40 mL. Thus, increasing reactor volume introduces a major challenge to the engineering of photocatalytic reactors and may explain the lower $\eta/[-\nu\Delta H_{OH}^{*}]$ values obtained by Ollis. As well, this demonstrates that photocatalytic reactors can be effectively ranked in terms of their efficiencies using PTEFs.

b) The $\eta/[-\nu\Delta H_{OH}^{*}]$ values obtained with Ollis' data seem to indicate independence of molecular structure. This is particularly true at higher concentrations, which points toward experiments with high pollutant concentrations as the best method for assessing with confidence equipment performance through PTEF values.

Case 4: This Thesis

Once PTEFs were obtained for the above mentioned references it was found relevant to establish how the PHOTO-CREC II reactor ranked in terms of PTEFs values with respect to the above described units. It should be recalled that PHOTO-CREC II was a 2.2 L volume reactor equipped with a 15 W lamp.

Figure. VI.19 $\{\eta/[-\nu\Delta H_{OH}^{\circ}]\}$ for different initial concentrations of model pollutant calculated from the data of Ollis (1985) for Dichloroethane; Monochloroacetic Acid; Dichloroacetic acid; Perchloroethylene.

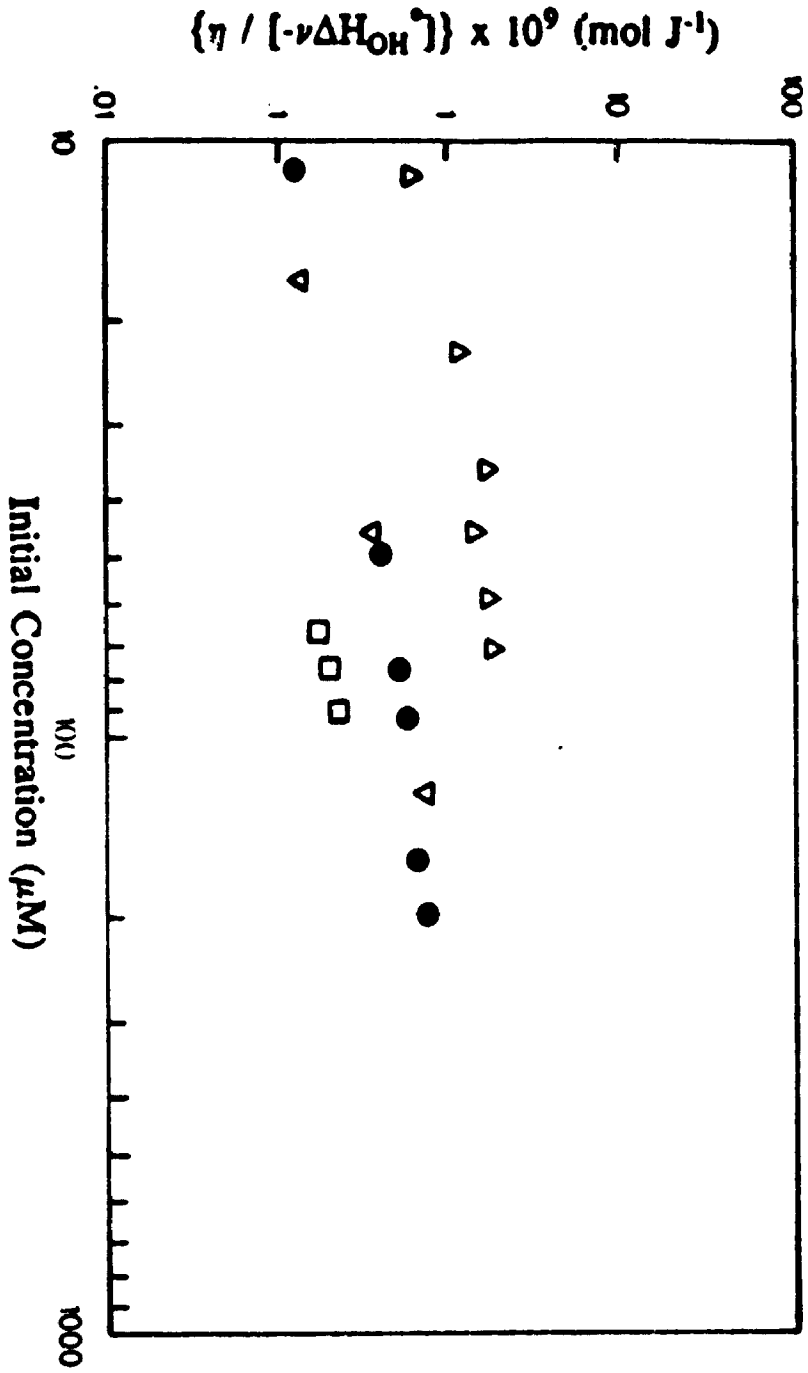
{η / [-νΔH_OH•]} x 10^9 (mol J^-1)
10
8
6
0
1000
Initial Concentration (μM)

Figure. VI.20 $\{\eta/[-\nu\Delta H_{OH}^{\bullet}]\}$ for different initial concentrations of model pollutants calculated from the data of this Thesis: Methylene Blue; Phenol.

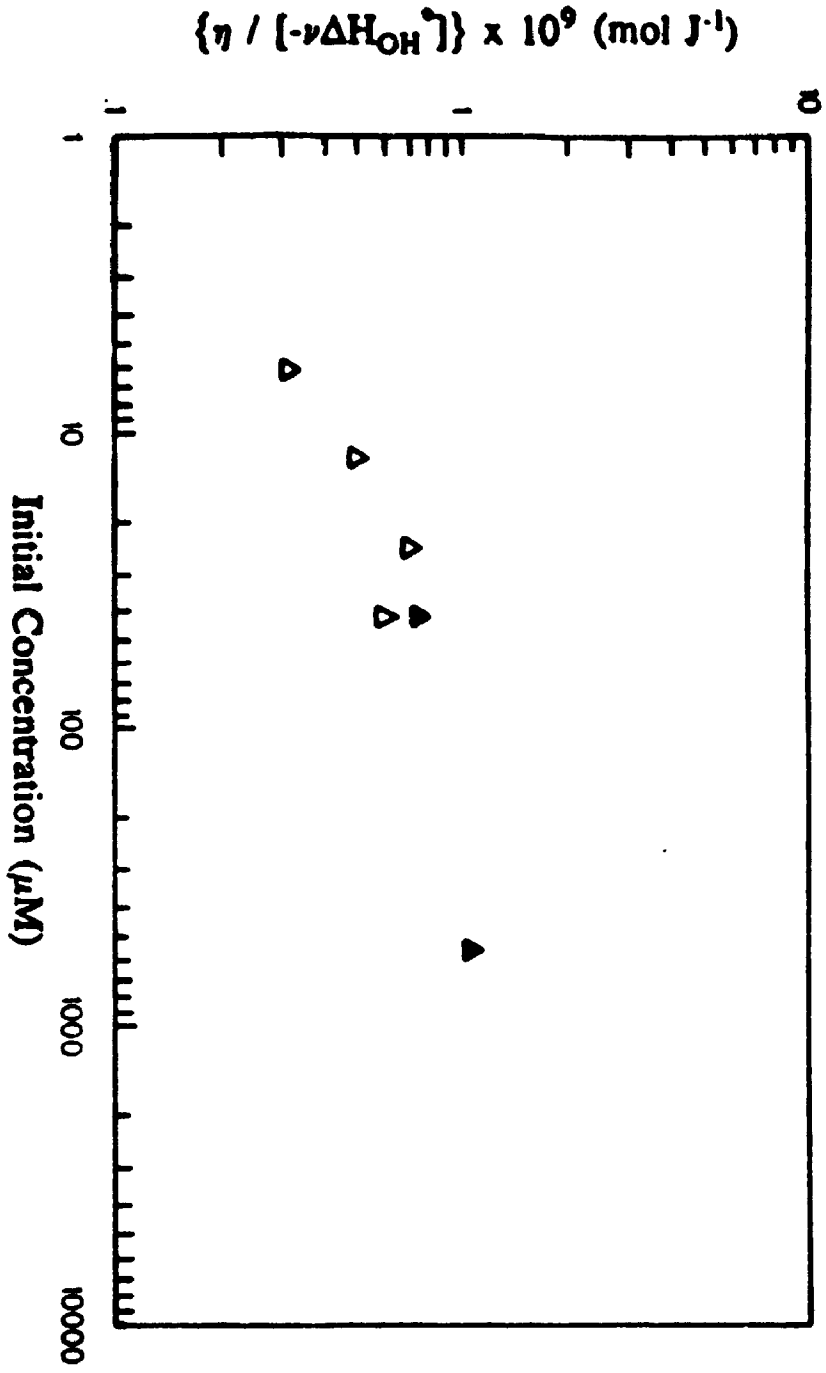
{η / [-νΔH_OH°]} x 10^9 (mol J^-1)
Initial Concentration (μM)
1
10
100
1000
10000

Results of PTEF with data of this Thesis, presented in Figure VI.19, show the following:

a) A maximum $\eta/[-\nu\Delta H_{OH}^{\bullet}]$ value of $\sim 10^{-9}$ mol J^{-1} was obtained. While these values are somewhat smaller than the best observed with the 90 mL reactor of Matthews ($2x10^{-9}$), they are, however, significantly higher than the ones in the 600 mL Ollis unit ($0.7\text{-}1.10^{-9}$). It is important to emphasize that results obtained with the PHOTO-CREC I (in between the lowest and highest PTEFs) were achieved with a unit having a volume 50 times larger than that of Matthews. This was achieved still keeping PTEFs in a comparable range.

b) Another interesting observation concerned the methylene blue and phenol experiments.The $\eta/[-\nu\Delta H_{OH}^{\bullet}]$ values for the two compounds fall in an almost single curve for PHOTO-CREC II (Figure VI.19), which also points to the small dependence of the PTEFs values on a particular molecular structure at higher concentrations. These results provide support for possible extrapolations of PTEFs values obtained in PHOTO-CREC II to other pollutants to be photoconverted eventually in the same reactor.

In summary, initial rate data of the technical literature and experimental results demonstrates that good PTEF efficiencies were achieved for a number of photocatalytic reactors. In particular, high PTEF values were achieved with PHOTO-CREC, as described in Fig. VI.21, in the context of a unit with the largest volume reported (2.2 L reactor). These high PTEF values, 1 x 10^{-9} and 2 x 10^{-9} mol J^{-1} for 150 and 500 mL min^{-1} water recirculation respectively, are encouraging and suggest a good potential for scaled-up versions of the PHOTO-CREC reactor.

Moreover, review of the PTEFs helps to demonstrate that efficiencies of current designs, 1-2 x 10^{-9} mol J^{-1}, are three orders of magnitude below the so-called "ideal" PTEF efficiency, 3 x 10^{-6} mol J^{-1}. Thus, there is still significant latitude for photocatalytic reactor technical improvements.

Figure. VI.21 Maximum Efficiency Factors $\{\eta / [-\nu\Delta H_{OH}^{*}]_{max}\}$ and reactor volume for several authors: Terzian; Matthews; Ollis; Valladares (this Thesis).

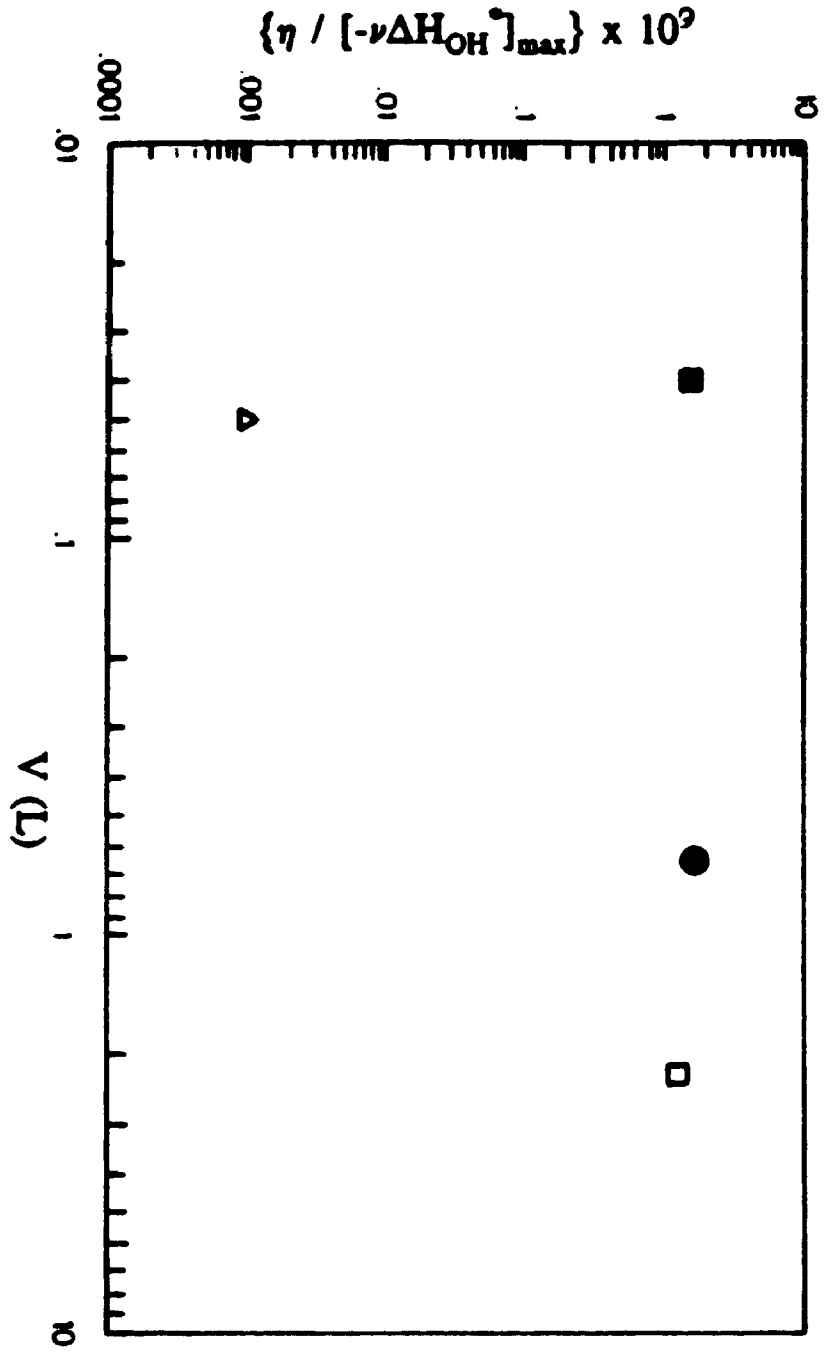
$\{\eta / [-\nu\Delta H_{OH}^{\circ}]_{max}\} \times 10^2$
1000
100
10
1
0.1
V (L)
10
1
0.1

VI.14. KINETIC MODELLING AND MASS TRANSFER PHENOMENA

Given the potential combined effects of mass transfer and the photocatalyzed reaction, a model including both effects was considered. This model is based in the following assumptions:

a) The process of mass transfer, as described in Figures VI.22 and VI.23 takes place between "bundle of fibers" (0.15 cm in diameter) with a ribbon shape, forming the mesh and the pollutant in the solution. These fiber bundles hold the immobilized TiO_2 and are contacted by the water stream.

b) The water stream flows perpendicular to the mesh of fiber bundles. This assumption is adequate considering the special design adopted for the PHOTO-CREC II reactor.

c) Water recirculation is high enough to assure that the pollutant concentration C(t,z) is a function only of the time on stream under irradiation.

d) The adsorption of the pollutant on the TiO_2 follows an equilibrium Langmuir isotherm: (refer to section IV.3)

$$q = K_1K_2\ C/(1+K_1C) \qquad (VI.4)$$

where:

- q = amount of pollutant adsorbed based on the unit weight of mesh (μmol/gmesh).
- C = pollutant concentration (μM).
- K_1 = adsorption constant (μM^{-1})
- K_2 = adsorption constant (μmol gmesh^{-1})

Thus, under these considerations and model assumptions the following pollutant mass balance in the photocatalytic unit can be considered:

Figure. VI.22 Schematic representation of the water flow patterns in the vicinity of the glass mesh illustrating the sudden changes in flow direction.

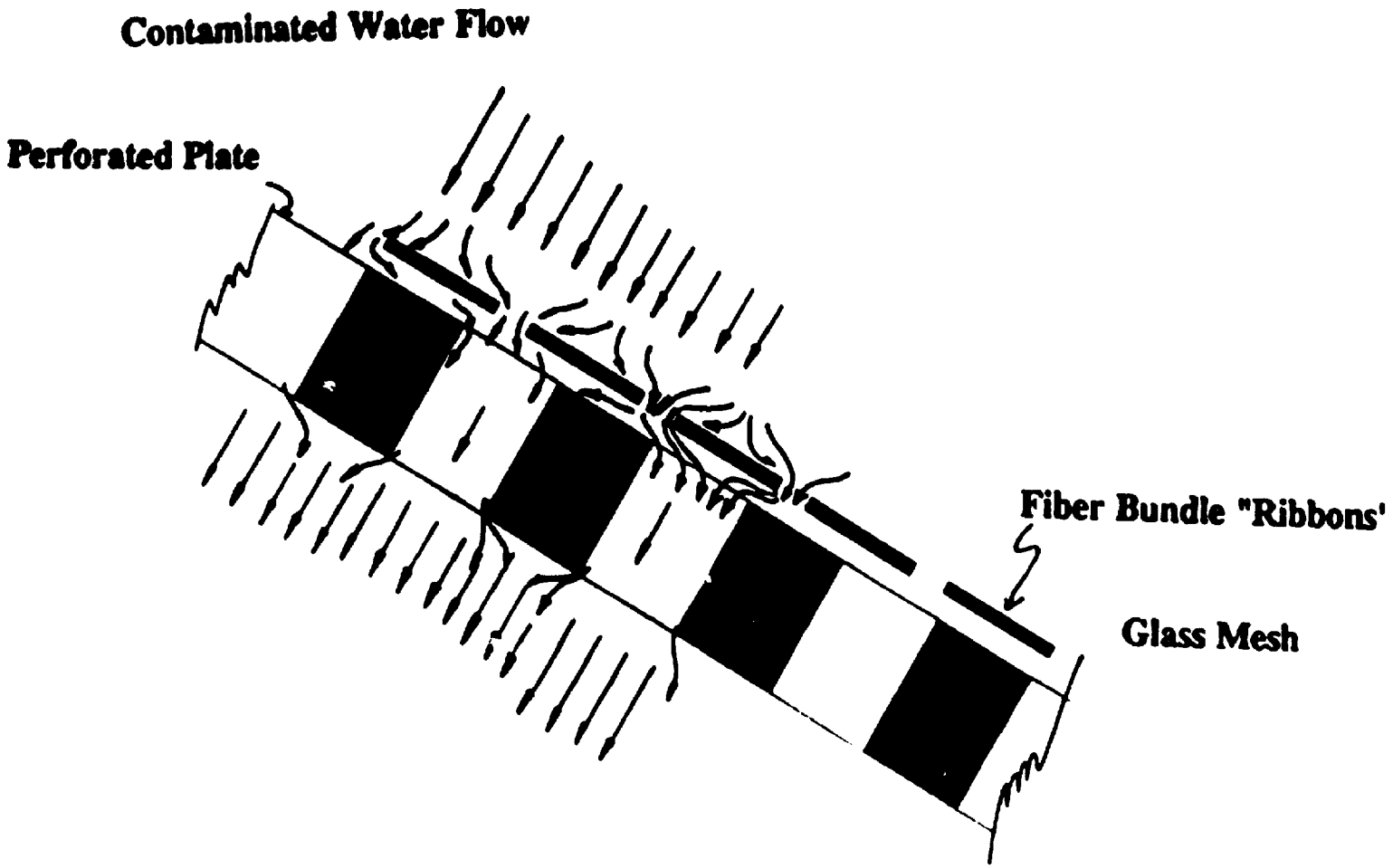
Contaminated Water Flow
Perforated Plate
Fiber Bundle "Ribbons'
Glass Mesh

Figure. VI.23 Schematic representation of the open mesh area and the glass mesh area with illustration of the square holes left open for the circulation of the fluid.

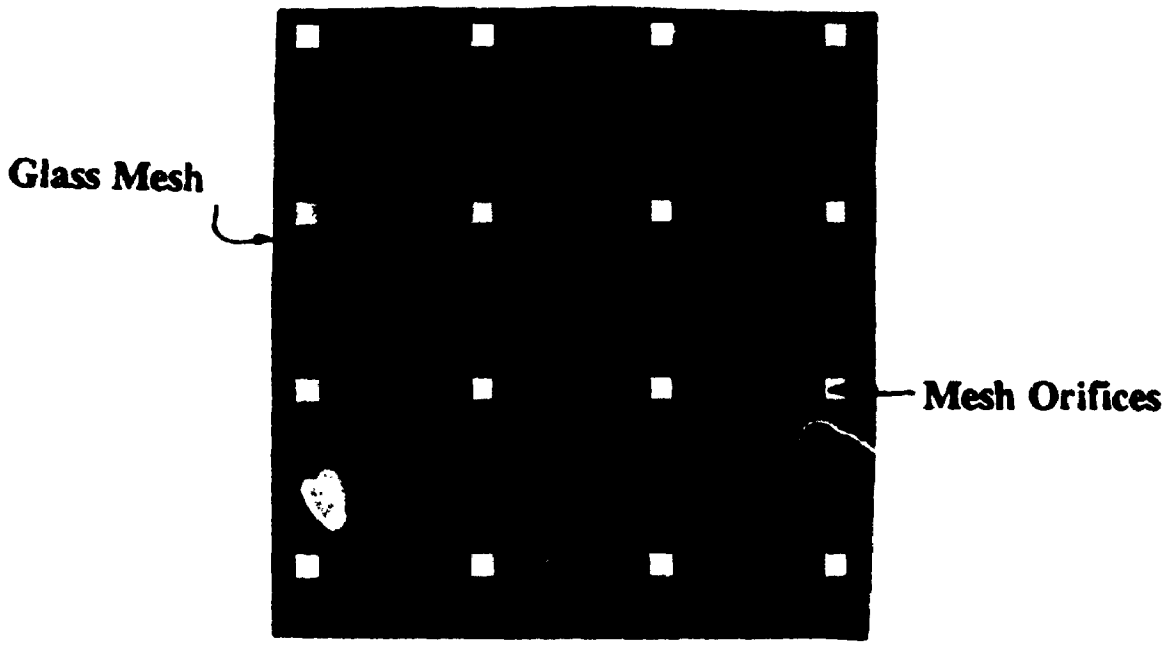
Glass Mesh
Mesh Orifices

$$([C]_t - [C]_{t+\Delta t})V = k_f A_m (C - C_I)\Delta t \qquad \text{(VI.5)}$$

where:

C = concentration of pollutant in the bulk phase (μM).

C_I = concentration of pollutant in the interface between the water and the bundle of fibers (μM).

k_f = mass transfer coefficient [L $dm^{-2}.s^{-1}$]

V = total volume of water [L]

t = irradiation time [s]

A_m = total external area of fiber bundles (dm^2)

taking, $\Delta C/\Delta t = dC/dt$ when $\Delta t \to 0$, it is possible to write:

$$-dC/dt = [k_f A_m/V](C - C_I) \qquad \text{(VI.6)}$$

This equation represents the change of pollutant concentration with time as a result of pollutant transfer through the interface of the fiber bundle.

Furthermore, a second mass balance can be established at the interface of each fiber bundle:

$$k_f A_m (C - C_I) = r\, w_m \qquad \text{(VI.7)}$$

where:

r = rate of pollutant photodegradation based on the unit weight of mesh [μmol $gmesh^{-1}$ s^{-1}]

w_m = total weight of impregnated mesh with TiO_2 [gmesh]

This equation expresses pollutant transfer through the boundary layer of the fiber bundle, making it equal to the amount of pollutant consumed by photochemical reaction.

It is frequently found that the photocatalytic reaction is irreversible and first order on the pollutant surface concentration. Then, it is possible to write:

$$r = -k P^a q \qquad \text{(VI.8)}$$

where:

k = kinetic constant for the photocatalytic reaction ($s^{-1} W^{-a}$)

P = electrical power of the lamp (W)

a = exponent involved in the function representing the influence of the electrical power of the lamp on the rate of photodegradation.

Considering these various assumptions the following relation results:

$$k_f A_m (C-C_I) = k P^a q w_m \qquad (VI.9)$$

Adsorption of the MeB pollutant on the catalyst surface takes place following a Langmuir model. The validity of this isotherm was demonstrated in the experiments under "dark conditions" in Section VI.3. Then Eq. (VI.9) can be modified to:

$$k_f A_m (C-C_I) = k K_1 K_2 P^a C_I w_m / (1+K_1 C_I) \qquad (VI.10)$$

Given that the "a" exponent can be considered equal to 1, as demonstrated in Section VI.9, the following set of equations have to be solved simultaneously:

$$-dC/dt = [k_f A_m/V] (C-C_I) \qquad (VI.11)$$

$$k_f A_m (C-C_I) = [k P K_1 K_2/(1+K_1 C_I)] C_I w_m \qquad (VI.12)$$

with $k_1 = k K_1 K_2 P$

In the proposed model there are three parameters influencing the change of concentration in the bulk k_f, k_1 and K_1. The K_1 parameter was already defined with independent adsorption experiments (initial period under dark conditions). The other two parameters, k_f and k_1, can be determined as follows:

a) The kinetic constant k_1 was determined at Q > 500 mL/min. From theory, it is known that if the flow rate is high enough, only one equation, instead of two [Eqs (VI.11) and (VI.12)], is required to model the reacting system;

$$-dC/dt = [(k_1C/(1+K_1C)]\ w_m/V \qquad (VI.13)$$

Moreover, if the concentration of pollutant is low enough, parameter estimation can be carried out under conditions where, $K_1C \ll 1$; then the resulting equation can be solved yielding

$$\ln [C/C_i] = - k_1.\ w/V_T.\ t$$

or

$$k_{app} = k_1.w_m/V = 0.0260\ s^{-1}$$

or

$$k_1 = 0.0260\ V/w_m\ (cm^3\ gcat^{-1}\ s^{-1})$$

b) Once the $k_1.w_m/V$ and k_1 are determined, there was only one parameter left, k_f. In order to simplify the mathematical approach, k_f was determined for pollutant concentration conditions where $K_1C \ll 1$. Under these conditions, it can also be stated that $K_1C_i \ll 1$ given that $C_i < C$.

Then the following set of equations is left for $Q < 500$ mL and $K_1C_i \ll 1$

$$dC/dt = [k_fA_m/V]\ (C-C_I) \qquad (VI.14)$$

$$k_fA_m(C-C_I) = k_1C_Iw_m \qquad (VI.15)$$

Rearranging Eq (IV.15) and writing C_i as a function of C,

$$C_I = [k_fA_m/(k_fA_m+k_1w_m)]\ C \qquad (VI.16)$$

and making a substitution of this result in Eq (VI.13) the following apparent kinetic constant is obtained:

$$k_{app} = 1/[1/k_1 w_m + V/k_f A_m] \qquad (VI.17)$$

Using the above equation and the experimental information obtained in separate experiments (k_1), it was possible to calculate the mass transfer constant (k_f). The calculation of k_f requires assessment of the fiber bundle area A_M in direct contact with the flowing water stream. The fiber bundles have the geometry of ribbons and are weaved in the form of a tissue with fibers placed at an orientation of 90°. Evaluation of the external surface of the total fiber bundles area used in the 15 baskets yielded an estimated area of 2.6×10^3 cm^2.

In order to provide a valid comparison of the extent of mass transfer in PHOTO-CREC II, a good indicator is the dimensionless Sherwood number Sh (1960). Sh and its correlation with the Reynolds number (Re) were calculated using the experimental k_f values and the following relations:

$$Sh = k_f \, d_{eq}/D_{AB} \qquad (VI.18)$$

where d_{eq} = diameter of the equivalent sphere having the same area per unit volume of fiber bundles with estimated thickness at 0.025 cm ($d_{eq} \sim 6$ fiber bundle tickness)

D_{AB} = diffusivity of MeB in water, estimated at 10^{-5} cm^2/s

$$Re = u \, \rho \, d_{eq}/\mu \qquad (VI.19)$$

where u = average velocity of the fluid in the proximity of the fiber bundle (space left between the fiber bundles) (cm.s^{-1})

ρ = density of the water (g.mL^{-1})

μ = viscosity of the water (g.cm^{-1}.s^{-1})

Experimental values obtained for Sh and Re are reported in Table VI.7. For Re changing from 6.6 to 30 a progressive increase of k_f was observed, and this was a good indicator of the data consistency. Also it was observed that the high Sh values, obtained in PHOTO-CREC II, are pressumably due to the special flow pattern of this unit. There were sudden changes of fluid direction in the vicinity of the fiber bundles (ribbons) supported in a perforated plate. Thanks to this design, it was possible to operate PHOTO-

Figure. VI.24 Correlation of the Sherwood Number (Sh) with the Reynolds Numbers (Re) for PHOTO-CREC II ( ) and for the following Models: Hobson and Thodos ( ); Sherwood, Pigford and Wilkie ( );Wilson and Geankoplis ( ) and Dwivedi and Upadhyay ( ).

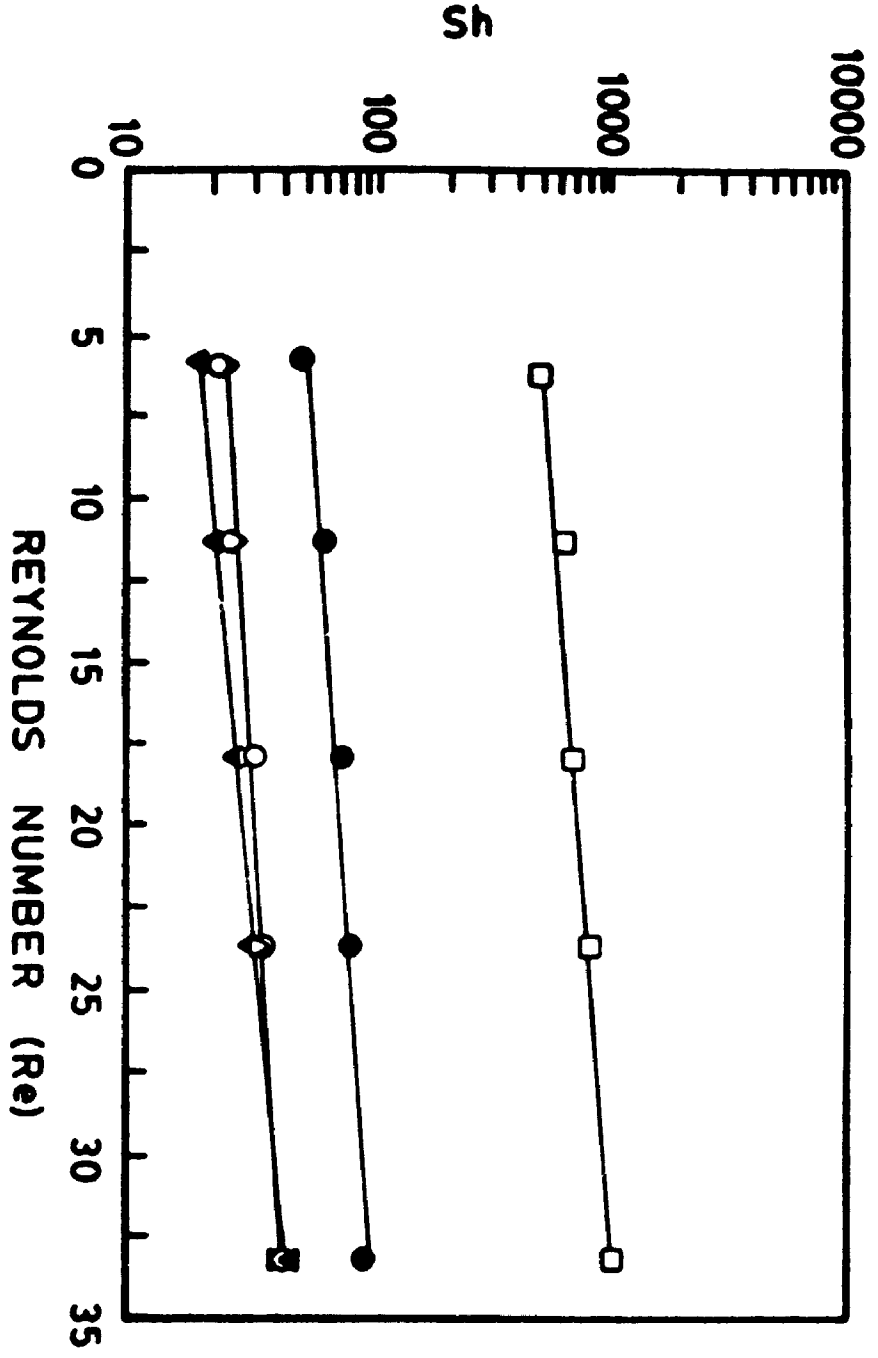
Sh
10000
1000
100
10
0
5
10
15
20
25
30
35
REYNOLDS NUMBER (Re)

TABLE VI.7

REYNOLDS AND SHERWOOD NUMBERS

Q (mL min^{-1})	v (cm s^{-1})	Re	k_{app} (s^{-1})	$k_f/10$ (cm s^{-1})	Sh
90	0.53	6.62	0.0154	3.17	475
150	0.88	11.0	0.0170	4.13	619
240	1.42	17.7	0.0178	4.74	711
320	1.90	23.7	0.0188	5.70	855
400	2.36	29.6	0.0196	6.69	1003

CREC II without mass transfer control, a remarkable result given the range of Reynolds numbers employed.

Furthermore, it was also interesting to compare the Sh values obtained with other values reported in the literature for the same range of Re numbers. Sh numbers were calculated using the following correlations for mass transfer in packed beds and liquid media:

-Correlation from Hobson and Thodos as reported by Bennet and Myers (1981),

-Correlation from Sherwood, Pigford and Wilkie as reported by King (1980),

-Correlation from Wilson and Geankoplis as reported by Geankoplis (1993),

-Correlation from Dwivedi and Upadhyay as reported by Brodkey and Hersey (1988).

It can be observed that the Sh numbers in PHOTO-CREC were always higher than the Sh values predicted by the models of packed beds of spheres. This difference ranged from 10-40 times and provides evidence of the high mass transfer achieved in the PHOTO-CREC II and of the relevance of the results obtained.

VI.15 CONCLUSIONS

Systematic experiments developed allowed the determination of physicochemical and efficiency characteristics of the proposed design system. The Langmuir adsorption Isotherm constants for the system methylene blue-TiO_2 on glass mesh obtained were to be $K_1 = 0.47 \pm 0.06\ \mu M^{-1}$ and $K_2 = 0.17 \pm 0.02\ \mu mol\ gmesh^{-1}$.

As well, at low concentrations, the photodegradation reaction showed first order kinetics and an apparent kinetic constant that changed in an inverse proportion with the initial MeB concentration. Furthermore, the water recirculation flow rate showed an influence in the kinetic constant: higher flow rates give higher kinetic constants. A constant value was reached after 500 mL/min. The light intensity and the apparent kinetic constant also showed a linear relation. The apparent quantum yields of the different experiments showed values in the range of 0.004 to 0.007, due mainly to the inherent low efficiency of the photocatalyst. The electrical energy per order (EE/O) obtained for the PHOTO-CREC II system (38-150) presented however encouraging values, in fact

they were the lowest values obtained in the open literature for photocatalytic reactors.

It was demonstrated that the PTEFs, obtained using data from a number of literature references, are independent or weakly dependent on pollutant chemical structure, being a characteristic of the specific photocatalytic reactor used. PTEF values in PHOTO-CREC II were in the range of 1×10^{9} which can be considered in the high level for PTEF values. This was particularly relevant considering the unit studied was with the largest volume for this level of PTEF.

Thus, the PTEF, established on the basis of photochemical and thermodynamic principles, can be used for optimizing designs and scaling up reactors operating with high light energy utilization. In particular, PTEF can be used for developing criteria for scaled versions of PHOTO-CREC.

A kinetic model that included the effect of mass transfer was also proposed. When the Sherwood numbers were compared with other correlations of the literature, they showed 10 to 30 times larger values. This provides evidence of the relevance of the proposed design, where changes in the direction of fluid elements close to the mesh are promoted.

CHAPTER VII
CONCLUSIONS

This research presents a photocatalytic reactor concept (PHOTO-CREC) for the photoconversion of water pollutants. In the context of the present study, the new unit was designed, manufactured, assembled, tested and operated in the course of systematic runs. As well, the performance of the PHOTO-CREC was compared with other reactor units previously reported in the technical literature.

Thus, in the context of this Thesis the following conclusions can be reported:

1. The PHOTO-CREC reactor was designed, built and successfully operated with model pollutants. The photoreactor has, as particular features, glass mesh with high TiO_2 loading on specially designed stainless steel baskets which allows for a carefully controlled water flow pattern and provides intimate contact of the illuminated TiO_2 and the pollutant dissolved in the water. The design also minimizes mass transfer controls on the photochemical reaction.
2. A method of direct impregnation of the TiO_2 anatase P25 from Degussa was developed. It was demonstrated in the laboratory that a direct TiO_2 immobilization on the glass mesh can be achieved with high loading (up to 8%) of a uniform TiO_2 distribution on a glass mesh matrix. With the impregnation method used, involving a particle dispersant (methanol-water solutions), TiO_2 is strongly bonded onto the glass mesh. The impregnated mesh, holding the TiO_2, is stable even after 150 hours under typical water flows with no detectable washing of TiO_2 particles. Moreover, by following the approach proposed,

thermal treatment (calcination) or other methods eventually affecting the anatase crystal structure are completely avoided. These findings are quite significant in order to take maximum advantage of the available mesh surface and maximize the TiO_2 irradiation.

3. Experiments developed allowed the determination of physicochemical and efficiency characteristics of the proposed design system.

The Langmuir adsorption Isoterm constants for the system methylene blue-TiO_2 on glass mesh obtained were found to be:

$K_1 = 0.47 \pm 0.07\ \mu M^{-1}$ and $K_2 = 0.17 \pm 0.02\ \mu mol\ gmesh^{-1}$.

As well at low concentrations, the photodegradation reaction showed first-order kinetics and an apparent kinetic constant that changed in an inverse proportion with the initial MeB concentration. However the water recirculation flow rate showed a linear relation on the apparent kinetic constant: higher flow rates give higher rate constants when water flow rate was changed from 100 mL/min to 500 mL/min. A constant value was reached after 500 mL/min. The light intensity and the apparent rate constant also showed a linear relation in this work. The quantum yields of the different experiments showed low values in the range of 0.004 to 0.007, due the inherent limitations of TiO_2. The electrical energy per order (EE/O) obtained for the PHOTO-CREC II system (38-150) presented encouraging values, if compared with the values obtained from the open literature for other photocatalytic reactors.

4. A kinetic model that included the effect of mass transfer was also proposed. When the Sherwood number from the model was compared with the model of Hobson and Todds and other models it showed to be 10 to 30 times bigger which provides evidence of the relevance of the proposed design proposed, where changes in the direction of fluid elements close to the mesh are promoted.

5. An efficiency index, *Photochemical-Thermodynamic Efficiency Factor* (PTEF) based on known thermodynamic and photochemical principles and with a general applicability to photocatalytic reactor systems was proposed in the context of this study. Thus, the need for criteria to compare photoreactor performance is addressed in the present study with the introduction of the "*Photochemical-Thermodynamic Efficiency Factor*"(PTEF).

   It was demonstrated that the PTEFs, obtained using data from a number of literature references, are independent or weakly dependent on pollutant chemical structure, being a characteristic of the specific photocatalytic reactor used. Thus, the PTEF, established on the basis of photochemical and thermodynamic principles, can be used for optimizing designs and scaling up reactors operating with high light energy utilization. In particular, PTEF could be used for developing criteria for scaled versions of PHOTO-CREC.

APPENDIX 1

QUANTUM YIELD CALCULATIONS

Experiments were developed to determine the light absorbed by the bare glass mesh and the supported TiO_2 photocatalyst. This was done by taking a UV diffuse reflectance spectrum at 365 nm and using an integrating sphere assembly (Simadzu Corporation). The absorbance showed the following values:

Absorbance for TiO_2 supported on glass mesh = 0.50 ± 0.05

Absorbance for the bare mesh = 0.15 ± 0.05

From these absorbances, the light fraction absorbed was calculated as follows:

Fraction absorbed by the bare mesh = $1 - 10^{-0.15} = 0.29$

Fraction Absorbed by the TiO_2 supported glass mesh = $1 - 10^{-0.5} = 0.69$

It can be concluded that the fraction absorbed by the bare mesh was 0.29, the fraction absorbed by the TiO_2 is 0.39 and the light transmitted through the mesh was 0.32. These results are illustrated in Fig.A1.

Thus, given the photon flux assessed by actinometry (potassium ferrioxalate actinometry) was 2×10^{-4} Einstein min^{-1}, it can be estimated that the photon rate absorbed by the TiO_2 was $\epsilon_{abs} = (1.05 \pm 0.05) \times 10^{-4}$ Einstein min^{-1}. This result was used for quantum yield calculations, using the following expression:

$$\phi = \frac{\text{Rate of photodegradation}}{\text{Photon rate absorbed by } TiO_2}$$

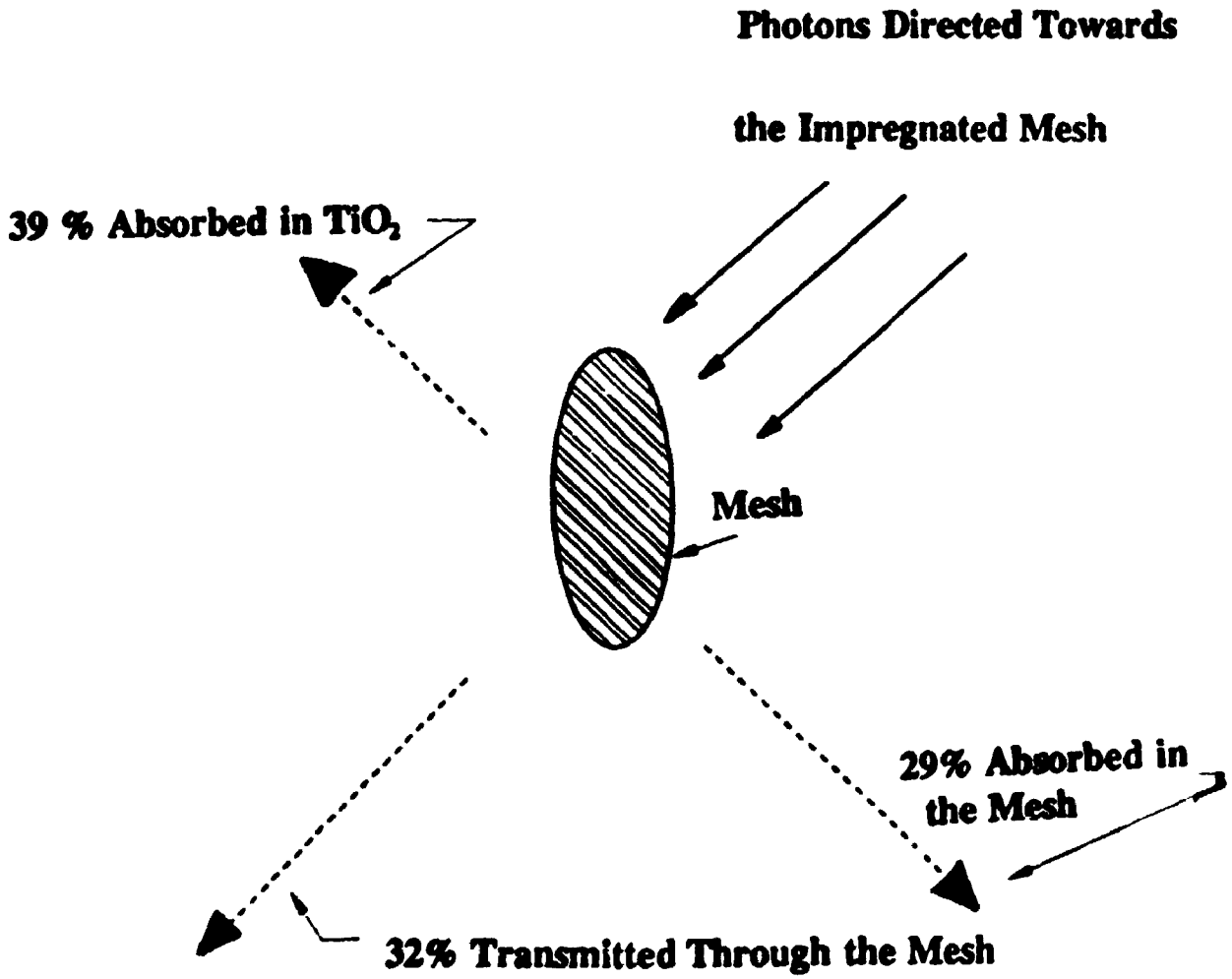
Photons Directed Towards
the Impregnated Mesh
39 % Absorbed in TiO_2
Mesh
29% Absorbed in
the Mesh
32% Transmitted Through the Mesh

REFERENCES.

Adamson, A. (1976) *Physical Chemistry of Surfaces*, Wiley, New York.

Al-Ekabi, H. and N. Serpone (1988) *J. Phys. Chem.*, 92, 5726.

Al-Ekabi and N. Serpone (1989) *Langmuir*, 5, 250.

Al-Ekabi, H. and A. Amiri (1990) In: *Proceedings of a Symposium on Advanced Oxidation Process*, Canada Center for Inland Waters, Burlington, Ontario, Canada.

Al-Ekabi, H., B. Butters, D. Delany, J. Ireland, N. Lewis, T. Powell and J. Story (1993) In: *Photocatalytic Purification and Treatment of Water and Air*, Ollis D.F. and Al-Ekabi H. (Eds.), Elsevier: Amsterdam, p 321.

Amhed S. and D.F. Ollis, (1984) *Solar Energy*, 32, 597.

Bahnemann, D., J. Cunningham, M.A. Fox, E. Pelizzetti, P. Pichat and N. Serpone (1994) In: *Aquatic and Surface Photochemistry*, Helz, G., Zepp, R. and Crosby, D., (Eds.), Lewis, Boca Raton, FL, p 261.

Barbeni, M., E. Premauro, E. Pelizzetti, E. Borgarello and N. Serpone (1985), *Chemosphere*, 14, 195.

Blanco, J. and S. Malato (1993) In: *Photocatalytic Purification and Treatment of Water and Air*, Ollis D.F. and Al Ekabi, H. (Eds.), Elsevier: Amsterdam, p 639.

Blake D., K. Magrini and J. Webb (1990) In: *Proceedings of A Symposium on Advanced Oxidation Processes*, Canada Center for Inland Waters, Burlington, Ontario, Canada.

Bolton, J.R., S. R. Cater and A. Safarzadeh-Amiri (1992) 203rd *ACS National Meeting*, San Francisco, Cal.

Bolton J.R. (1990) In: *Proceedings of a Symposium on Advanced Oxidation Processes*, Canada Center for Inland Waters, Burlington, Ontario, Canada.

Bolton, J.R. (1995) *Proceedings of the First Interamerican Conference on Environmental Issues*, Valladares, J. and de Lasa H. (Eds.), San Salvador, El Salvador.

Bolton J.R. and S.R. Cater, (1994) In: *Aquatic and Surface Photochemistry*, Helz, G., Zepp, R. and Crosby, D., (Eds.), Lewis, Boca Raton, FL, p 467.

Bockelmann, D., R. Goslich, D. Weichgrebe and D. Bahnemann (1993) In: *Photocatalytic Purification and Treatment of Water and Air*, Ollis D.F. and Al-Ekabi, H. (Eds.), Elsevier: Amsterdam p 771.

Borgarello, E. and N. Serpone (1986) *Inorg. Chem.*, 25, 4499.

Braun A.M., L. Jakob and E. Oliveiros (1993) In: *Photocatalytic Purification and Treatment of Water and Air*, Ollis, D.F. and Al Ekabi, H. (Eds.), Elsevier: Amsterdam, p 511.

Cabrera, M.I., D.M. Alfano and A.E. Cassano (1994) *Ind. Eng. Chem. Res.* 33, 303.

Carey, J.H., J. Lawrence and H.M. Tosine (1976), *Bull. Environ. Contam. Toxicol.*, 16, 697.

Carey, J.H. (1990) In: *Proceedings of A Symposium on Advanced Oxidation Processes*, Canada Centre for Inland Waters, Burlington, Ontario, Canada

Chen-Yung, H., C. Lee and D.F.Ollis (1983) *J. Catal.*, 82, 418.

Davis, A. and O. Hao (1992) *J. Catal.*, 136, 629.

Davis, A. and O. Hao (1991) *J. Catal.*, 131, 285.

de Lasa, H. and J. Valladares (1993) "Novel Photocatalytic Reactor for the Mineralization of Water Pollutants" Final Report, *Ministry of the Environment and Energy of Ontario.*

Dwivedi, P.N. and S.N. Upadhyay (1988) In: *Transport Phenomena. A Unified Approach*. Brodkey, R.S. and Hersey, H.C. (Eds.), p 621.

Edwards, B. (1995) In: *Proceedings of the First Interamerican Conference on Environmental Issues*, Valladares, J. and de Lasa H. (Eds.), San Salvador, El Salvador.

Fox, M.A. and M. Dulay (1993) *Chem. Rev.*, 93, 341.

Fujishima, A. and K. Honda (1972) *Nature*, 138, 37.

Glaze W.H., J.F. Kenneke and J. Ferry (1993) *Environ. Sci. Technol.*, 27, 17.

Herrmann, J.M., J.Disdier and P.Pichat (1988) *J. Phys, Chem.*, 90, 6028.

Hobson, M. and G. Thodos (1982) In: *Momentum Heat and Mass Transfer*, Bennett C.O. and Myers J.E.(Eds),McGraw Hill, New York, p 590.

Hypotec Ltd., (1993) *Hysim 386 - The Truly Processes Simulator,* Software Licensed to the University of Western Ontario.

Levenspiel, O., (1974) *Chemical Reaction Engineering*, Wiley, New York.

Mariangelli, R. and D.F. Ollis (1977) *AIChE J*, 23, 415.

Matthews, R.W. (1987) *J. Phys. Chem.* 91, 3328.

Matthews, R.W. (1988a) *J. Catal.*, 111, 264.

Matthews, R.W. (1988b) *J. Catal.*, 113, 549.

Matthews, R.W. (1988c) *J. Phys. Chem.* 92, 6853.

Matthews, R.W. (1989) *J. Chem. Soc., Faraday Trans*, 85 (6), 1291.

Matthews, R.W. (1991) In: *Proceedings of the Eighth International Conference on Photochemical Conversion and Storage of Solar Energy*, Palermo, Italy, Pelizzetti, E. and Schiavello M. (Eds.), p 427.

Matthews, R.W. (1993) In: *Photocatalytic Purification and Treatment of Water and Air*, Ollis D.F. and Al-Ekabi, H., (Eds.), Elsevier: Amsterdam, p 121.

Murov, S.L., I. Carmichael and G.L. Hug (1993) *Handbook of Photochemistry*, Dekker, New York, p 299.

Ollis, D.F., C.Y. Hsiao, L. Budiman and C.L. Lee (1984) *J. Catal.*, 88, 89.

Ollis, D.F. (1985) *Environ. Sci. Technol.*, 19, 480.

Ollis, D.F., E. Pelizzetti and N. Serpone (1989) *Photocatalysis, Fundamentals and Applications,* Wiley, New York, p 603.

Ollis, D.F. (1990) *Proceedings of the Eighth International Conference on Photochemical Conversion and Storage of Solar Energy,* Pelizzetti E. and Schiavello, M. (Eds.), Palermo, Italy, p 593.

Pacheco J.E., M. Mehos, C. Turchi and H. Link (1993) *Photocatalytic Purification and Treatment of Water and Air*, Ollis, D.F. and Al-Ekabi, H., (Eds.), Elsevier: Amsterdam, p 547.

Pelizzetti, E., E. Borgarello and N. Serpone (1985) In: *Photoelectrochemistry, Photocatalysis and Photoreactors,* M. Schiavello, Ed., Reidel, Dordrecht, Netherlands, p 305.

Pelizzetti, E. and N. Serpone (Eds.) (1986) *Homogeneous and Heterogenous Photocatalysis*, Reidel, Dordrecht, Netherlands.

Peral, J. and D. F. Ollis **(1993)** *Photocatalytic Purification and Treatment of Water and Air*, Ollis, D.F. and Al-Ekabi, H. (Eds.), Elsevier: Amsterdam, p 741.

Pruden, A. and D. Ollis **(1980)** *J. Catal.*, 66, 383.

Pruden, A. and D. Ollis **(1983a)** *J. Catal.*, 82, 404.

Pruden, A. and D. Ollis **(1983b)** *Environ. Sci. Technol.*, 17, 10.

Okamoto, K., Y. Yamamoto and H. Tanaka **(1985)**, *Bull. Chem. Soc. Jpn.*, 58, 2023.

Robertson M. K. and R.B. Henderson **(1990)** "Fluid Purification" *USA Patent #* 4, 892, 712.

Serpone, N., E. Borgarello, R. Harris, P. Cahill and M. Borgarello **(1986)** *Solar Energy Materials*, 14, 121.

Serpone, N., D. Lawless, R. Terzian, C. Minero and E. Pelizzetti **(1991)** *Photochemical Conversion and Storage of Solar Energy*, Pelizzetti, E. and Schiavello, M. (Eds.), p 451.

Serpone, N., E. Pelizzetti and H. Hidaka **(1993)**, *Photocatalytic Purification and Treatment of Water and Air*, Ollis D.F. and Al-Ekabi, H. (Eds.) Elsevier: Amsterdam, p 225.

Serpone N., E. Pelizzetti and H. Hidaka **(1993)** *Photocatalytic Purification and Treatment of Water and Air*, Ollis, D.F. and Al-Ekabi H. (Eds.), Elsevier: Amsterdam, p 771.

Serpone, N. **(1994)** "A Decade of Heterogeneous Photocatalysis In Our Laboratory: Pure and Applied Studies in Energy Production and Environmental Detoxification", *Res. Chem. Intermed.* 20, p 953.

Sclafani, A., A. Brucato and L. Rizzutti **(1993)** *Photocatalytic Purification and Treatment of Water and Air*, Ollis, D.F. and Al Ekabi, H. (Eds.), Elsevier: Amsterdam, p 533.

Sherwood T.K., R.L. Pigford and C.R. Wilkie **(1980)** In: *Separation Processes*, King C.J. (Ed.), Mc Graw Hill, New York, p 527.

Sun L., K. Schindler, A. Hoy and J. Bolton **(1994)** In: *Aquatic and Surface Photochemistry*, Helz, G., Zepp, R. and Crosby, D. (Eds.), Lewis, Boca Raton, FL, p 409.

Sun, L. and J.R. Bolton (1995) *J. Phys. Chem.*, (submitted)

Sundstrom, D. and H. Klei (1979), *Waste Water Treatment*, Prentice, Englewood Cliffs, N.J.

Tanaka, H., K. Harada and S Murata (1986), *Solar Energy*, 36, 159.

Terzian, R., N. Serpone, C. Minero and E. Pelizzetti (1991) *J. Catal.* 128, 352.

Thurchi, C.S. and D.F. Ollis (1988) *J. Phys. Chem.*, 92, 6852.

Turchi, C.S., M. Mehos and J. Pacheco (1993) *Photocatalytic Purification and Treatment of Water and Air*, Ollis, D.F. and Al-Ekabi, H., (Eds.) Elsevier: Amsterdam, p 789.

Valladares, J.E., (1991) *M.Sc. Thesis*, The University of Western Ontario, London, Ontario, Canada.

Valladares, J. and J.R. Bolton (1993) *Photocatalytic Purification and Treatment of Water and Air*, Ollis, D. F. and Al-Ekabi, H., (Eds.), Elsevier: Amsterdam, p 111.

Weedon, A. (1994) In: Proccedings of *The First International Conference on Advanced Oxidation Technologies for Water and Air Remediation*, London, Canada, p 127.

Wei, T., Y. Wang and C. Wan (1990) *J. Photochem. Photobiol. A: Chem.*, 55, 118.

Wilson and C.J. Geankoplis (1993) In: *Transport Proceses and Unit Operations*, Geankoplis C.J., (Eds.), p 448.

Wolfrum, E. and C.S. Turchi (1992) *J. Catal.* 136, 626.

Xu, Y., P. Menassa and C. Langford (1988) *Chemosphere*, 17, 1971.

Yue P.L. (1985a) In: *Photoelectrochemistry, Photocatalysis and Photoreactors*, M. Schiavello, (Ed.), Dordrecht, Neetherlands, 527.

Yue P.L. (1985b) In: *Photoelectrochemistry, Photocatalysis and Photoreactors*, M. Schiavello (Ed.), Dordrecht, Neetherlands, p 619.

Yue P.L. (1985c) In: *Photoelectrochemistry, Photocatalysis and Photoreactors*, M. Schiavello, (Ed.), Dordrecht, Neetherlands, p 575.

Yue, P.L., (1993) *Photocatalytic Purification and Treatment of Water and Air*, Ollis D.F. and Al-Ekabi, H. (Eds.), Elsevier, Amsterdam, p 111.

Zhang,Y.,J.C. Crittenden and D.W.Hand (1994) *Chemistry and Industry*, September, p 717.